Evolution of Hydrothermal Fluids in the Alta Stock, Central Wasatch Mountains, Utah

U.S. GEOLOGICAL SURVEY BULLETIN 1977

AVAILABILITY OF BOOKS AND MAPS OF THE U.S. GEOLOGICAL SURVEY

Instructions on ordering publications of the U.S. Geological Survey, along with prices of the last offerings, are given in the current-year issues of the monthly catalog "New Publications of the U.S. Geological Survey." Prices of available U.S. Geological Survey publications released prior to the current year are listed in the most recent annual "Price and Availability List." Publications that are listed in various U.S. Geological Survey catalogs (see back inside cover) but not listed in the most recent annual "Price and Availability List" are no longer available.

Prices of reports released to the open files are given in the listing "U.S. Geological Survey Open-File Reports," updated monthly, which is for sale in microfiche from the U.S. Geological Survey, Books and Open-File Reports Section, Federal Center, Box 25425, Denver, CO 80225. Reports released through the NTIS may be obtained by writing to the National Technical Information Service, U.S. Department of Commerce, Springfield, VA 22161; please include NTIS report number with inquiry.

Order U.S. Geological Survey publications **by mail** or **over the counter** from the offices given below.

BY MAIL

Books

Professional Papers, Bulletins, Water-Supply Papers, Techniques of Water-Resources Investigations, Circulars, publications of general interest (such as leaflets, pamphlets, booklets), single copies of Earthquakes & Volcanoes, Preliminary Determination of Epicenters, and some miscellaneous reports, including some of the foregoing series that have gone out of print at the Superintendent of Documents, are obtainable by mail from

U.S. Geological Survey, Books and Open-File Reports
Federal Center, Box 25425
Denver, CO 80225

Subscriptions to periodicals (Earthquakes & Volcanoes and Preliminary Determination of Epicenters) can be obtained ONLY from the

Superintendent of Documents
Government Printing Office
Washington, D.C. 20402

(Check or money order must be payable to Superintendent of Documents.)

Maps

For maps, address mail orders to

U.S. Geological Survey, Map Distribution
Federal Center, Box 25286
Denver, CO 80225

Residents of Alaska may order maps from

Alaska Distribution Section, U.S. Geological Survey,
New Federal Building - Box 12
101 Twelfth Ave., Fairbanks, AK 99701

OVER THE COUNTER

Books

Books of the U.S. Geological Survey are available over the counter at the following Geological Survey Public Inquiries Offices, all of which are authorized agents of the Superintendent of Documents:

- **WASHINGTON, D.C.**--Main Interior Bldg., 2600 corridor, 18th and C Sts., NW.
- **DENVER, Colorado**--Federal Bldg., Rm. 169, 1961 Stout St.
- **LOS ANGELES, California**--Federal Bldg., Rm. 7638, 300 N. Los Angeles St.
- **MENLO PARK, California**--Bldg. 3 (Stop 533), Rm. 3128, 345 Middlefield Rd.
- **RESTON, Virginia**--503 National Center, Rm. 1C402, 12201 Sunrise Valley Dr.
- **SALT LAKE CITY, Utah**--Federal Bldg., Rm. 8105, 125 South State St.
- **SAN FRANCISCO, California**--Customhouse, Rm. 504, 555 Battery St.
- **SPOKANE, Washington**--U.S. Courthouse, Rm. 678, West 920 Riverside Ave..
- **ANCHORAGE, Alaska**--Rm. 101, 4230 University Dr.
- **ANCHORAGE, Alaska**--Federal Bldg, Rm. E-146, 701 C St.

Maps

Maps may be purchased over the counter at the U.S. Geological Survey offices where books are sold (all addresses in above list) and at the following Geological Survey offices:

- **ROLLA, Missouri**--1400 Independence Rd.
- **DENVER, Colorado**--Map Distribution, Bldg. 810, Federal Center
- **FAIRBANKS, Alaska**--New Federal Bldg., 101 Twelfth Ave.

Evolution of Hydrothermal Fluids in the Alta Stock, Central Wasatch Mountains, Utah

By DAVID A. JOHN

U.S. GEOLOGICAL SURVEY BULLETIN 1977

U.S. DEPARTMENT OF THE INTERIOR
MANUEL LUJAN, JR., Secretary

U.S. GEOLOGICAL SURVEY
Dallas L. Peck, Director

UNITED STATES GOVERNMENT PRINTING OFFICE, WASHINGTON : 1991

For sale by the
Books and Open-File Reports Section
U.S. Geological Survey
Federal Center, Box 25425
Denver, CO 80225

CONTENTS

FIGURES

TABLES

Evolution of Hydrothermal Fluids in the Alta Stock, Central Wasatch Mountains, Utah

By David A. John

ABSTRACT

The Alta stock is a small, composite granodiorite to quartz monzodiorite stock that lies between the Park City and Cottonwood mining districts in the central Wasatch Mountains, Utah. The stock was tilted about 20° east subsequent to its emplacement, and present exposures of the stock represent paleodepths ranging from about 3.7 km on the east to 6.3 km on the west. Primary crystallization of biotite before hornblende suggests initial magmatic water contents of 3 to 4 weight percent. Calculations based on biotite compositions suggest that oxygen fugacity during crystallization was between nickel–nickel oxide and hematite-magnetite buffers and that the oxidation state may have slightly increased during crystallization and from shallow to deeper depths in the stock. Amphibole phenocrysts have conspicuous patchy compositional zoning similar to that reported in other shallow intrusions and characterized by systematic increases in Mg, Ca, and Mn and decreases in Fe, Al, Ti, Na, and K with increasing Si. Compositional zoning may indicate interaction of the amphibole with an aqueous fluid during crystallization. Fluid-inclusion data, however, suggest that vapor saturation of the magma may not have occurred until temperatures approached the solidus (725–770 °C). In the upper part of the stock at depths ≤5 km, magmatic fluids either boiled, forming high-salinity brine (35–70 weight percent NaCl equivalent) and low-salinity vapor phases, or else high-salinity brines were directly exsolved from the crystallizing magma. In deep parts of the stock at depths >5 km, magmatic fluids were supercritical and of low to moderate salinity (≤12 weight percent NaCl equivalent).

The hydrothermal system is characterized by pervasive, generally weak, deuteric alteration. This alteration is characterized by partial sericitization of plagioclase, chloritization of biotite, and development of turbid perthite crystals. Stable-isotope relations and fluid-inclusion data suggest that alteration occurred at temperatures near 500 °C from magmatically derived fluids. Weak fracture-controlled alteration also is present. Early veins contain calcic amphibole (hornblende), K-feldspar, and epidote. These are followed by biotite+magnetite (±K-feldspar), quartz±K-feldspar, quartz+pyrite±sericite, and pyrite+chlorite. All veins except pyrite+chlorite initially formed at temperatures near 470–550 °C from dilute (≤10 weight percent NaCl equivalent), nonboiling fluids that were probably derived from magmatic fluids. Veins and joints have strong preferred northeast orientations that parallel regional structures. Veins are much less abundant than in the nearby Mayflower stock and in the vicinity of typical porphyry copper-related intrusions elsewhere, suggesting that fracture permeability was much lower in the Alta stock than in mineralized intrusions.

The hydrothermal system of the Alta stock developed in several ways distinct from intrusion-hosted porphyry copper systems. These include the following: (1) Early fluids had relatively high $a_{Ca}{}^{2+}/a^2{}_{H}{}^{+}$ ratios that stabilized calcic amphibole; (2) late fluids deposited chlorite instead of sericite, probably indicating relatively high $a_{Mg}{}^{2+}/a^2{}_{H}{}^{+}$ ratios; (3) there is only weak fracture-controlled alteration; (4) most veins formed from relatively dilute fluids, including early, high-temperature veins; (5) pressure remained near lithostatic throughout crystallization and cooling of the stock; and (6) there is no stable-isotope evidence for incursion of meteoric water. Most of these differences probably are the result of the Alta stock being emplaced at somewhat greater depths than most porphyry copper stocks and possibly having slightly lower initial water contents: both of these factors would lead to low fracture permeability.

INTRODUCTION

Recent papers describing an orthomagmatic model for the generation of porphyry copper and molybdenum deposits by Burnham (1979a, 1981, 1985) and Burnham and Ohmoto (1980) have emphasized the role of exsolution of magmatic fluids during crystallization of shallowly emplaced granitic magmas. In this model, early release of fluids may lead to concentration of ore-forming elements, hydrofracturing, and hydrothermal alteration characteristic of these deposits. These authors argue that relatively volatile-rich magmas and shallow levels of emplacement may be more important factors in the gen-

Manuscript approved for publication, February 4, 1991.

eration of porphyry copper–molybdenum deposits than specific sources for calc-alkaline magmas or unusually high concentrations of metals, sulfur, and chlorine in the magma.

The Alta stock, a small, composite granodiorite to quartz monzodiorite intrusion in the central Wasatch Mountains, Utah (fig. 1), has many features similar to intrusions that host porphyry copper deposits. Other temporally equivalent intrusions in the central Wasatch Mountains (Park City and Cottonwood mining districts) formed significant precious- and base-metal mineralization, both within intrusive rocks and in the surrounding sedimentary wall rocks. The Alta stock, however, generally lacks stockwork veins, intense hydrothermal alteration, and disseminated copper sulfide mineralization typical of porphyry copper-related intrusions.

This study was undertaken to examine the evolution of magmatic and hydrothermal fluids in a well-exposed, weakly altered and weakly mineralized system that is similar in many aspects to porphyry copper intrusions. By comparing results from the poorly mineralized Alta stock with those from porphyry copper systems, it was hoped that differences between barren and mineralized systems would become more apparent. This study emphasized the determination of the presence or absence of a fluid phase during crystallization and the spatial and temporal evolution of the hydrothermal system within the Alta stock. Small Fe-Cu skarns that formed along the margins of the Alta stock were not studied. Studies undertaken included systematic mapping of veins and fractures in the stock, electron-microprobe analyses of mafic minerals, fluid-inclusion studies of igneous rocks and hydrothermal veins, and reconnaissance stable-isotope analyses.

Acknowledgments

This paper is an outgrowth of part of a Ph.D. thesis completed at Stanford University. I wish to thank my thesis advisor, M.T. Einaudi, for much help and many ideas. W.J. Moore introduced me to the geology of the Wasatch Mountains, and D.P. Cox encouraged me to undertake this study. T.G. Theodore and T.F. Lawton introduced me to the world of fluid inclusions and helped with interpretation of the fluid-inclusion data. L.C. Calk helped with the microprobe analyses, and R.L. Oscarson assisted with the SEM work. Discussions with G.K. Czamanske and S.D. Ludington were helpful in interpreting the microprobe and SEM data. R.H. Brigham provided most of the stable-isotope data, and discussions with him and J.R. O'Neil helped with the interpretation of these data. Some of the samples used in this study were collected by W.J. Moore and M.L Sorensen. Reviews of early versions of the manuscript by M.T. Einaudi, T.G. Theodore, and S.D. Ludington measurably improved it.

GEOLOGY OF THE ALTA STOCK

The Alta stock is a small (approximately 10 km^2) composite intrusion that is one of 11 middle Tertiary (31–42 Ma) calc-alkaline stocks in the central Wasatch Mountains (fig. 1). The regional geologic setting of igneous rocks in the central Wasatch Mountains was recently summarized by John (1987, 1989). Previous studies of the Alta stock were made by Calkins and Butler (1943) and Wilson (1961). Studies of metamorphism related to emplacement of the stock have been made by Smith (1972), Cranor (1974), Moore and Kerrick (1976), and Bowman and Cook (1981). Kemp and Bowman (1984) studied skarns that locally formed along the margins of the stock. Mineralization in and around the stock was described by Calkins and Butler (1943) and James (1978), and Belt (1969) described reconnaissance geochemical sampling of the stock. Estimated depths of emplacement and fluid-inclusion populations of the Alta and other stocks in the central Wasatch Mountains were described by John (1987, 1989).

The Alta stock consists of two major phases (equigranular and porphyritic), a discontinuous mafic border phase, and numerous pegmatite and aplite bodies that intrude Paleozoic sedimentary rocks (fig. 2; Calkins and Butler, 1943; Wilson, 1961). The two major phases are a medium-grained, more or less equigranular phase and a vaguely to strongly porphyritic phase with a fine-grained aplitic groundmass. The equigranular phase forms most of the western and outer parts of the stock, and the porphyritic phase forms the eastern and inner parts of the stock (fig. 3). Contacts between the phases vary from sharp and intrusive along the southern margin of the porphyritic phase near Lake Mary (fig. 4) to obscure and gradational along the northern margin of the porphyritic phase. Near Lake Mary the porphyritic phase truncates foliation, jointing, and aplite dikes in the equigranular phase. Textures of the eastern part of the stock are highly variable, and, owing to poor outcrop, contacts between different textural types are not exposed. Wilson (1961) suggested that the porphyritic phase resulted from injection of partially crystallized magma into the equigranular phase and subsequent pressure quenching of this magma (Jahns and Tuttle, 1964).

The mineralogy of major phases of the stock is fairly uniform except for slight variations in modal contents of biotite and hornblende, which are the main mafic silicate minerals. Clinopyroxene was an early crystallizing phase but was almost entirely resorbed by the magma and is now only found as small inclusions in cores of plagioclase crystals. Magnetite is the dominant

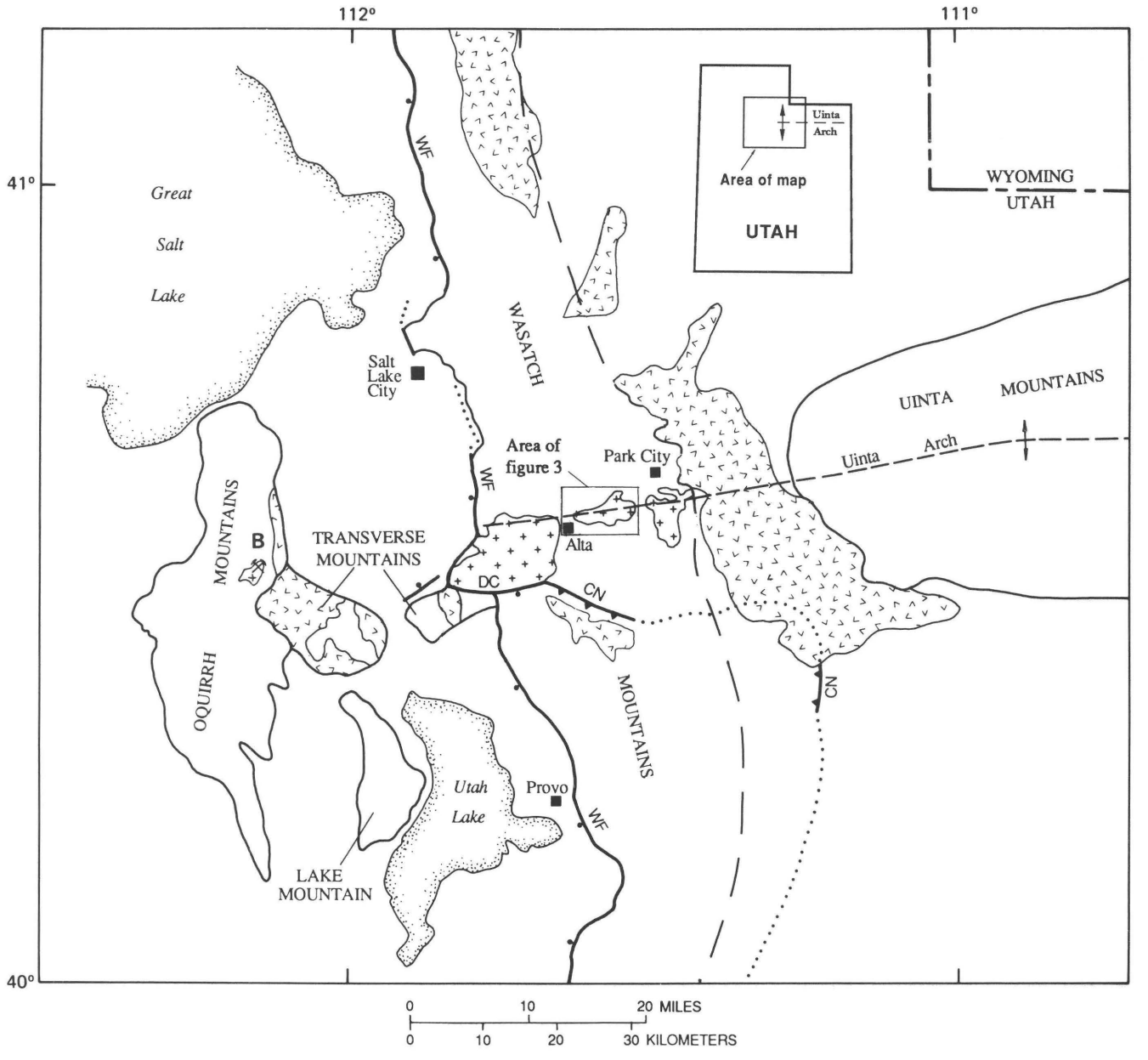

EXPLANATION

- Volcanic rocks (Tertiary)
- Granitic rocks (Tertiary)
- Contact
- Normal fault—Dotted where concealed. Bar and ball on downthrown side
- Thrust fault—Dotted where concealed. Sawteeth on upper plate
- Anticline
- Approximate extent of Wasatch Mountains

Figure 1. Central Wasatch Mountains and surrounding region, showing distribution of middle Tertiary igneous rocks and major structures. Geology simplified from Hintze (1980). Abbreviations: B, Bingham mine; CN, Charleston-Nebo thrust fault; DC, Deer Creek fault; WF, Wasatch fault zone.

Fe-Ti oxide mineral and appears to be a liquidus phase; ilmenite is sparse to absent in most samples. Sphene forms euhedral phenocrysts throughout most of the stock. Modal and chemical analyses indicate that the composition of the stock varies from quartz monzodiorite to granodiorite with a slight increase in silica contents from the margin inward and toward the eastern part of the stock (fig. 5, table 1). Most of the stock is metaluminous, although the most felsic part of the stock is weakly corundum normative (table 1).

John (1987, 1989) showed that the central Wasatch Mountains have been tilted east about 20° since the emplacement of the Alta stock. Paleodepths of present exposures of the Alta stock were estimated to range from about 6.3 km on the west to about 3.7 km on the east, corresponding to lithostatic pressures varying from about 1.7 kbars on the west to 1.0 kbar on the east.

HYDROTHERMAL ALTERATION OF THE ALTA STOCK

Hydrothermal alteration of the Alta stock generally is weak and mostly consists of pervasive deuteric alteration. Other types of alteration include fine-grained, shreddy biotite that locally replaces hornblende and is present in the groundmass of rocks in the eastern part of the stock; thin K-feldspar selvages around hornblende veins; and thin sericitic selvages on quartz and quartz+pyrite veins. Deuteric alteration is present throughout the stock and appears to be unrelated to megascopic or microscopic fractures. This alteration consists of variable amounts of fine-grained white mica (sericite) replacing plagioclase, chlorite + sphene + magnetite replacing biotite along crystal margins and cleavage planes, sphene locally rimming magnetite, and perthite forming in potassium feldspar and antiperthite in plagioclase. In more strongly altered rocks, epidote partially replaces plagioclase and biotite, prehnite locally replaces biotite, and potassium feldspar becomes turbid and more coarsely perthitic.

Seven vein types were distinguished during field studies (table 2). Early veins (type 1) are hornblende + K-feldspar + sphene ± quartz ± magnetite ± epidote. Plagioclase crystals along the margins of type 1 veins range from unaltered to partially replaced and overgrown by K-feldspar to sericitized. Many type 1 veins have thin (≤1 cm) white selvages of potassium feldspar (approximately $Or_{91}Ab_9$). Most hornblende crystals are euhedral and appear to have filled open spaces that were later filled by quartz. Epidote (±magnetite ±pyrite) veins (type 2) are present sporadically in the eastern part of the stock and locally cut hornblende veins. Biotite + magnetite veins (type 3) locally cut hornblende veins. Type 3

Figure 2. Alta stock, looking west. Alta stock forms light-colored rocks seen in lower half and at skyline on left side of photograph. Peak on left side of the photograph is Mt. Millicent. High peak in background is Dromedary Peak, which is composed of Proterozoic and Paleozoic sedimentary rocks. Lake Mary is in center of photograph and Twin Lakes Reservoir is on far right side. Grassy clearcuts in lower part of photograph are ski runs. Brighton is just to right of photograph.

veins also may contain quartz, K-feldspar, pyrite, chalcopyrite, and molybdenite. Wall-rock alteration of plagioclase varies from partial replacement by K-feldspar to fresh or weakly sericitized, similar to other plagioclase crystals outside the immediate vein selvage. Potassium feldspar crystals along vein margins are fresh.

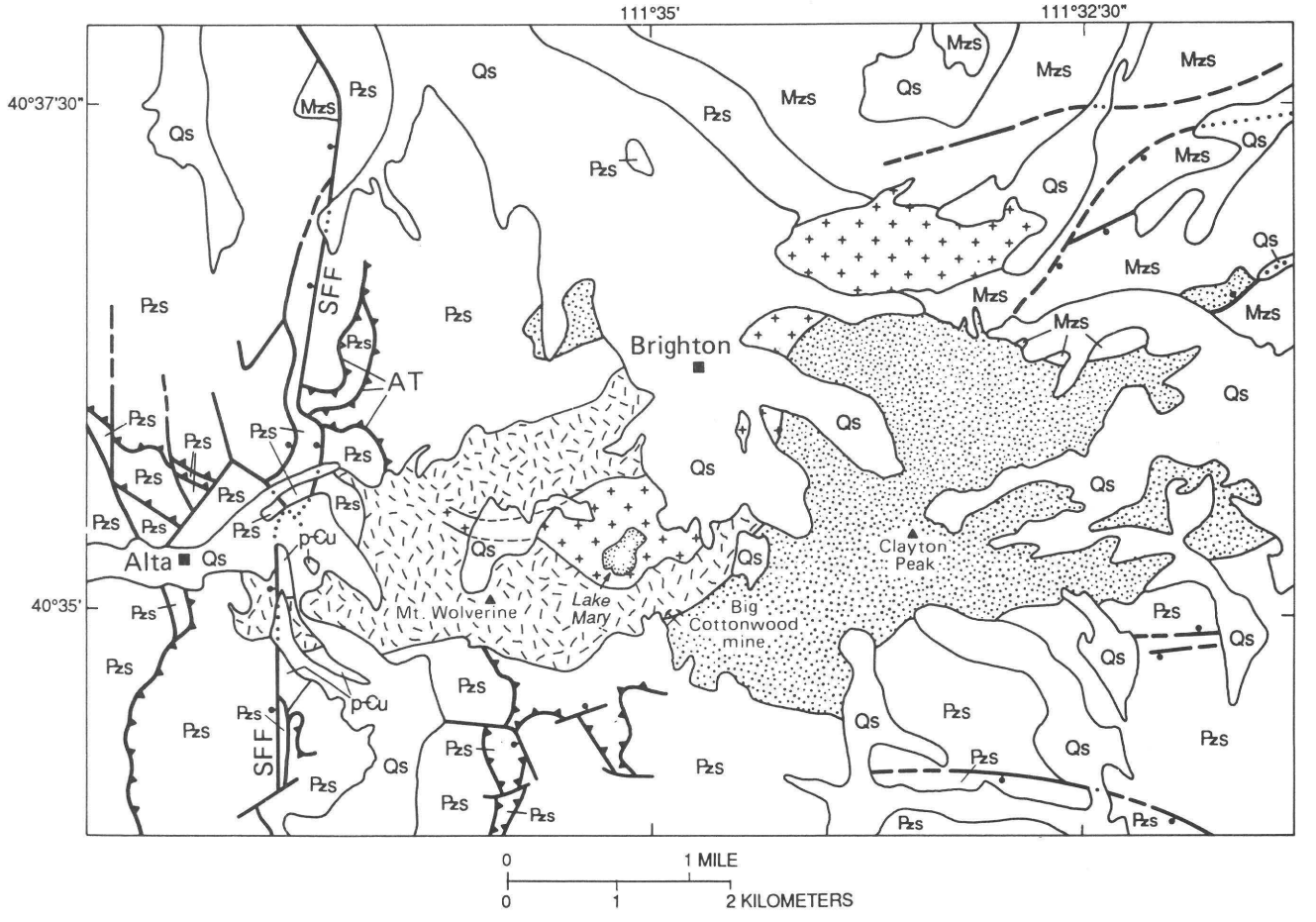

EXPLANATION

- Qs — Quaternary surficial deposits
- Porphyry phase — Alta stock
- Equigranular phase — Alta stock
- Clayton Peak stock
- Mzs — Mesozoic sedimentary rocks
- Pzs — Paleozoic sedimentary rocks
- p€u — Precambrian sedimentary, metamorphic, and intrusive rocks, undivided
- Contact—Dashed where approximately located
- Normal fault—Dashed where approximately located; dotted where concealed. Bar and ball on downthrown side
- Thrust fault—Sawteeth on upper plate

Figure 3. Alta stock and vicinity. Geology simplified from Baker and others (1966) and Crittenden (1965). Abbreviations: SFF, Silver Fork fault; AT, Alta Grizzly thrust.

Quartz veins (type 4), generally containing small amounts of K-feldspar, cut the biotite + magnetite veins. Plagioclase crystals along the margins of type 4 veins generally are sericitized, and biotite crystals are chloritized. Quartz + pyrite veins (type 5), generally with coarse-grained sericite selvages, locally cut biotite + magnetite veins. Plagioclase, biotite, and hornblende are sericitized in vein selvages, whereas potassium feldspar varies from unaltered to sericitized. Vuggy quartz veins partially filled with fine-grained chlorite + pyrite (type 6) cut all the above types of veins. Plagioclase along vein margins is sericitized, and biotite is chloritized. Potassium feldspar appears fresh or weakly sericitized. The latest veins (type 7) are pyrite + chlorite that coat joint surfaces (fig. 6). These veins lack vein selvages.

MINERALIZATION ASSOCIATED WITH THE ALTA STOCK

Weak, fracture-controlled base-metal mineralization is present within the Alta stock. Thin (generally ≤2 mm), widely spaced biotite + magnetite ±quartz ±pyrite veins, locally containing small amounts of chalcopyrite and (or) molybdenite, are present throughout the stock but are nowhere abundant. These veins are similar to early veins in porphyry copper deposits (Titley, 1982). Thicker, milky white quartz veins containing chalcopyrite and pyrite are locally present near Mt. Wolverine (James, 1978).

Two types of mineralization are present in wall rocks around the Alta stock. These are small Fe-Cu skarns and Ag-Pb-Zn fissure and replacement ores. Skarns locally contain pods of massive magnetite ± bornite ± chalcopyrite ± pyrrhotite in a complex gangue of silicate minerals (for example, Big Cottonwood mine; fig. 3). Ag-Pb-Zn sulfide ores are present in fault zones (particularly thrust faults) and replace carbonate rocks where these rocks intersect mineralized faults (Calkins and Butler, 1943; James, 1978). Most of the Ag-Pb-Zn ores were found west of the Silver Fork fault (fig. 3) in the Cottonwood mining district.

FRACTURES AND VEINS IN THE ALTA STOCK

Joints and mineral-coated joints (veins) are present throughout the Alta stock, and reconnaissance studies of the distribution, orientation, and abundance of joints and veins are described below. Traverses were made across all parts of the stock, and data on the types, orientations, and abundances of veins and fractures were measured at approximately 250 locations spaced at fairly uniform intervals (approximately 60–100 m) along these traverses (fig. 7*A*).

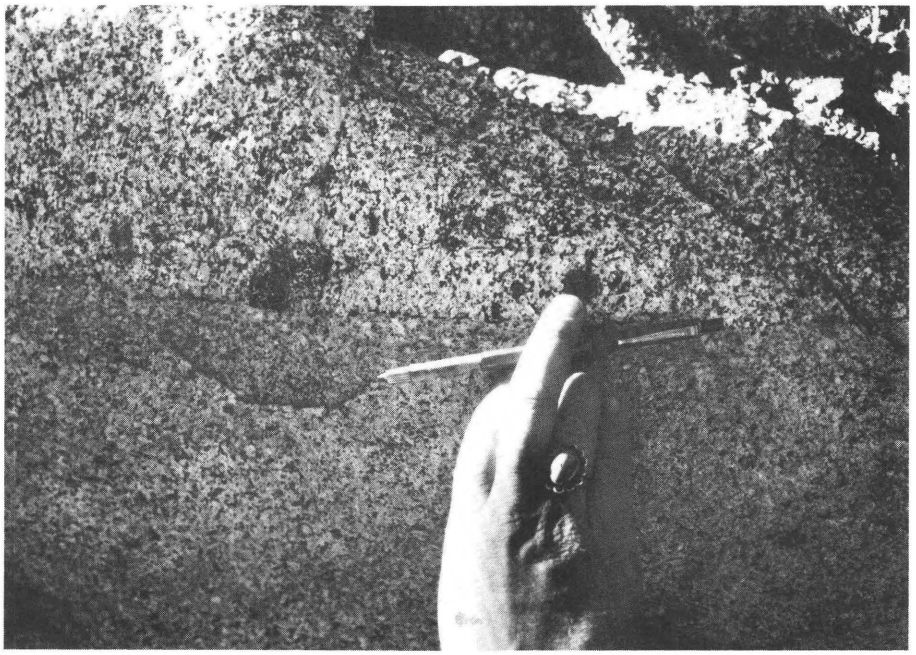

Figure 4. Intrusive contact between equigranular and porphyritic phases of Alta stock. Foliation defined by parallel alignment of mafic minerals and flattened mafic inclusions in equigranular phase (upper half of photograph) is truncated by porphyritic phase (lower half of photograph). Photograph taken on western shore of Lake Mary.

Types and Relative Ages

Joints are well developed throughout most of the stock and tend to form one or two well-defined sets. Spacing between joints varies from about 2 cm to >1 m. Most joints have approximately planar surfaces and appear to be continuous along strike for several to tens of meters. No strike separation was found on joints, which suggests that movement was dominantly normal to the surface of the joint. Wilson (1961, pl. 2) found that joint sets in the equigranular and porphyritic phases have different orientations and spacings, but this relationship was not confirmed in the present study.

A small percentage of joints are coated with hydrothermal minerals and are shown as veins (fig. 7). Most veins are thin, with average widths of 1 to 2 mm; few veins exceed 1 cm in width. Aplite and pegmatite dikes also are common and predate all vein types. Pyrite + chlorite veins (type 7) are the most abundant veins; they are present at nearly every outcrop and cut all other types of veins. Veins are not offset by the contact between the porphyritic and equigranular phases, indicating that the vein-forming hydrothermal system postdates emplacement of the porphyritic phase.

Distribution and Orientations

The distribution and orientations of veins are shown in figure 7. Hornblende+K-feldspar veins are notably sparse in the eastern (upper) part of the stock, whereas epidote veins are concentrated in this part of the stock (fig. 7*A*). Hornblende+K-feldspar veins are concentrated along the western, northern, and southern mar-

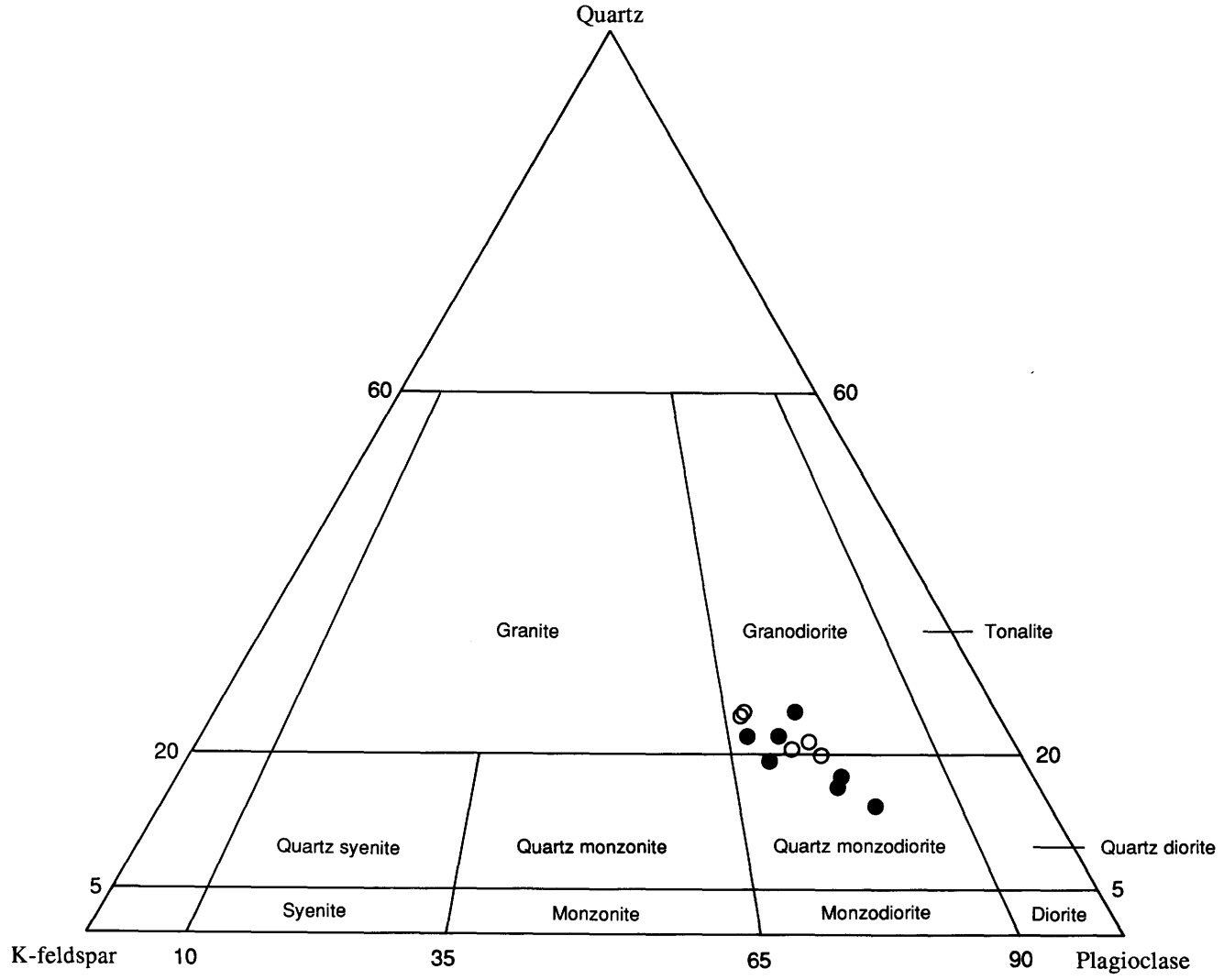

Figure 5. Modal quartz, plagioclase, and K-feldspar contents recalculated to 100 percent for samples of Alta stock on the basis of point counts of stained slabs. Solid circles, samples of equigranular phase; open circles, samples of porphyritic phase. Compositional fields from Streckeisen (1976).

Table 1. Chemical analyses, CIPW norms, and modal analyses of the Alta stock

[Major-element analyses except FeO made by wavelength-dispersive X-ray fluorescence spectroscopy (analyst, A. Bartel). FeO, F, and Cl determined by wet chemical methods (analyst, K. Stewart). Minor-element analyses made by energy-dispersive X-ray fluorescence (analysts, J. Taggert and T. Vercoutere)]

Sample	82-PC-17	83-PC-206	83-PC-272	83-PC-276
SiO_2 (wt %)	62.9	63.5	63.9	67.2
Al_2O_3	16.4	16.6	16.0	15.5
Fe_2O_3	2.48	2.53	2.30	1.56
FeO	2.43	2.13	2.15	1.71
MgO	2.25	1.81	2.19	1.61
CaO	4.84	4.39	4.21	2.73
Na_2O	3.66	3.88	3.70	3.38
K_2O	2.99	3.14	3.08	4.22
TiO_2	.58	.58	.58	.50
P_2O_5	.32	.32	.29	.26
MnO	.08	.08	.05	.03
LOI	.23	.31	.67	.58
Total	99.16	99.27	99.12	99.28
F	.05	.05	.06	.05
Cl	.018	.010	.025	.013
Ba (ppm)	1,300	1,750	2,000	1,350
Ce	102	110	125	80
Cr	20	13	26	18
Cu	<20	146	<20	310
La	58	67	80	52
Nb	8	14	13	13
Ni	6	10	15	4
Rb	91	116	109	184
Sr	680	696	745	450
Y	20	20	25	20
Zn	59	60	56	27
Zr	177	176	227	161

gins of the stock (fig. 7*A*). Both biotite+magnetite veins and quartz+pyrite+chlorite veins are concentrated in the western (deeper) parts of the stock (fig. 7*B*, *C*).

Stereographic plots suggest that joints and veins have regular orientations (fig. 8). Joints have two dominant orientations: approximately N. 35° E. dipping 80° NW. and N. 85° E. dipping 80° NW. (fig. 8*A*). All veins except type 7 pyrite+chlorite veins have similar orientations to the joints (fig. 8*B*). Pyrite+chlorite veins are more systematically oriented than other types of veins, with a dominant trend of N. 38° E., 76° NW. subparallel to one set of joints (fig. 8*C*).

The approximate total number of megascopic fractures per meter (joints + veins) varies from <1/m to >20/m, although the number of veins generally is less than 1–2/m. The integrated fracture density (total length of veins/area of outcrop; Haynes and Titley, 1980), measured in three locations where veins are most abundant, ranges from 0.08/cm to 0.16/cm. There is no obvious correlation between abundance of joints and veins with depth in the stock or between abundance of fractures with location relative to the margins of the stock.

Comparison of Fracture Data in the Alta Stock to Other Areas in the Central Wasatch Mountains

Villas and Norton (1977) showed that there are two dominant trends of veins in the nearby Mayflower stock: N. 50° E., 80° NW. and N. 50° W., 80° SW. They noted that the northeast-trending set is parallel to major fissures in the Park City mining district, but that there was no regional counterpart to the northwest-trending set. They suggested that these fracture sets were conjugate shear fractures formed at high

Table 1. Chemical analyses, CIPW norms, and modal analyses of the Alta stock—Continued

Sample	82-PC-17	83-PC-206	83-PC-272	83-PC-276
Normative minerals (weight percent)				
Quartz	17.33	17.67	19.11	23.69
Corundum	—	—	—	1.04
Orthoclase	17.86	18.75	18.49	25.27
Albite	31.30	33.17	31.80	28.98
Anorthite	19.70	18.80	18.24	12.00
Diopside	1.96	.87	.84	—
Hypersthene	6.35	5.16	6.34	5.16
Magnetite	3.64	3.71	3.39	2.29
Ilmenite	1.11	1.11	1.12	.96
Apatite	.75	.75	.68	.61
Modal analyses (volume percent)				
Quartz	13.6	18.7	20.8	21.5
Plagioclase	52.6	44.5	46.9	44.6
K-feldspar	15.9	22.0	16.8	22.0
Biotite	4.6	6.4	7.5	9.9
Hornblende	10.8	6.0	6.4	.8
Opaque oxides	1.8	1.5	1.5	.6
Sphene	.5	1.0	.3	.5
Apatite	.1	.1	tr	tr
Other	Z	All, Z	Cpx, Z	All, Z

Abbreviations: LOI, loss on ignition at 900 °C; tr, trace; All, allanite; Cpx, clinopyroxene; Z, zircon.

Sample descriptions (see fig. 11 for sample locations):

82-PC-17—marginal part of Alta stock, equigranular phase

83-PC-206—interior part of Alta stock, equigranular phase

83-PC-272—upper part of Alta stock, equigranular phase; plagioclase moderately sericitized and biotite moderately chloritized,

83-PC-276—upper part of Alta stock, porphyritic phase, hornblende partially replaced by biotite

temperatures during emplacement and cooling of the Mayflower stock. They also showed that the abundance of mineralized fractures ranges from about 6 to 21 per meter in the upper part of the Mayflower stock and decreases downward.

Numerous silicic, lamprophyric, and andesitic dikes, which intrude the Alta and Little Cottonwood stocks and the wall rocks between them, are shown on maps of the Dromedary Peak and Brighton quadrangles (Crittenden, 1965; Baker and others, 1966). The dikes tend to have three major trends—N. 5° W. to N. 10° E., N. 40–60° E., and N. 80° E. to E.-W.—and most appear to have steep dips. Major joint sets in the Little Cottonwood stock mapped by Crittenden (1965) have orientations similar to the dikes.

Fractures in the Alta stock have fairly systematic orientations subparallel to regional fracture patterns and lack a strong set of conjugate shear fractures similar to those present in the Mayflower stock. These data suggest that most of the fractures in the Alta stock formed by tensile stresses and were localized in directions of regional weaknesses. Burnham (1985) has suggested that fracture patterns in typical porphyry copper systems are preferentially concentrated where wall rocks initially have relatively uniform tensile strengths. In contrast, for wall rocks that initially possess major zones of weaknesses, Burnham suggests that localization of fractures in directions of regional weaknesses and release of energy during second (resurgent) boiling lead to early failure and concentration of decompressional energy into these

Table 2. Vein assemblages in the Alta stock

Type	Mineralogy	Typical width (millimeters)	Relative abundance	Selvage
1	Hornblende + K-feldspar + sphene ± quartz ± magnetite ± epidote	1–10 (generally ≤1–2)	Moderate	White K-feldspar (0–5 mm)
2	Epidote ± magnetite ± pyrite	1–2	Sparse except at east end	
3	Biotite + magnetite ± quartz ± K-feldspar ± pyrite ± chalcopyrite ± molybdenite	<1–2	Moderate	Local K-feldspar (<1–2 mm)
4	Quartz ± K-feldspar	1–10	Sparse	
5	Quartz + pyrite ± sericite selvages	1–50	Generally sparse	Sericite (1–10 mm)
6	Quartz + chlorite + pyrite	1–10	Generally sparse	Narrow sericite
7	Pyrite + chlorite	<1–3	Abundant	

zones, stopping development of extensive "porphyry-type fracture systems." This latter process may have occurred in the Alta stock.

The abundance of mineralized fractures (veins) in the vicinity of the Mayflower vein system in the Mayflower stock is about 5 to 20 times greater than in the Alta stock. Fossil fracture permeability of the Alta stock cannot be estimated accurately because the apertures of the fractures are unknown (Snow, 1970; Norton and Knapp, 1977). However, if aperture widths in the Alta stock are similar to those estimated by Villas and Norton (1977) for the Mayflower stock and if the abundance of mineralized fractures is an accurate representation of the number of fractures that were open during circulation of hydrothermal fluids, then fracture permeability of the Alta stock was about an order of magnitude less than that in the Mayflower stock. The integrated fracture densities measured in the Alta stock are considerably lower than those measured by Haynes and Titley (1980) and Titley and others (1986) in the Sierrita, Arizona, porphyry copper deposit and are similar to values that these authors measured several kilometers outside of the mineralized zone, suggesting that the fracture permeability in the Alta stock is considerably lower than in porphyry copper systems.

CRYSTALLIZATION SEQUENCE AND ESTIMATION OF H_2O CONTENTS OF THE MAGMA

The mineralogy and crystallization sequence of the Alta stock suggest that the magma of the Alta stock had initial H_2O contents around 3 to 4 weight percent, which may be less than typical porphyry copper-related intrusions. In the Alta stock, textural evidence indicates that both biotite and hornblende crystallized relatively early, but that biotite began to crystallize before hornblende (fig. 9; John, 1987). The presence of hornblende as an early phenocrystic phase indicates magmatic H_2O contents ≥3 weight percent for bulk compositions similar to the Alta stock (Burnham, 1979a). Comparison of the mineral crystallization sequence of the Alta stock (fig. 9) with Naney's (1983) experimental studies of a synthetic granodiorite with a composition similar to the most felsic parts of the Alta stock suggests water contents of about 3.5 to 4.25 weight percent (fig. 10). Comparison of the crystallization sequence of the Alta stock to experimental crystallization studies of the Oligocene Fish Canyon Tuff at 2 kbars (Johnson and Rutherford, 1989a), which has a whole-rock composition similar to most of the Alta stock, also suggests low H_2O contents in the magma (approximately 3 weight percent) and vapor undersaturation during most of the crystallization (mole fraction of H_2O in the fluid phase approximately 0.25; Johnson and Rutherford, 1989a, fig. 10).

Mineral-crystallization sequences and estimates of magmatic H_2O contents of porphyry copper intrusions are seldom reported. Dilles (1984, 1987) noted that in the Yerington batholith, biotite crystallized before hornblende in the premineralization granodiorite phase, but that biotite and hornblende crystallized simultaneously in the quartz monzonite porphyry and porphyritic quartz monzonite phases, indicating somewhat higher H_2O contents in the mineralizing intrusions. He suggested that H_2O contents of the quartz monzonite porphyry and porphyritic quartz monzonite were >4 weight percent. Burnham's (1979a, 1981, 1985; Burnham and Ohmoto, 1980) model for porphyry copper systems suggests crystallization of hornblende before biotite. These data suggest that the initial H_2O contents of the Alta stock might have been slightly less than in typical porphyry copper intrusions.

COMPOSITIONS OF PRIMARY BIOTITE AND AMPHIBOLE AS INDICATORS OF MAGMATIC FLUID

The compositions of biotite and amphibole can be sensitive indicators of the temperature and of the oxygen and water fugacities of crystallization (Wones, 1981), although the effects of subsolidus reequilibration and alteration must be understood before these parameters can be estimated. Several studies of porphyry copper systems and of shallow plutonic complexes suggest that the oxidation state, and in some cases the oxygen fugacity as well, increased during crystallization and cooling (for example, see Murakami, 1969; Czamanske and Wones, 1973; Mason, 1978; Chivas, 1981; Hendry and others, 1985). In contrast to these oxidizing trends, oxygen fugacity decreases with falling temperature, a trend that is typical of closed systems where the oxidation state maintains values close to oxygen buffer curves (for example, see Dodge and others, 1969; Lipman, 1971; Hildreth, 1979). An increasing oxidation state during crystallization is reflected in higher Mg/(Mg+Fe) contents of biotite and hornblende as crystallization progresses. Czamanske and Wones (1973), Mason (1978), Chivas (1981), and Hendry and others (1985) attributed exsolution of a vapor phase from the magma and subsequent diffusive loss of hydrogen as the most likely cause of oxidation during crystallization. However, a numerical model of the effects of vapor exsolution on magmatic oxygen fugacity by Candela (1986) suggests that this process is an ineffective method for increasing oxygen fugacity in normal granodioritic magmas, and that some other process, such as introduction of meteoric water, must account for increasing oxidation state.

The compositions of biotite and hornblende in 26 samples of the Alta stock were determined by electron microprobe (fig. 11). Analyses were made of phenocrysts, groundmass crystals, small inclusions in the interiors of plagioclase crystals, and hydrothermal crystals. Ferrous/ferric iron ratios were determined for four biotite separates by wet chemical analysis of ferrous iron and recalculation of microprobe analyses. Representative analyses of biotite and hornblende are given in tables 3 and 4, respectively.

Biotite Compositions

Biotite in the Alta stock has relatively low Fe/(Fe+Mg) ratios (0.31 to 0.51) compared with values from biotite in the Sierra Nevada batholith (Dodge and others, 1969; Ague and Brimhall, 1988), the California Coast Ranges (Dodge and Ross, 1971), and Japanese granitoids (Czamanske and others, 1981). Biotite phenocryst compositions are very similar to those of biotite in other intrusions in the Wasatch Mountains (Nash, 1982; Aiken, 1982; D.A. John, unpub. data, 1990); in the least altered biotite in the Santa Rita (Jacobs and Parry,

Figure 6. Type 7 pyrite+chlorite veins in Alta stock. Subparallel pyrite+chlorite veins are well developed along one joint set. Note felt-tip marking pen for scale.

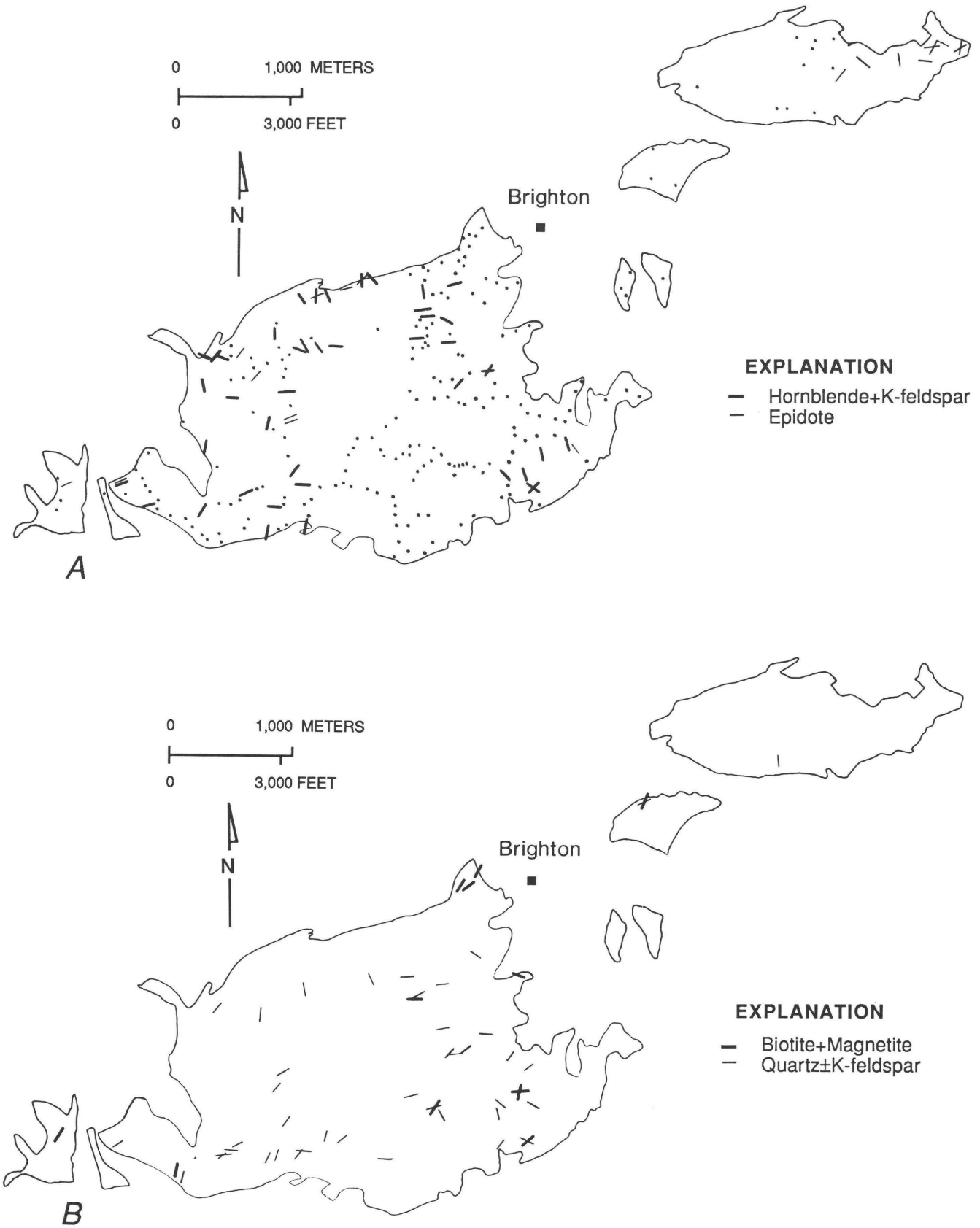

Figure 7. Distribution and orientations of veins in Alta stock. See figure 3 for location. *A*, Type 1 hornblende-bearing veins and type 2 epidote veins. Dots show other locations where fracture data were collected. *B*, Type 3 biotite+magnetite and

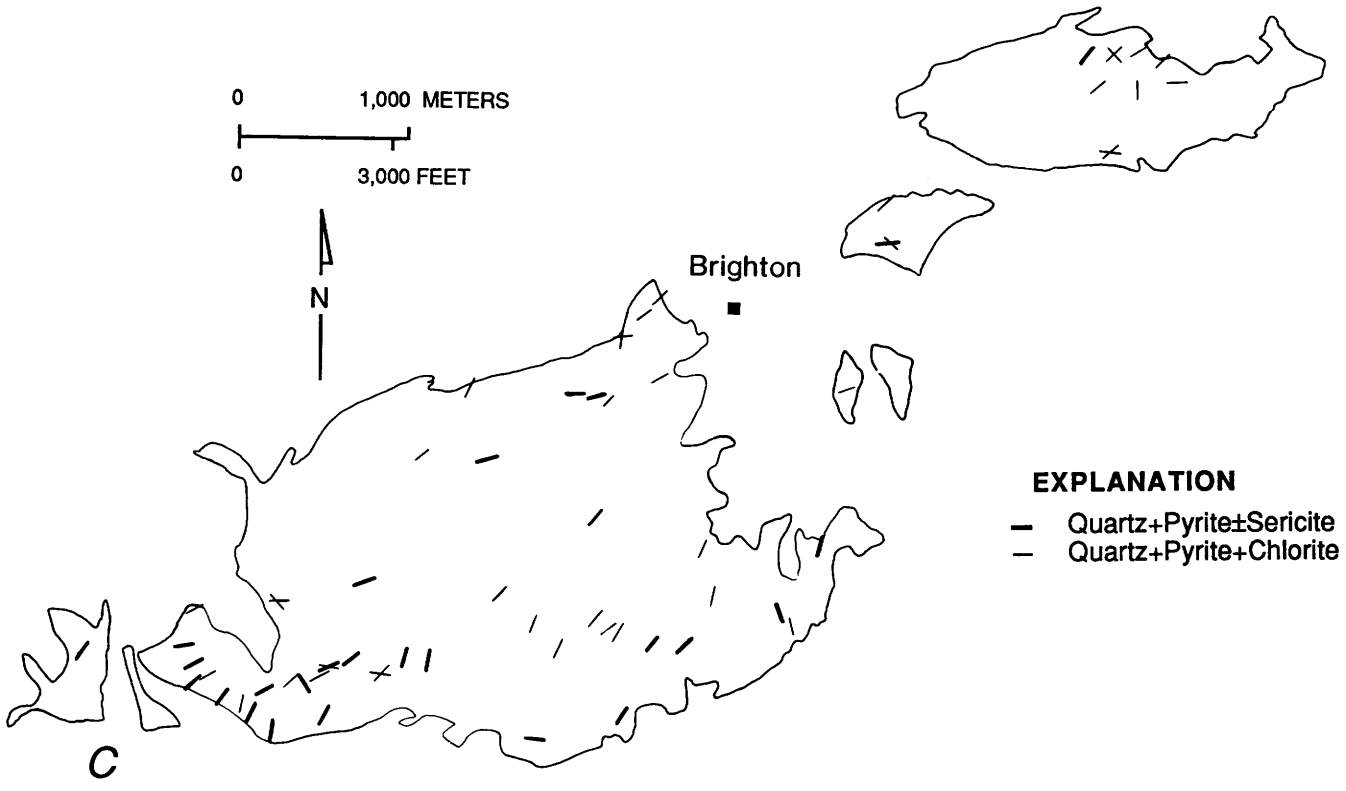

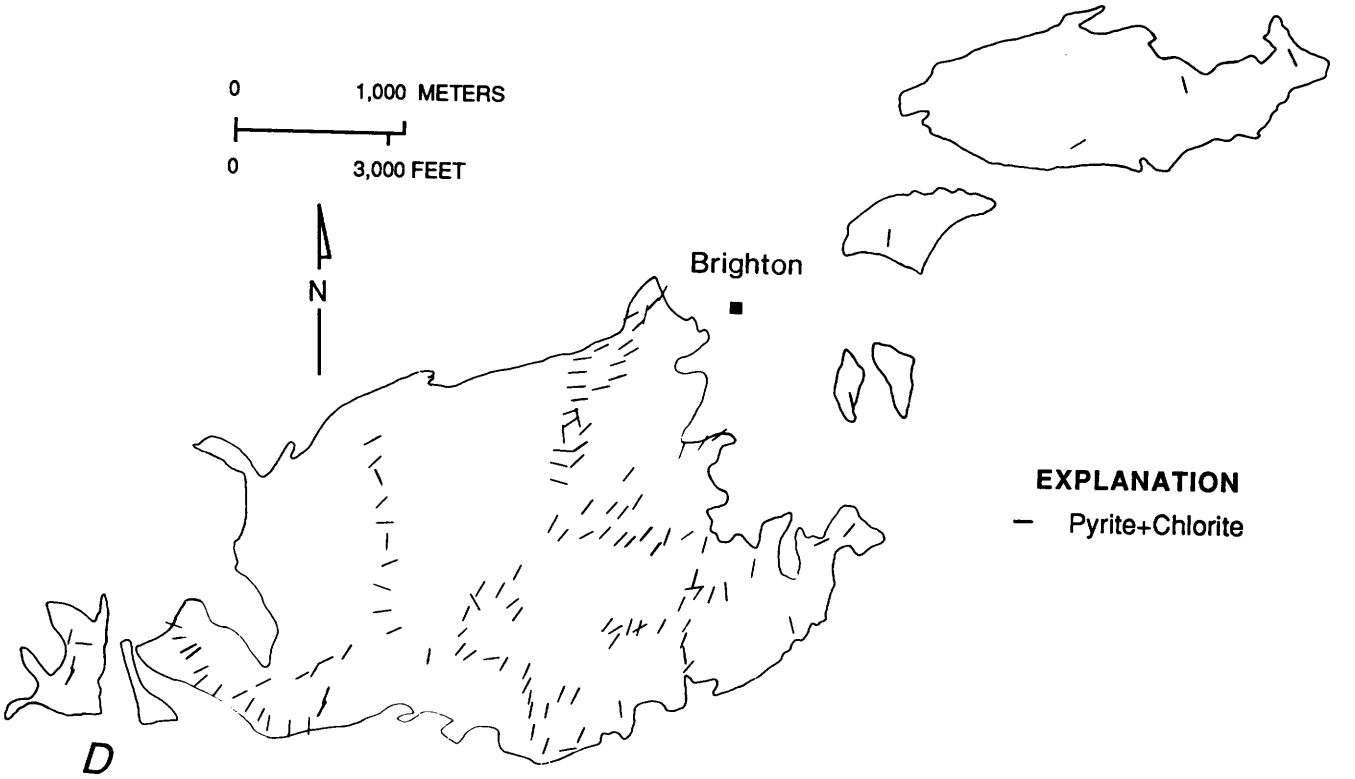

type 4 quartz±K-feldspar veins. *C*, Type 5 quartz+pyrite±sericite and type 6 quartz+pyrite+chlorite veins. *D*, Type 7 pyrite+chlorite veins.

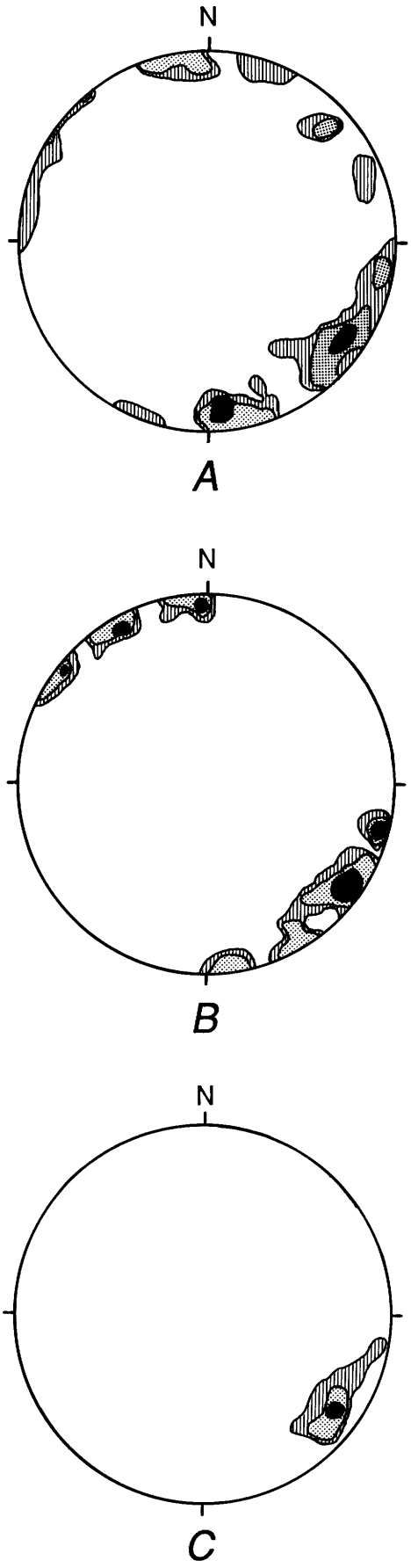

1979), Bingham (Czamanske and Moore, 1973; Lanier and others, 1978), and Yerington (Dilles, 1984, 1987) porphyry copper deposits; and in the Fish Canyon Tuff (Whitney and Stormer, 1985).

Most biotite phenocrysts show only weak Fe-Mg zoning, with either nearly constant Fe/(Fe+Mg) ratios or Fe/(Fe+Mg) ratios that are slightly lower for rims compared with cores (table 3). Four samples along the margin of the stock show the opposite trend, however, with two samples showing strong Fe-enrichment from core to rim [for example, Fe/(Fe+Mg) increases from 0.39 to 0.48 from core to rim in sample 83-PC-253, table 3]. In crystals that show significant core to rim zoning, most of the crystal is fairly homogeneous, with only the rims having large Fe-Mg variation from the rest of the crystal. Titanium and barium contents also decrease from core to rim in crystals showing Fe-Mg zoning (table 3), which is consistent with falling temperature and progressive crystallization (Barriere and Cotten, 1979) and with the change from magmatic to hydrothermal conditions (Jacobs and Parry, 1979).

Two textural types of "hydrothermal" biotite are present: (1) thin veins associated with magnetite, quartz, K-feldspar, and, locally, some sulfide minerals, and (2) fine-grained clots of shreddy biotite that are present as replacements of hornblende phenocrysts and as small crystals in the groundmass. Shreddy biotite was analyzed in one sample and has a composition very similar to the rim compositions of biotite phenocrysts (sample 83-PC-276, table 3). Vein biotite of three samples has significantly lower Ti and Ba and higher Si contents than do biotite phenocrysts in the same sample, and lower Ti contents than the shreddy biotite in sample 83-PC-276 (fig. 12, table 3). Fe/(Fe+Mg) ratios of vein biotite are variable and overlap phenocryst compositions (fig. 12, table 3).

Estimation of Intensive Parameters Using Biotite Compositions

Temperatures of biotite crystallization were estimated to help evaluate the oxidation state during crystallization of the Alta stock. These estimates used

◀ **Figure 8.** Lower-hemisphere equal-area net projection of poles of structural data in Alta stock. *A*, Joints in Alta stock, 336 measurements. Contour intervals at 2 (lined), 3 (stippled), and 4 (black) percent per 1-percent area. *B*, Types 1 through 6 veins in the Alta stock, 206 measurements. Contours at 3 (lined), 4 (stippled), and 5 (black) percent per 1-percent area. *C*, Type 7 pyrite+chlorite veins, 255 measurements. Contours at 5 (lined), 6.5 (stippled), and 8 (black) percent per 1-percent area.

the Ti and Fe contents of biotite and empirical equations derived by Dilles (1984, 1987) and Luhr and others (1984) for biotite coexisting with quartz and sphene or ilmenite. These geothermometers are based on regression of Fe-Ti oxide temperatures from volcanic rocks and oxygen-isotope temperatures in plutonic and metamorphic rocks against the ratio of mole fractions of Ti and Fe in octahedral sites in biotite. Temperatures were estimated using the Dilles (1984) geothermometer because it is based on a larger data set and includes lower temperature samples than does the geothermometer of Luhr and others (1984). The accuracy of the Dilles geothermometer is unknown, but Dilles (1984) suggests an error of +50 °C over the temperature range of 450 °C to >900 °C.

Temperature estimates (figs. 12, 13; table 3) are fairly consistent with known biotite phase relations (Wones and Eugster, 1965; Naney, 1983; Johnson and Rutherford, 1989a) and with solidus temperatures estimated from the experimental studies of Piwinskii (1968) and Naney (1983). Several temperature estimates in the eastern part of the stock, however, may be too high (>900 °C), and several estimates in the western part of the stock are slightly subsolidus (650–700 °C). The anomalously high temperatures may be due to the lack of a Ti-bearing phase during early crystallization; in particular, these samples do not contain phenocrystic sphene and contain little, if any, ilmenite. All biotite phenocrysts showing Fe-Mg zoning have higher calculated core temperatures than rim temperatures (fig. 13). These data suggest that most biotites may have retained their high-temperature compositions, and that compositional zoning is the result of progressive crystallization.

Estimates of oxygen fugacity were made using temperatures calculated from the Dilles (1984, 1987) calibration, biotite compositions, and biotite stability relations from Wones and Eugster (1965) and Wones (1972) using the expression $\log f_{H_2O} = 7409/T + 4.25 + 0.5 \log f_{O_2} + 3 \log a_{annite} - \log a_{sanidine} - \log a_{magnetite}$ for biotite coexisting with quartz, magnetite, and potassium feldspar. The activity of annite was calculated as $a_{annite} = X^3_{Fe^{+2}} X^2_{OH}$, where $X_{Fe^{+2}}$ is the mole fraction of Fe^{+2} in the octahedral site and X_{OH} is the mole fraction of OH in the hydroxyl site. For these calculations, Fe^{+2} was assumed equal to 0.75 total Fe (average of Fe^{+2}-Fe^{+3} determinations; see fig. 14), $a_{sanidine}$ equal to 0.8, and $a_{magnetite}$ equal to 0.8. H_2O pressure was assumed equal to total pressure, and f_{H_2O} values were taken from Burnham and others (1969). Calculated oxygen fugacities range from about $10^{-10.9}$ to $10^{-15.7}$ bars (fig. 13). Calculated oxygen fugacities are between the Ni-NiO (NNO) and hematite-magnetite (HM) buffers and are about 0.5 to 2 log units above the titanite-magnetite-quartz (TMQ) buffer (Wones, 1989), in general agreement with estimates from Fe^{+3}-Fe^{+2} contents of biotite (fig. 14) and with the lack of stable clinopyroxene in the later stages of crystallization and the near-absence of ilmenite. Biotite crystals showing strong compositional zoning generally suggest crystallization along oxygen-buffered paths, with rims having compositions indicating lower temperatures and lower oxygen fugacities (fig. 13). In general, the western samples and hydrothermal biotite have calculated temperatures and oxygen fugacities that suggest crystallization at slightly higher oxidation states than for the eastern phenocrysts (fig. 13).

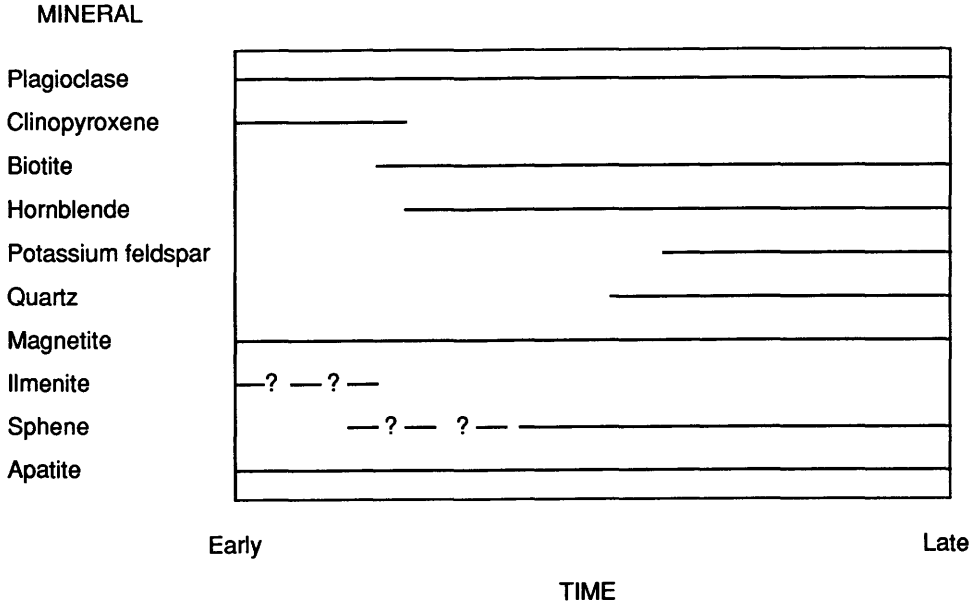

Figure 9. Sequence of mineral crystallization in Alta stock. Relative ages of crystallization based on textural relations among minerals. Queried segments indicate uncertain timing.

These calculations are subject to large errors resulting from uncertainties in estimates of temperatures, pressures, and activities of biotite and potassium feldspar. Temperature uncertainties of ±50 °C result in oxygen-fugacity uncertainties of ±0.7 log units. Uncertainties in other parameters lead to smaller uncertainties, but oxygen-fugacity estimates are probably no better than ± 1 log unit.

The effects of $P_{H_2O}<P_{total}$ (water-undersaturated magma) were estimated using Burnham's (1979b) water-silicate melt model assuming 3 percent H_2O in the melt. Water undersaturation reduces calculated f_{O_2} values by 0.5 to 0.7 log units. If core compositions of biotite represent crystallization under $P_{H_2O}<P_{total}$ conditions, and if rim compositions represent crystallization at $P_{H_2O}=P_{total}$, then compositionally zoned crystals suggest slight increases in the oxidation state during crystallization. The increases in oxidation state are similar in magnitude to those calculated by Candela (1986) but are considerably smaller than the increases suggested by Czamanske and Wones (1973). There is no indication of an increase in oxygen fugacity during crystallization, even in strongly zoned crystals.

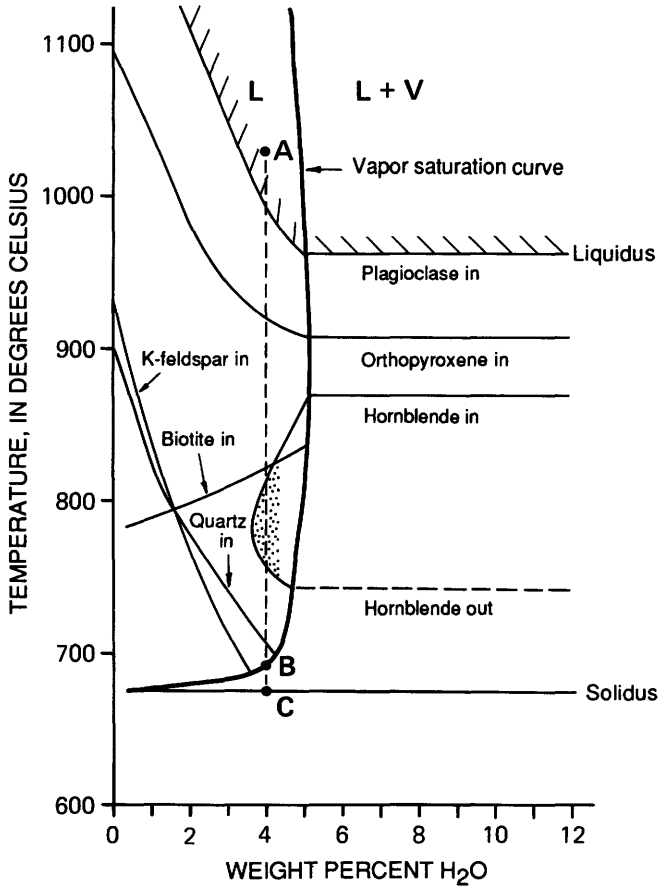

Figure 10. Temperature plotted vs. weight percent H_2O at 2 kbars total pressure, showing phase relations for a synthetic granodiorite composition (modified from fig. 4 of Naney, 1983). Stippled field shows range of H_2O contents where biotite will crystallize before hornblende and possible range of H_2O contents for Alta stock. Points A, B, and C portray possible crystallization path described in text. Abbreviations; L, liquid; V, vapor.

Amphibole Compositions

Amphibole in the Alta stock shows a wide range of textures, compositions, and compositional zoning. Compositions span the range from magnesio-hornblende to actinolite (table 4; Leake, 1978). Most amphibole in the Alta stock is compositionally similar to amphibole in other intrusions in the Wasatch Mountains (Aiken, 1982; Nash, 1982; D.A. John, unpub. data, 1990). Amphibole phenocrysts in the Alta stock are not replaced by fibrous, fine-grained actinolitic amphibole and do not contain pyroxene cores as they do in the Clayton Peak stock (Aiken, 1982). The amphibole phenocrysts have low Fe/(Fe+Mg) ratios and low total Al, Ti, Na, and K concentrations compared with primary amphibole in the Sierra Nevada batholith (Dodge and others, 1968; Ague and Brimhall, 1988), the California Coast Ranges (Dodge and Ross, 1971), Japanese granitoids (Czamanske and others, 1981), the Fish Canyon Tuff (Whitney and Stormer, 1985; Johnson and Rutherford, 1989a), and most other "igneous" amphibole (Leake, 1968; Helz, 1982).

Most analyzed amphibole crystals in the Alta stock contain two types of compositional zoning: (1) overall core to rim zoning, and (2) irregular patchy zoning. In general, neither type of zoning is optically discernible except as vague changes in pleochroism. However, patchy compositional zoning is readily apparent in backscattered SEM images (fig. 15).

Patchy compositional zoning is present in most samples and is similar to zoning in amphibole described by Czamanske and Wones (1973), Chivas (1981), and Hendry and others (1985). This zoning consists of small domains that are highly enriched in Al, Fe, Ti, Na, and K and depleted in Si, Mg, Mn, and Ca relative to adjacent domains. These domains appear to be discontinuous and are not obviously related to concentric growth zones, mineral inclusions, or any alteration visible under the microscope (fig. 15). Domains within single crystals may vary by as much as 0.7 Si atoms per unit cell (23 oxygens). Despite the complex distribution of compositional domains, overall compositional trends are well defined, as shown in figure 16, where variations of major elements are plotted against silicon atoms per unit cell. Regular increases in Mg, Mn, and Ca and decreases in Fe, Al^{VI}, Ti, Na, and K are apparent with increasing Si. The compositional trends are similar to trends observed by Chivas (1981) for the Inamumu zoned pluton,

Guadalcanal, Solomon Islands, and by Hendry and others (1985) for the Christmas intrusive complex, Arizona. The apparent compositional gap between 7.2 and 7.3 Si atoms per unit cell reported by Chivas (1981) as a possible break between igneous and subsolidus amphibole is not present in the Alta stock, and vein amphibole falls on both sides of this previously reported "break."

Most analyzed crystals also show overall core to rim zoning, with Al^{IV}, Fe/(Fe+Mg), Ti, Na, and K decreasing and Si, Mg, Mn, and Ca increasing from core to rim (table 4). However, rims in four samples show opposite trends, although the variation in Fe/(Fe+Mg) is not nearly as extreme as in biotite that shows this reverse type of zonation (table 3). Iron-enrichment trends are only found in samples located along the margin of the stock, although only one of these samples contains biotite showing the same trend (sample 83-PC-253).

Hydrothermal amphibole from early hornblende+K-feldspar+quartz+sphene veins was analyzed in two samples. The amphibole ranges from actinolitic hornblende to actinolite (fig. 16) and is compositionally inhomogeneous. These samples span the range of compositions found in amphibole phenocrysts from the same sample, and in sample 83-PC-253 they show the same Fe-enrichment trend from core to rim as shown by amphibole phenocrysts (table 4).

Interpretation of Compositional Zoning in Amphibole

Complex patchy zoning in amphibole similar to zoning found in the Alta stock has been interpreted by Czamanske and Wones (1973), Chivas (1981), and Hendry and others (1985) as the result of fluctuating oxygen fugacity during both igneous and hydrothermal crystallization. Chivas (1981) notes that the smooth compositional variations and overall variations between textural types in the Inamumu zoned pluton are consistent with fluctuating but generally increasing oxygen fugacity from early magmatic through late magmatic to early hydrothermal crystallization. He also correlates high f_{O_2} domains (Si-, Mg-, and Ca-rich) with periods of fluid exsolution and suggests that Fe, Ti, Na, K, and Cl are partitioned into the fluid phase in preference to the amphibole. In contrast, for amphibole in "barren" intrusions, Chivas notes that there is little evidence for the former presence of a fluid phase, and that the amphibole either shows Fe-enrichment with increasing Si or shows very irregular compositional trends. Mason (1978) also suggests that Mg-enrichment of amphibole rims is the result of increasing oxygen fugacity during crystallization.

Overall compositional trends of amphibole in the Alta stock suggest both falling temperature and increas-

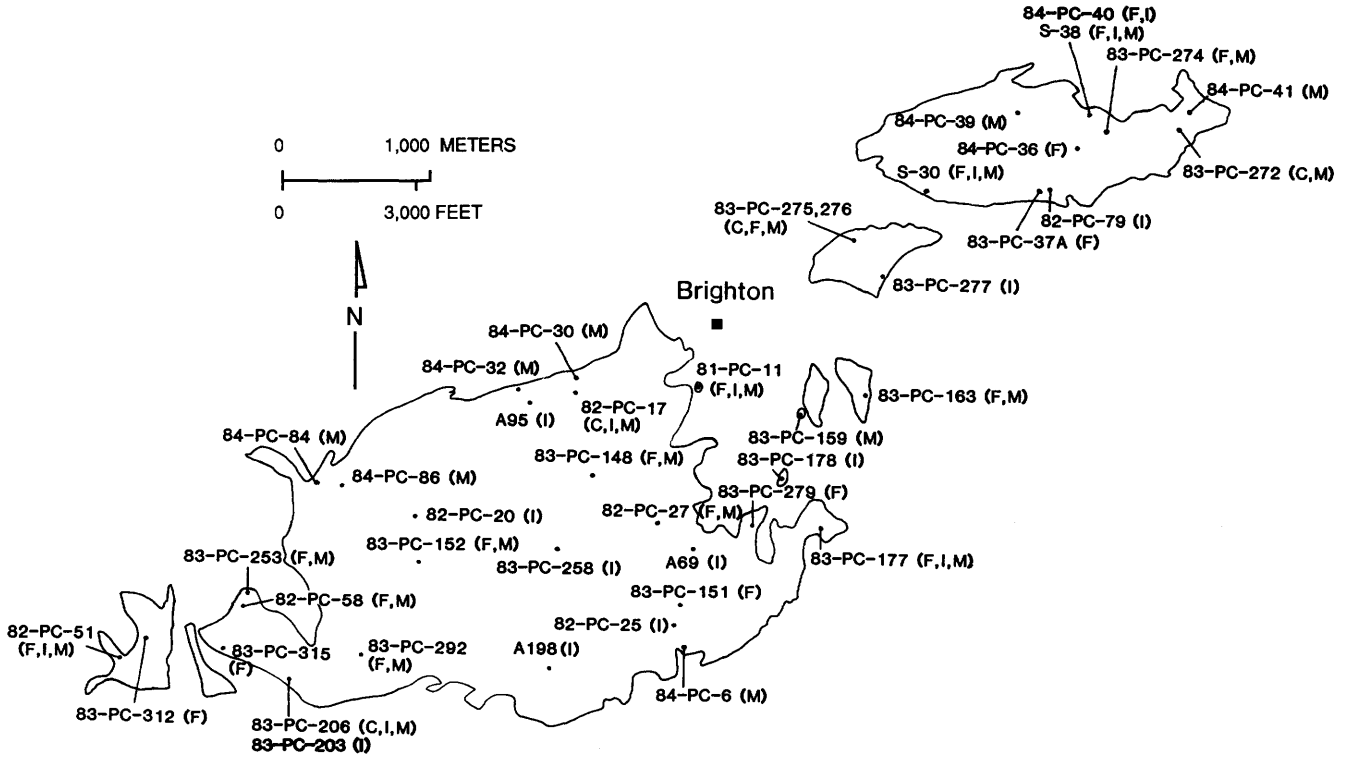

Figure 11. Locations of Alta stock samples used in chemical analyses (C) and in microprobe (M), stable-isotope (I), and fluid-inclusion (F) studies. See figure 3 for location.

Table 3. Representative microprobe analyses of biotite in the Alta stock

[n.a., not analyzed]

Sample Spot[1]	83-PC-276 6A (core)	83-PC-276 7A (rim)	83-PC-276 3 (shred)	83-PC-276 2A (vein)	83-PC-253 4 (inc)	83-PC-253 1 (core)	83-PC-253 2 (rim)	S-30 1A (core)	S-30 2A (rim)	83-PC-148 4 (pheno)	83-PC-148 1 (vein)
SiO_2	36.78	37.96	38.35	38.48	36.45	37.10	36.98	36.74	37.24	37.17	38.26
Al_2O_3	14.08	13.79	13.58	14.57	15.57	14.48	14.52	14.04	14.17	14.63	14.44
FeO*	15.83	15.30	15.60	15.30	17.70	16.07	18.89	17.11	16.25	16.90	16.96
MgO	13.99	14.79	15.10	14.11	11.72	14.04	11.60	13.46	13.71	13.49	14.16
MnO	.23	.22	.31	.29	.38	.30	.34	.32	.24	.40	.44
TiO_2	4.19	3.50	3.20	2.93	4.09	3.80	3.86	4.16	3.66	3.89	2.36
K_2O	8.97	9.29	9.41	9.38	9.52	9.42	9.28	8.95	8.93	9.62	9.10
Na_2O	.11	.07	.07	.07	.07	.11	.08	.11	.10	.11	.10
CaO	.00	.01	.01	.02	.11	.01	.02	.01	.03	.02	.04
BaO	1.00	.07	.08	.03	.72	.26	.19	1.04	.82	n.a.	n.a.
F	.71	1.05	.85	.91	.45	.60	.43	.47	.55	.59	.63
Cl	.15	.06	.15	.05	.14	.08	.06	.17	.16	.11	.08
Total	96.04	96.11	96.71	96.14	96.92	96.27	96.25	96.58	95.86	96.93	96.57
Total (–O =F+Cl)	95.71	95.65	96.32	95.75	96.70	96.00	96.06	96.34	95.59	96.66	96.29
Structural formula based on 11 oxygens											
Si	2.760	2.815	2.833	2.845	2.735	2.769	2.793	2.761	2.797	2.763	2.838
Al^{IV}	1.240	1.185	1.167	1.155	1.265	1.231	1.207	1.239	1.203	1.237	1.162
Al^{VI}	.006	.021	.016	.115	.112	.043	.086	.005	.052	.045	.101
Fe	.994	.949	.964	.946	1.111	1.003	1.193	1.075	1.021	1.051	1.052
Mg	1.565	1.634	1.662	1.555	1.311	1.562	1.306	1.507	1.535	1.495	1.565
Mn	.015	.014	.019	.018	.024	.019	.022	.020	.015	.025	.028
Ti	.237	.195	.178	.163	.231	.213	.219	.235	.207	.218	.132
Sum VI	2.817	2.813	2.839	2.797	2.789	2.840	2.826	2.842	2.830	2.834	2.878
K	.859	.879	.887	.885	.911	.897	.894	.858	.856	.912	.861
Na	.016	.010	.010	.010	.010	.016	.012	.016	.015	.016	.014
Ca	.000	.001	.001	.002	.009	.001	.002	.001	.002	.002	.003
Ba	.033	.002	.003	.001	.024	.008	.006	.034	.027		
F	.169	.246	.199	.213	.107	.142	.103	.112	.131	.139	.148
Cl	.019	.008	.019	.006	.018	.010	.008	.022	.020	.014	.010
Fe/(Fe+Mg)	.388	.367	.367	.378	.459	.391	.477	.416	.399	.413	.402
Biotite temp(°C)[2]	791	731	692	669	736	744	690	755	726	735	574

* Total Fe as FeO

[1]Core=core of biotite phenocryst; rim=rim of biotite phenocryst; pheno=average of entire phenocryst; inc=biotite inclusion in plagioclase phenocryst; shred=shreddy, hydrothermal biotite; vein=hydrothermal vein-filling biotite

[2]Biotite temperature calculated from Dilles (1987)

Table 4. Representative microprobe analyses of amphibole in the Alta stock

Sample	83-PC-272	83-PC-272	84-PC-86	84-PC-86	84-PC-86	83-PC-253	83-PC-253	83-PC-253	83-PC-253	82-PC-27	82-PC-27	82-PC-27	82-PC-27
Spot[1]	3 (core)	4 (rim)	1 (core)	2 (rim)	3 (inc)	4 (core)	5 (rim)	2 (vein)	3 (vein-rim)	1 (inc)	2 (inc)	3 (core)	4 (rim)
SiO_2	49.77	50.31	48.00	50.00	46.57	50.50	50.29	51.25	49.89	43.45	50.07	50.72	51.48
Al_2O_3	5.36	5.09	6.89	5.41	7.73	4.98	5.04	4.58	5.44	9.47	5.10	5.07	4.64
FeO*	11.00	10.75	13.53	13.01	14.30	11.73	11.95	11.84	12.96	16.36	13.67	11.99	11.67
MgO	16.52	16.74	14.40	15.09	13.58	15.90	15.77	16.08	15.19	11.73	14.60	16.07	16.38
MnO	.53	.51	.60	.60	.59	.57	.54	.32	.40	.55	.64	.70	.68
TiO_2	1.23	1.16	1.28	.87	1.35	.72	.72	.54	.69	1.68	.83	.78	.59
CaO	12.01	11.85	12.04	12.21	12.01	12.25	12.23	12.49	12.28	12.00	12.61	12.34	12.40
Na_2O	1.24	1.21	1.18	.90	1.25	.97	.93	.86	.96	1.37	.69	.91	.82
K_2O	.53	.50	.64	.47	.77	.39	.42	.38	.45	1.15	.41	.44	.37
F	.46	.52	.25	.25	.28	.31	.32	.35	.33	.18	.21	.21	.21
Cl	.08	.07	.06	.05	.08	.03	.03	.02	.03	.15	.04	.05	.05
Total	98.73	98.71	98.87	98.86	98.51	98.35	98.24	98.71	98.62	98.09	98.87	99.28	99.29
Total (–O=F+Cl)	98.52	98.48	98.75	98.74	98.37	98.21	98.10	98.56	98.47	97.98	98.77	99.18	99.19
Structural formula based on 23 oxygens													
Si	7.139	7.196	6.973	7.212	6.839	7.272	7.259	7.341	7.207	6.552	7.245	7.249	7.332
Al^{IV}	.861	.804	1.027	.788	1.161	.728	.741	.659	.793	1.448	.755	.751	.668
Al^{VI}	.045	.054	.153	.132	.177	.117	.117	.114	.134	.235	.115	.103	.111
Fe	1.320	1.286	1.644	1.570	1.756	1.413	1.443	1.418	1.566	2.063	1.654	1.433	1.390
Mg	3.531	3.568	3.118	3.244	2.972	3.412	3.392	3.432	3.270	2.636	3.149	3.423	3.477
Mn	.064	.062	.074	.073	.073	.070	.066	.039	.049	.070	.078	.085	.082
Ti	.133	.125	.140	.094	.149	.078	.078	.058	.075	.191	.090	.084	.063
Sum VI	5.093	5.095	5.129	5.113	5.127	5.090	5.096	5.061	5.094	5.195	5.086	5.128	5.123
Ca	1.846	1.816	1.874	1.887	1.890	1.890	1.892	1.917	1.901	.939	1.955	1.890	1.892
Na	.345	.336	.332	.252	.356	.271	.260	.239	.269	.401	.194	.252	.226
K	.097	.091	.119	.086	.144	.072	.077	.069	.083	.220	.076	.080	.067
F	.209	.235	.115	.114	.130	.130	.146	.159	.151	.085	.096	.095	.095
Cl	.019	.017	.015	.020	.012	.007	.007	.005	.007	.038	.010	.012	.012
Fe/(Fe+Mg)	.345	.265	.345	.326	.371	.293	.298	.292	.324	.439	.345	.295	.286
Pressure (kbars)[2]	.42	.22	1.54	.47	2.18	.17	.22	-.13	.50	3.59	.27	.20	-.10

FeO*=All Fe as FeO

[1]Core=core of hornblende phenocryst; rim=rim of hornblende phenocryst; inc=small hornblende inclusion in plagioclase phenocryst; vein=vein amphibole; vein-rim=rim of amphibole crystal in vein

[2]Pressure calculated from total aluminum content using equation of Johnson and Rutherford (1989b)

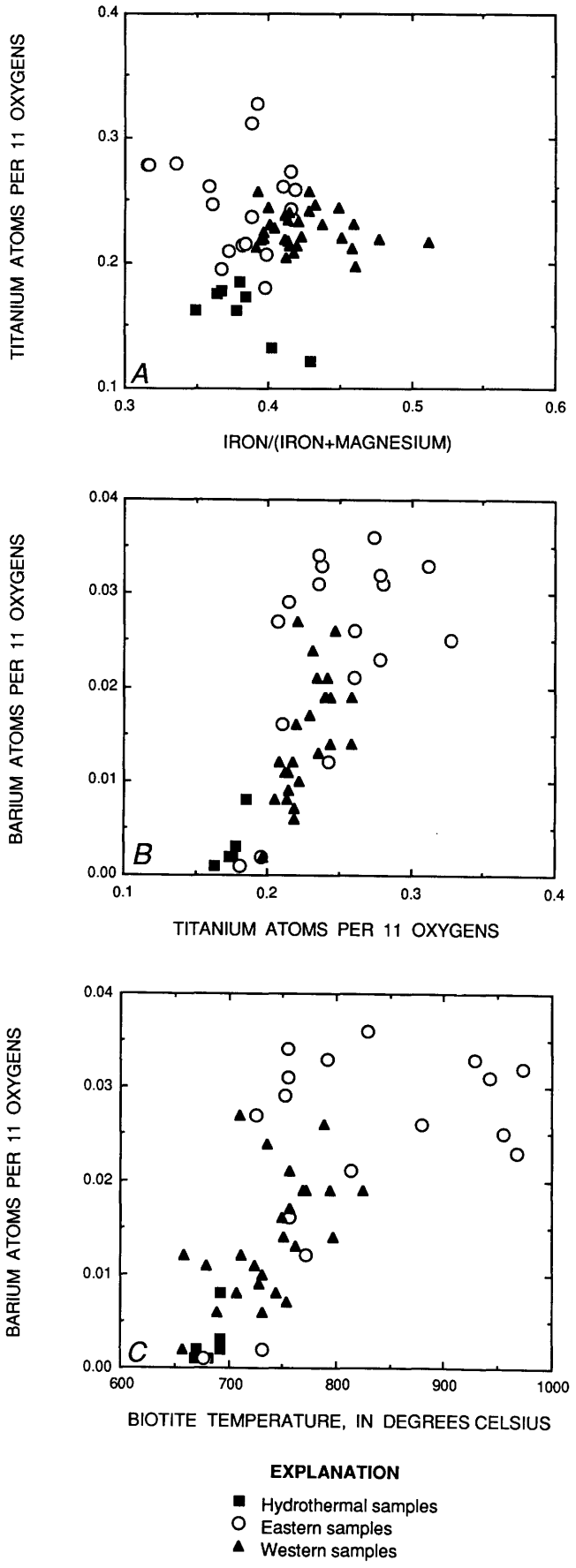

ing oxidation state during progressive crystallization. The strong positive correlation between Al^{IV}, Ti, Na, and K contents and their depletion from core to rim and from inclusions to phenocrysts is consistent with decreasing temperature during crystallization (Helz, 1982). However, decreasing Fe/(Fe+Mg) ratio with decreasing temperature is the opposite trend expected from experimental studies and suggests an increase in the oxidation state during crystallization (Helz, 1982). Decreasing Ti also is consistent with an increase in the oxidation state (Helz, 1982). The magnitude of the change in the oxidation state is indeterminable, however.

The compositional overlap between hydrothermal amphibole and amphibole phenocrysts and the lack of obvious signs of recrystallization or replacement of early amphibole by more siliceous, late amphibole suggest that at least some of the more siliceous amphibole phenocrysts crystallized in the presence of a hydrothermal, possibly magmatic(?) fluid. The presence of K-feldspar, sphene, and, locally, magnetite in hornblende veins suggests that early hydrothermal fluids had high K, Na, Ti, Al, and Fe contents, and that these elements could have been partitioned into minerals other than amphibole. Alternatively, amphibole with higher Fe, Al, Ti, Na, and K contents may not be stable under subsolidus conditions.

In summary, amphibole compositional trends are complex but generally suggest increasing oxidation state with decreasing temperature. It is not obvious, however, when the interaction of the Alta stock with an aqueous phase began, and the magnitude of the change in oxidation state is unknown. The origin of patchy compositional zoning in amphibole remains poorly understood.

Hornblende Geobarometry

Recent empirical (Hammarstrom and Zen, 1986; Hollister and others, 1987) and experimental (Johnson and Rutherford, 1989b) studies show that the aluminum content of hornblende in granitic magma varies linearly with pressure of crystallization. Thus, the aluminum content of hornblende can be used as a geobarometer in

◀ **Figure 12.** Biotite compositions in Alta stock based on electron-microprobe analyses. Eastern and western samples separated by approximate depth of crystallization: eastern samples, ≤5.2 km; western samples, >5.2 km. *A*, Ti atoms per 11 oxygens vs. Fe/(Fe+Mg). Note that hydrothermal biotite has considerably lower Ti contents than igneous biotite. *B*, Ba atoms per 11 oxygens vs. Ti atoms per 11 oxygens. *C*, Ba atoms per 11 oxygens vs. calculated biotite equilibration temperature. Note that Ba content decreases with decreasing temperature. See text for description of calculation of biotite temperature.

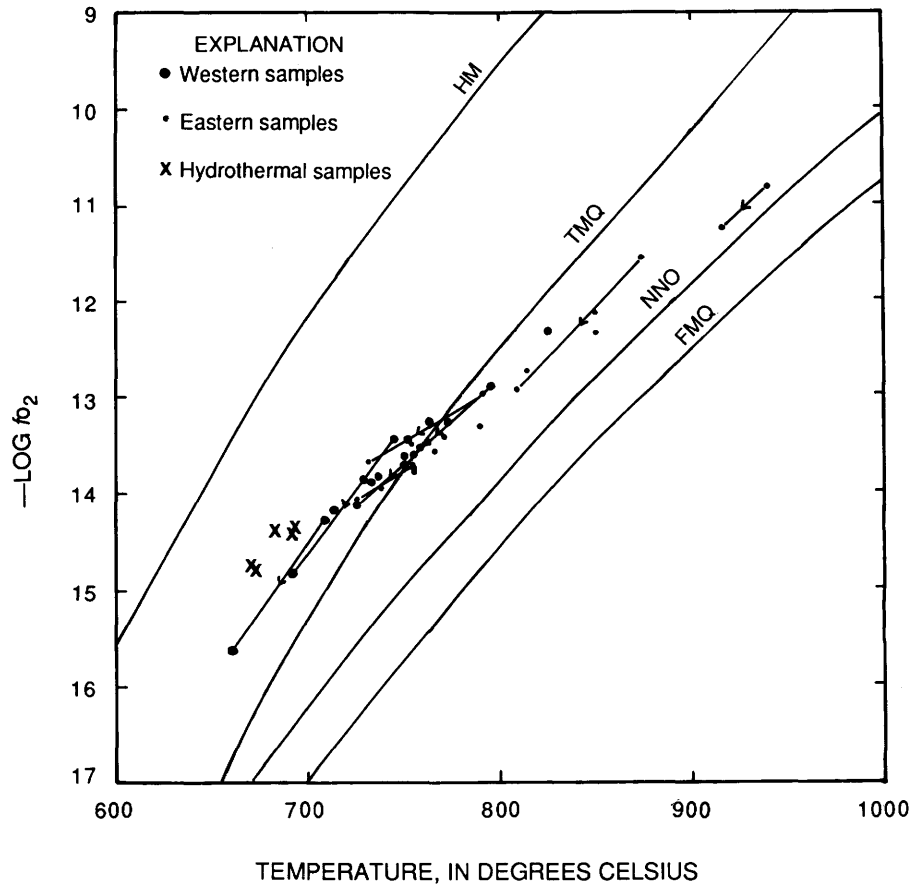

Figure 13. Calculated temperature plotted vs. estimated log oxygen fugacity (f_{O_2}) for biotite from Alta stock. See text for methods of calculation. Tie lines connect zoned crystals; arrows point to rims. Eastern and western samples separated by approximate depth of crystallization: eastern samples, ≤5.2 km; western samples, >5.2 km. HM and FMQ are, respectively, the hematite-magnetite and fayalite-magnetite-quartz oxygen buffer curves from Chou (1978), NNO is the nickel-nickel oxide buffer curve of Huebner and Sato (1970), and TMQ is titanite-magnetite-quartz buffer curve of Wones (1989) calculated at 1,400 bars. TMQ equilibria are adjusted for clinopyroxene compositions of Alta stock.

rocks where hornblende crystallizes with quartz, plagioclase, K-feldspar, biotite, magnetite, and sphene or ilmenite, as is common during the later stages of crystallization of granodiorite and tonalite magma. Data used in calibration of the hornblende geobarometers are for pressures between 2 to 8 kbars, and Johnson and Rutherford (1989b) and Hollister and others (1987) suggest errors in pressure estimates of ±0.5 and ±1.0 kbar, respectively, for pressures between 2 and 8 kbars. The three equations of the hornblende geobarometer diverge at high pressures (>5 kbars) but yield nearly identical results at low pressures (2 kbars).

The hornblende geobarometers were applied to hornblende crystals in the Alta stock using aluminum contents estimated from electron-microprobe analysis (table 4). Pressures estimated using the experimentally derived equation of Johnson and Rutherford (1989b) range from 4.1 kbars to negative values; most pressure estimates are ≤1.0 kbar (table 4). Many samples yield >2 kbars ranges in pressure estimates between adjacent domains within single crystals. Pressures estimated using hornblende rim compositions, which should yield the most accurate estimates of pressure, range from 3.3 kbars to negative values; most are ≤0.5 kbar. Pressures estimated using the equations of Hammarstrom and Zen (1986) and Hollister and others (1987) are similarly low and variable.

The hornblende geobarometer does not appear to yield reasonable estimates of the pressure of crystallization of the Alta stock. Based on pressures estimated from regional field relations, contact-metamorphic mineral assemblages in wall rocks of the Alta stock, and fluid-inclusion data, final pressures of crystallization of the Alta stock varied from about 1.7 kbars on the west

side of the stock to 1.0 kbar on the east side of the stock (John, 1987, 1989). These values are thought to be accurate within ±0.5 kbar and are more reasonable than the highly variable or negative pressures estimated for many samples using the hornblende geobarometer.

There are several possible reasons for the failure of the hornblende geobarometer in the Alta stock, including (1) lack of calibration of the geobarometer at low pressures (<2 kbars); (2) partial reequilibration of hornblende phenocrysts at low pressures and (or) low temperatures; or (3) the effects of other variables, such as vapor saturation, on composition of hornblende crystallizing at low pressures. Most hornblende phenocrysts in the Alta stock contain numerous systematic compositional variations that appear coupled to variations in aluminum content (that is, increasing Fe, Ti, Na, and K contents, and decreasing Si, Ca, and Mn contents with increasing Al; see fig. 16). Thus, it is unlikely that low-temperature or low-pressure reequilibration of aluminum content has taken place and is the cause of the low and highly variable pressure estimates for the Alta stock (see also Hammarstrom and Zen, 1986). It is more likely that a combination of low-pressure crystallization of the magma, at least partially during vapor-saturated conditions, and the lack of calibration of the hornblende geobarometer at low pressures leads to the poor results given by the hornblende geobarometer in the Alta stock.

STABLE-ISOTOPE STUDIES

Reconnaissance studies of hydrogen- and oxygen-isotope compositions of minerals in the Alta stock were made to assess the possible role of meteoric water in the evolution of the hydrothermal system. Mineral separates from 16 samples representing several types of alteration and spread throughout the stock were analyzed for oxygen and (or) hydrogen isotopes. Sample locations are given in figure 11.

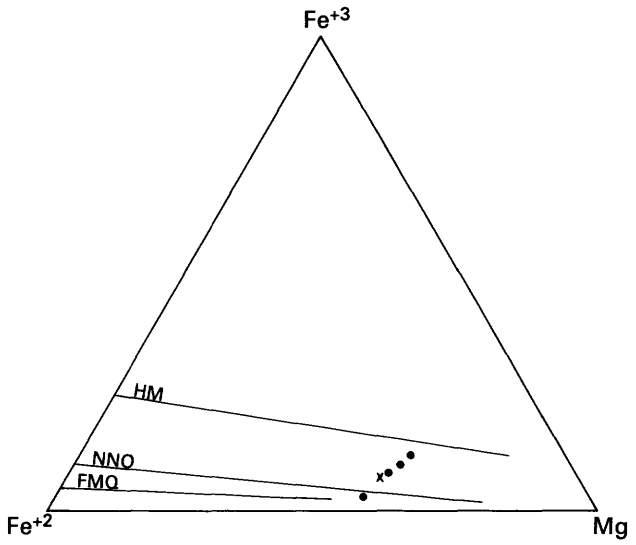

Figure 14. Fe^{+2}-Fe^{+3}-Mg (mole ratios) in biotite from Alta stock. HM, NNO, and FMQ oxygen buffer curves (defined in fig. 13 legend) from Wones and Eugster (1965). X, analysis from Wilson (1961).

Methods

Isotopic analyses of hydrogen and (or) oxygen were made on mineral separates using standard techniques for extraction of hydrogen and oxygen (Bigeleisen and others, 1952; Clayton and Mayeda, 1963; Borthwick and Harmon, 1982). Water contents of hydrous minerals were measured by a manometer during extraction of hydrogen gas. Isotopic compositions of prepared gasses were measured using gas ratio mass spectrometers and are reported in standard delta notation relative to standard mean ocean water (SMOW). Analytical precision is 0.1–0.2 permil for $\delta^{18}O$ and approximately 1 permil for δD.

Results

Results of the isotopic analyses gathered in this study are presented in table 5, along with previous analyses reported by Taylor (1968). Oxygen-isotope compositions of primary quartz and primary K-feldspar show rather restricted ranges of $\delta^{18}O$ from +8.3 to +9.7 and +7.3 to +8.0 permil, respectively. Fractionation between quartz and K-feldspar is normal (>1 permil) in six of the seven samples, suggesting isotopic equilibrium. Whole-rock $\delta^{18}O$ values measured by Taylor (1968) are between the quartz and K-feldspar values (+8.0 and +8.4 permil) and somewhat higher than the +6.5 to +7.5 permil values reported by Kemp and Bowman (1984). These data suggest that the primary whole-rock oxygen-isotope composition of the Alta stock is about +7 to +8 permil. Two samples of hydrothermal vein quartz yielded $\delta^{18}O$ values of +9.5 and +11.5 permil (samples 83-PC-203 and 84-PC-40, table 5).

Quartz–K-feldspar pairs having normal oxygen-isotope fractionation are used with the equations of Bottinga and Javoy (1973, 1975) to calculate temperatures of isotopic equilibration (table 5). These temperatures range from 407 °C to about 560 °C. Oxygen-isotope fractionations involving other minerals in one sample (A95, table 5) also suggest equilibration temperatures near 500 °C (Bottinga and Javoy, 1975). Quartz in one sample (82-PC-79) is relatively depleted (+8.3 permil), whereas K-feldspar is isotopically similar to other samples (+7.7). The reason for the depletion in this quartz is unknown.

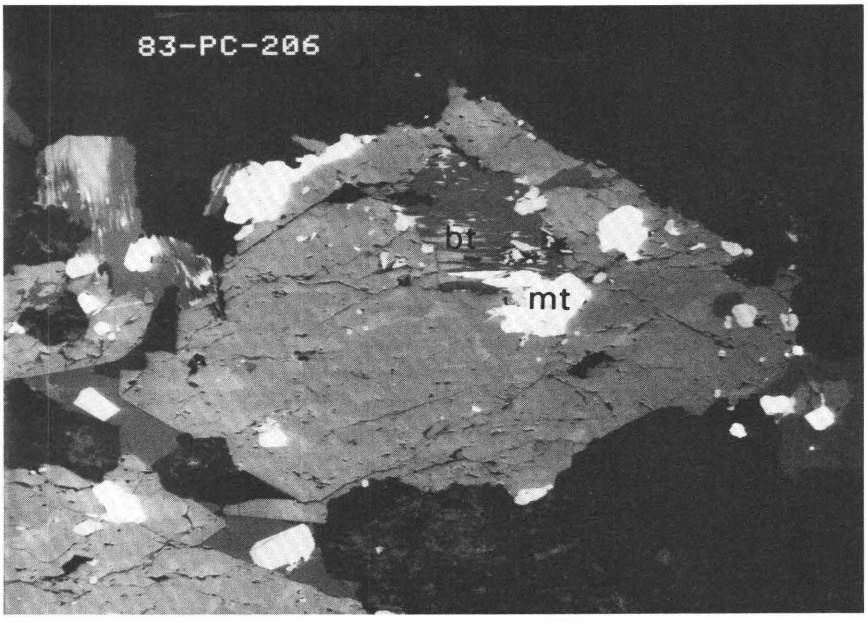

A

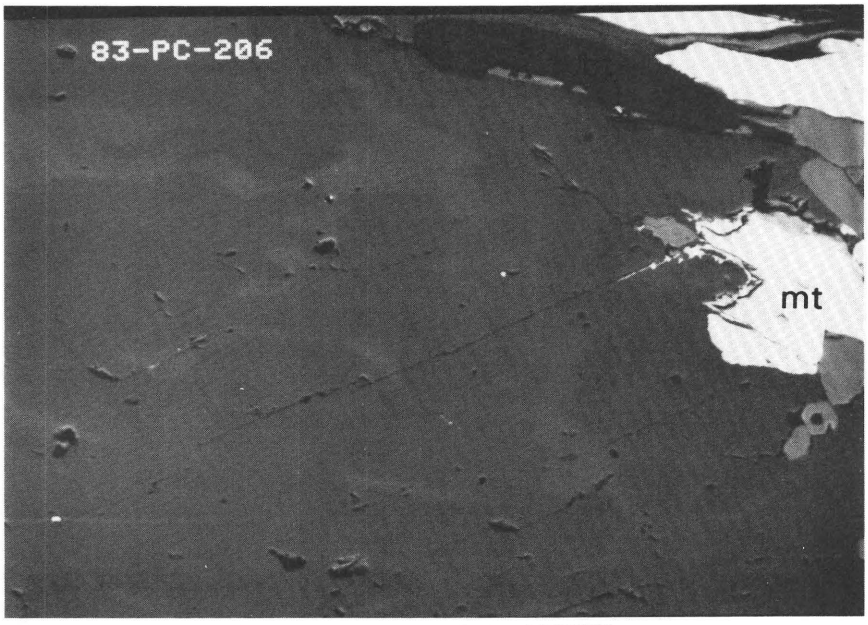

B

Figure 15. Backscattered SEM images of hornblende phenocrysts in Alta stock (sample 83-PC-206), showing patchy compositional zoning. *A*, Subhedral hornblende phenocryst containing small, partially chloritized biotite inclusion (bt) and magnetite inclusions (mt). Patchy compositional zoning shown by slight variations in brightness; lighter colored areas contain higher concentrations of Fe, Al, Ti, K, and Na than darker areas that contain higher concentrations of Si, Mg, and Ca. *B*, Enlargement of *A* showing irregular compositional domains.

Hydrogen-isotope analyses of biotite and mixtures of biotite and chlorite have δD values ranging from –86 to –109 permil. These values are relatively light compared with those of most igneous biotite (for example, see Nabelek and others, 1983; Brigham, 1984). There are no obvious relationships between δD and position in the stock, but δD generally increases with increasing amounts of structurally bound water in partially chloritized samples (fig. 17).

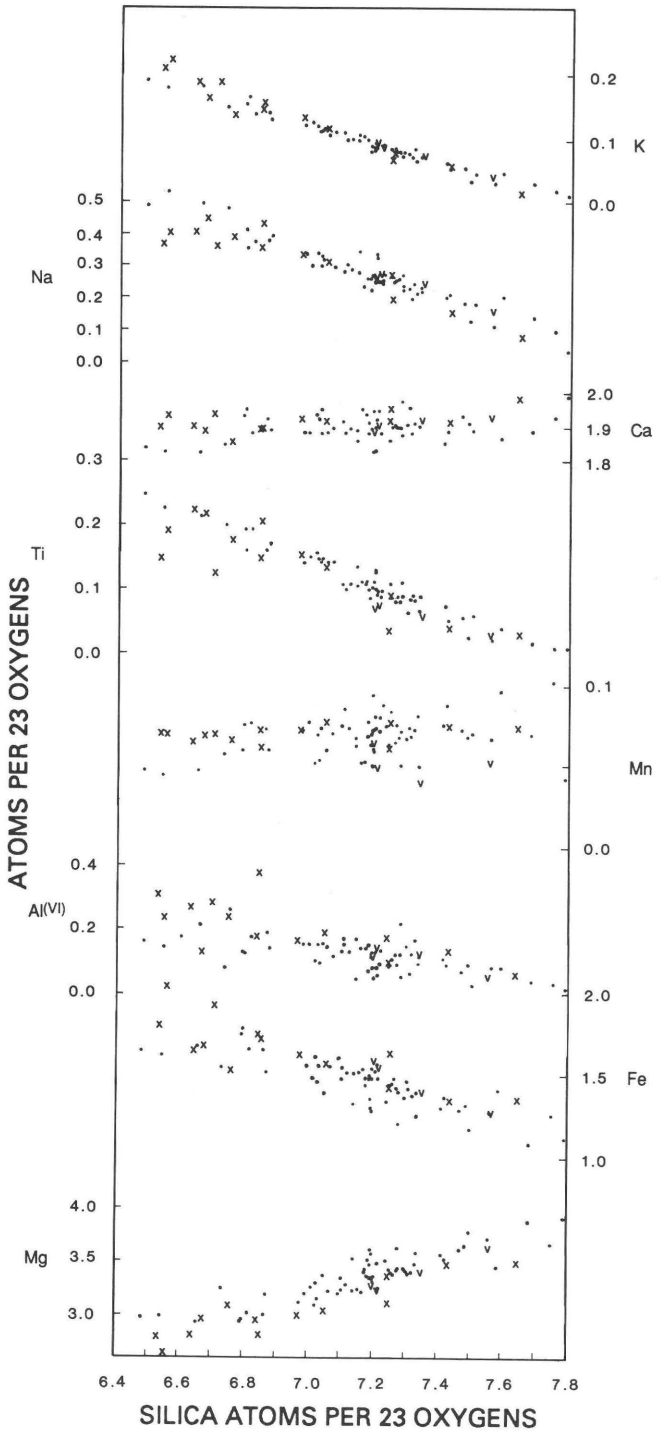

Figure 16. Variations of Al^{VI}, Mg, Fe, Ti, Ca, Mn, Na, and K with Si content (in atoms per 23 oxygens) in amphibole crystals from Alta stock. There are a total of 78 analyses from 25 samples. X, small amphibole inclusions in plagioclase phenocrysts; V, vein amphiboles.

Hydrogen-isotope analyses of three chlorite samples from two different parageneses (two samples of chloritized biotite phenocrysts and one sample of a type 6 vein) are nearly identical, with δD values of about –75 permil. These values are notably enriched in deuterium by 10 to 30 permil relative to fresh biotite. The increase in δD during chloritization is similar to the trend found in the Notch Peak stock by Nabelek and others (1983) and is opposite to the trends found in systems where meteoric-water interaction has been demonstrated (for example, Criss and Taylor, 1983) and to the trend reported for chloritization of biotite in the Little Cottonwood stock along the Wasatch fault zone (Bromley and others, 1985). Nabelek and others (1983) and Taylor (1988) have suggested that deuterium enrichment during chloritization indicates alteration resulting from subsolidus interaction of magmatic fluids in an essentially closed system.

Isotopic compositions of fluids in equilibrium with measured $\delta^{18}O$ and δD values of quartz, K-feldspar, and biotite at 500 °C and 700 °C were calculated using equations for water-mineral fractionations from Bottinga and Javoy (1973) and Suzuoki and Epstein (1976) (table 5). Calculated water compositions lie within the "magmatic-water" box of Taylor (1974) over the temperature range of 500–700 °C, although deteurium values straddle the low end of this range (fig. 18). The isotopic composition of hydrothermal fluids in equilibrium with sample 83-PC-203 at 500 °C, calculated from measured $\delta^{18}O$ and δD values for vein quartz and vein chlorite using equations of Bottinga and Javoy (1973) and Graham and others (1987), also lies within the magmatic-water box (fig. 18). Thus, calculated water compositions are consistent with the idea that isotopic reequilibration at 500 °C only involves waters that are compatible with magmatic origins.

Discussion

Oxygen-isotope fractionations between quartz and K-feldspar have values indicative of isotopic reequilibration at subsolidus temperatures (approximately 500 °C). Isotopic reequilibration at subsolidus temperatures is consistent with petrographic observations that suggest subsolidus processes (for example, unmixing of potassium feldspar and plagioclase, formation of myrmekite, and other forms of "deuteric alteration"), with feldspar equilibration temperatures of <500 °C estimated from the two-feldspar geothermometer (Whitney and Stormer,

Table 5. Oxygen and deuterium analyses of minerals and rocks in the Alta stock

Sample	Mineral	$\delta^{18}O$[1]	δD[1]	$\%H_2O$[2]	Temperature [3]
81-PC-11	Quartz	9.4,9.2			494
	K-feldspar	7.7,7.6			
	Biotite		-89	3.82	
S-38	Quartz	9.1,9.1			472
	K-feldspar	7.3,7.4			
	Biotite		-95	3.28	
82-PC-20	Quartz	9.2,9.1			559
	K-feldspar	7.9,7.6			
	Biotite		-102	3.28	
82-PC-17	Quartz	9.3			518
	K-feldspar	7.8,7.7			
	Biotite		-109	2.93	
82-PC-79	Quartz	8.3,8.3			
	K-feldspar	7.8,7.7			
	Biotite (+chlorite) [4]	4.1,4.1	-101	4.10	
S-30	Biotite		-89	3.82	
83-PC-177	Biotite (+chlorite)		-98	4.39	
83-PC-203	Quartz (vein)	9.5			
	Chlorite (vein)		-71	11.13	
83-PC-277	Chlorite (after biotite)		-76	10.57	
83-PC-178	Biotite (+chlorite)		-87	4.59	
82-PC-25	Biotite (+chlorite)		-100	3.91	
83-PC-258	Chlorite (after biotite)		-75	9.23	
82-PC-51	Biotite (+chlorite)		-86	5.05	
84-PC-81	Biotite		-100	2.81	
84-PC-54	Biotite		-105	3.19	
84-PC-40	Vein quartz	11.5			
[5]A95	Quartz	9.7			482
	K-feldspar	8.0			
	Andesine	7.3			
	Hornblende	5.5			
	Biotite	4.3			
[5]A69	Groundmass	7.0			
[5]A58	Quartz	8.9			
	Whole rock	8.0			
[5]A198AP1	Quartz	9.7			
	Whole rock	8.4			
[5]A198AP2	Quartz	9.6			407
	K-feldspar	7.5			

[1]Parts permil ($^{o}/_{oo}$) relative to standard mean ocean water (SMOW)
[2]Water contents of biotite and chlorite directly measured during extraction of water for deuterium analysis
[3]Oxygen-isotope equilibration temperatures, in degree Celsius (°C), for quartz–K-feldspar pairs calculated from Bottinga and Javoy (1973)
[4]Impure mineral separates containing variable but generally small amounts of chlorite as reflected by the water yields
[5]Samples from Taylor (1968)

1977; Brown and Parsons, 1981), and with fluid-inclusion data that indicate the widespread presence of hydrothermal fluids at these temperatures (see the section on fluid-inclusion studies below).

Calculated water compositions and measured δD values for chlorite and $\delta^{18}O$ values for hydrothermal quartz suggest that there has been little interaction of meteoric water with the Alta stock, despite pervasive subsolidus alteration and isotopic reequilibration. Present-day meteoric waters in the Wasatch Mountains are quite light ($\delta^{18}O$=–17.5, δD=–130 permil; Bromley and others, 1985) and probably also were quite light in the early Oligocene [J.R. O'Neil, oral commun., 1985; see also Bowman and others (1987) for meteoric-water values from the nearby Bingham porphyry copper deposit]. If chloritization were the result of the introduction of meteoric water, chlorite should be strongly depleted in deuterium (fig. 17). Also, quartz veins should be strongly depleted in $\delta^{18}O$ (calculated $\delta^{18}O_{quartz}$=–14.3 permil at 500 °C; Bottinga and Javoy, 1973). Thus, the stable-isotope data are compatible with an essentially closed-system deuteric alteration that has not been modified by the influx of large volumes of meteoric ground water.

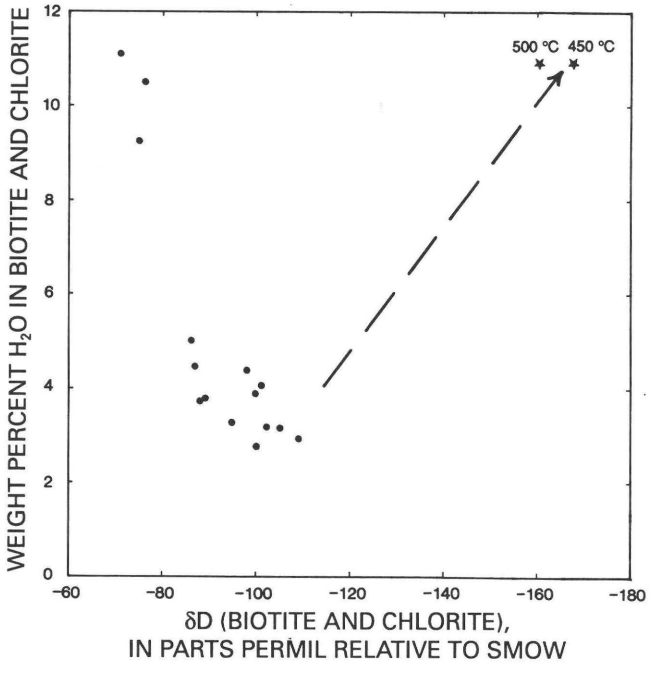

Figure 17. δD plotted vs. water contents of biotite and chlorite in Alta stock. High water contents of most biotite are result of partial chloritization of biotite. Trend expected from progressive chloritization with meteoric waters (for example, see Criss and Taylor, 1983) is shown as dashed line. Stars, approximate compositions of chlorite formed from meteoric water calculated at 450 °C and 500 °C using present-day meteoric-water composition (Bromley and others, 1985) and equation of Suzuoki and Epstein (1976). SMOW, standard mean ocean water.

FLUID-INCLUSION STUDIES

Scope and Types of Materials Studied

Fluid inclusions were studied both to look for direct evidence of fluids trapped at magmatic temperatures and to characterize distribution and temporal development of hydrothermal fluids. Fluid inclusions were studied petrographically in about 150 samples of the stock and of veins cutting the stock, and heating and freezing experiments were conducted on approximately 1,735 fluid inclusions in 22 samples (appendix 1). Reconnaissance crushing experiments were made on samples used in the heating and freezing studies. Daughter minerals in opened inclusions in igneous quartz were examined by SEM methods in sample S-38. Because the ages of fluid

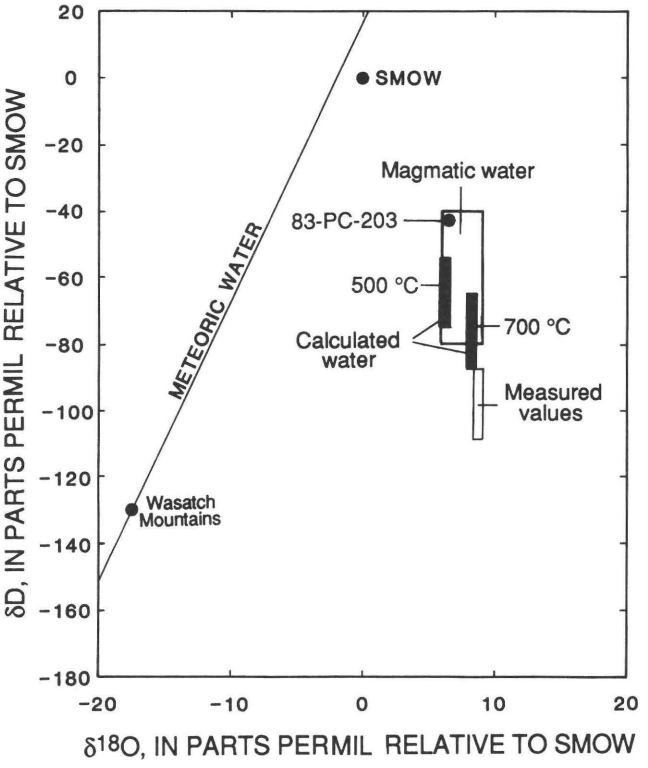

Figure 18. $\delta^{18}O$ and δD relations for Alta stock. Measured and estimated whole-rock values (using estimated whole-rock $\delta^{18}O$ values and biotite δD values) are shown along with calculated compositions of waters in equilibrium with whole-rock values at 500 °C and 700 °C. Water compositions are calculated from equations in Bottinga and Javoy (1973) and Suzuoki and Epstein (1976). Composition of water in equilibrium with sample 83-PC-203 at 500 °C is calculated from measured $\delta^{18}O$ and δD values for vein quartz and chlorite, respectively, and equations in Bottinga and Javoy (1973) and Graham and others (1987). Magmatic-water box is from Taylor (1974). Meteoric-water line from Craig (1961). Values for present-day meteoric water in Wasatch Mountains from Bromley and others (1985). SMOW, standard mean ocean water.

inclusions relative to one another were ambiguous in most samples, fluid inclusions were studied in 14 samples containing both igneous and hydrothermal quartz. The seven other samples were of igneous rock that did not have veins near the sample. Heating and freezing data were collected on all major types of veins except types 2 and 7, but owing to the paucity of veins, generally only one vein type and its host rock were studied from a single outcrop. Sample localities are shown in figure 11. Experimental methods for heating and freezing experiments were given by John (1989).

Petrographic Characteristics of Fluid Inclusions in the Alta Stock

Based on room-temperature phase relations, four types of fluid inclusions are distinguished in the Alta stock: type 1, liquid rich; type 2, vapor rich; type 3, high salinity; and type 4, mixed H_2O-CO_2 (fig. 19).

Type 1 fluid inclusions contain liquid plus vapor at room temperature (fig. 19*A*). Vapor contents range from <5 to about 30 volume percent. Crushing experiments indicate that small amounts of CO_2 are present in some of the vapor bubbles. Small birefringent and (or) opaque daughter(?) crystals occasionally are present in type 1 fluid inclusions.

Type 2 fluid inclusions contain a large vapor bubble and smaller amounts of liquid (fig. 19*A*, *B*). Vapor contents generally are >60 volume percent. Crushing experiments suggest that CO_2 probably is the main component in many vapor bubbles. Type 2 fluid inclusions are relatively uncommon.

Type 3 fluid inclusions contain liquid plus vapor plus halite at room temperature (fig. 19*B*, *C*). Vapor contents tend to be small (<20 volume percent). Other birefringent and opaque daughter minerals, including hematite and calcite, are present locally, and sylvite is identified in one sample. Type 3 fluid inclusions are subdivided into three types (3a, 3b, and 3c) based on their homogenization behavior and the presence or absence of sylvite. In type 3a fluid inclusions halite dissolves at temperatures lower than liquid-vapor homogenization, whereas in type 3b fluid inclusions halite dissolution takes place at temperatures greater than liquid-vapor homogenization. Type 3c fluid inclusions contain daughter crystals of sylvite in addition to halite.

Type 4 fluid inclusions are uncommon and have only been identified in two samples. At room temperature, these inclusions have three phases: CO_2 vapor, CO_2 liquid, and H_2O-rich liquid. The volume percent of CO_2 varies from about 20 to 35 percent, corresponding to about 5 to 10 mole percent CO_2 (Burruss, 1981).

Attempts were made to classify fluid inclusions in a temporal sense as primary, secondary, or pseudosec-

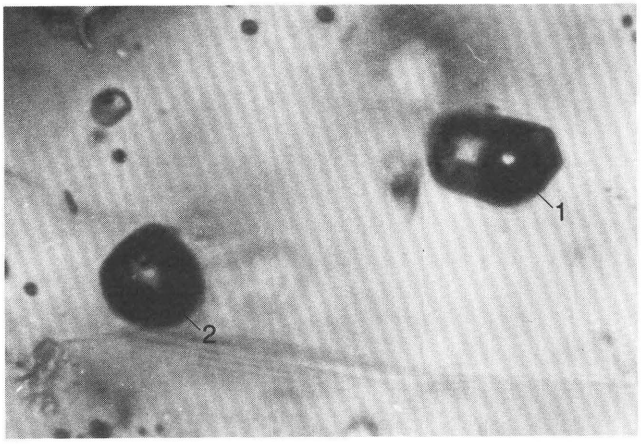

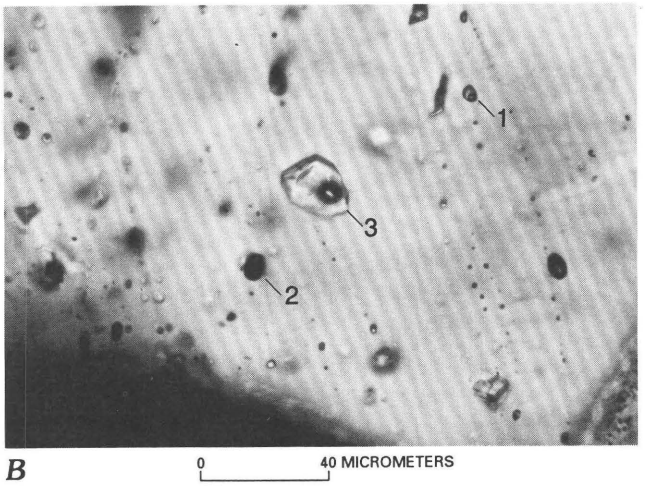

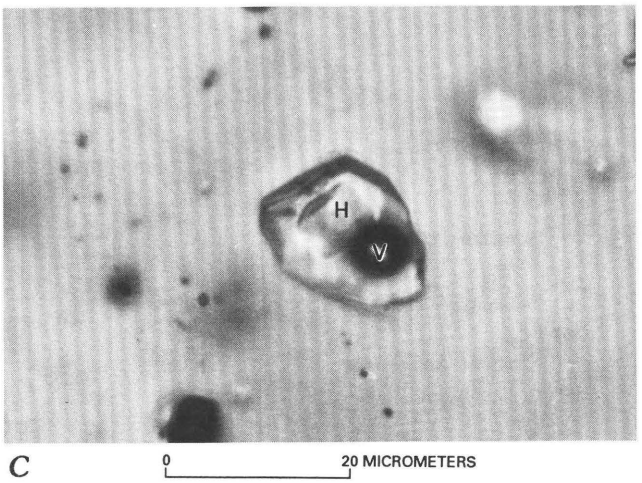

Figure 19. Photomicrographs of fluid inclusions in Alta stock. *A*, Type 1 (liquid-rich) and type 2 (vapor-rich) fluid inclusions. Igneous quartz in sample S-38. *B*, Types 1, 2, and 3 (high-salinity) fluid inclusions. Igneous quartz in sample S-38. *C*, Enlargement of *B* showing type 3 fluid inclusion containing halite cube (H) and vapor bubble (V).

ondary using the criteria of Roedder (1984). In most samples, however, the relative ages of various types of fluid inclusions could not be unequivocally determined owing to (1) either very sparse or extremely abundant numbers of fluid inclusions and (2) the lack of crystal growth features. Despite attempts to avoid measuring secondary fluid inclusions, pressure-corrected homogenization temperatures suggest that most fluid inclusions in igneous quartz crystals were trapped at subsolidus temperatures and are therefore secondary.

Distribution of Fluid-Inclusion Populations

Liquid-rich (type 1) fluid inclusions are present in igneous quartz throughout the Alta stock, whereas vapor-rich and high-salinity fluid inclusions (types 2 and 3) are restricted to the eastern, upper portions of the stock (fig. 20). Some exceptions to this overall distribution scheme are present in a downfaulted block west of the Silver Fork fault and at several topographic highs. Fluid-inclusion populations in igneous quartz were divided into two types based on the presence or absence of high-salinity (type 3) fluid inclusions. The approximate three-dimensional distribution of these two sample populations is shown in figure 21, where samples have been projected onto a N. 80° E. cross section. An extremely regular distribution of fluid-inclusion populations in igneous quartz is present, with high-salinity (type 3) fluid inclusions restricted to the upper parts of the Alta stock. An approximately planar surface dipping about 15° E. separates igneous quartz crystals that contain high-salinity fluid inclusions (+liquid-rich fluid inclusions) (eastern samples) from samples that only contain liquid-rich fluid inclusions (western samples). Vapor-rich (type 2) fluid inclusions also are limited to the upper (eastern) part of the stock, although they are not present in all samples that contain high-salinity fluid inclusions. The one sample lying above this surface that does not contain type 3 fluid inclusions (sample 83-PC-163) apparently does not contain any fluid inclusions trapped prior to vein formation (see the section on fluid inclusions in eastern samples below). One sample along the northern margin of the Alta stock contains type 3 fluid inclusions and lies slightly below this surface. The surface is offset and apparently repeated by the Silver Fork fault in the westernmost part of the stock (fig. 21). Apparent offset of the surface is comparable to the amount of movement on the Silver Fork fault estimated by Calkins and Butler (1943) using stratigraphic offset. The surface separating the two fluid-inclusion populations in the Alta stock is subparallel to the inferred

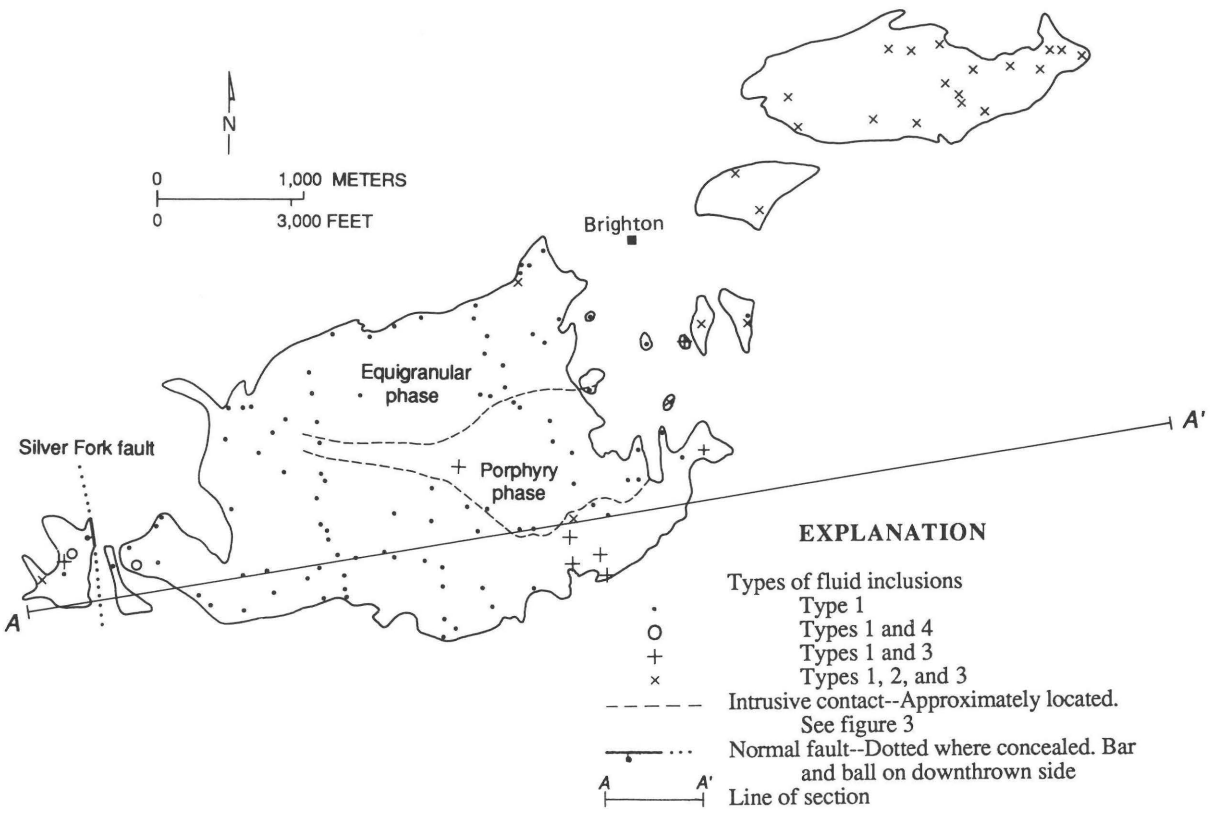

Figure 20. Distribution of fluid-inclusion types in igneous quartz in Alta stock. See figure 3 for location. Section *A-A'* shown in figure 21.

preintrusion surface (fig. 21) and is subparallel to a similar, but slightly offset, surface separating samples of the Clayton Peak stock that contain high-salinity fluid inclusions from samples that lack high-salinity fluid inclusions (John, 1989, fig. 6).

Heating and Freezing Experiments

Salinities of types 1 and 2 fluid inclusions were calculated from the freezing point depression using the equation of Potter and others (1978). Salinities of types 3a and 3b fluid inclusions were calculated from halite dissolution temperatures using the equations of Potter and Brown (1977) and Chou (1987). Salinities of type 3c fluid inclusions were calculated using halite and sylvite dissolution temperatures and data from Sterner and others (1988). Salinities of type 4 fluid inclusions were calculated from melting temperatures of CO_2-hydrate using the relations of Bozzo and others (1975).

Western Samples

Fluid inclusions in igneous quartz were studied in 10 samples from the western part of the stock (fig. 22). Eight of these samples also contain quartz veins, whose fluid inclusions were also studied. These veins represent all major types of veins except type 2 (epidote) and type 7 (pyrite+chlorite) veins. Nearly all fluid inclusions observed in both igneous and vein quartz are liquid-rich (type 1) inclusions containing liquid + vapor at room temperature and homogenizing to the liquid phase. Sparse type 4 (liquid CO_2-bearing) fluid inclusions are present in two samples but are not discussed further because of insufficient data.

Homogenization temperatures range from about 180 °C to 445 °C in igneous quartz and from 200 °C to 410 °C in the quartz veins (fig. 22). Calculated salinities of type 1 inclusions range from 0 to 16 weight percent NaCl equivalent, although nearly all are less than 12 percent (fig. 23). With few exceptions, only minor differ-

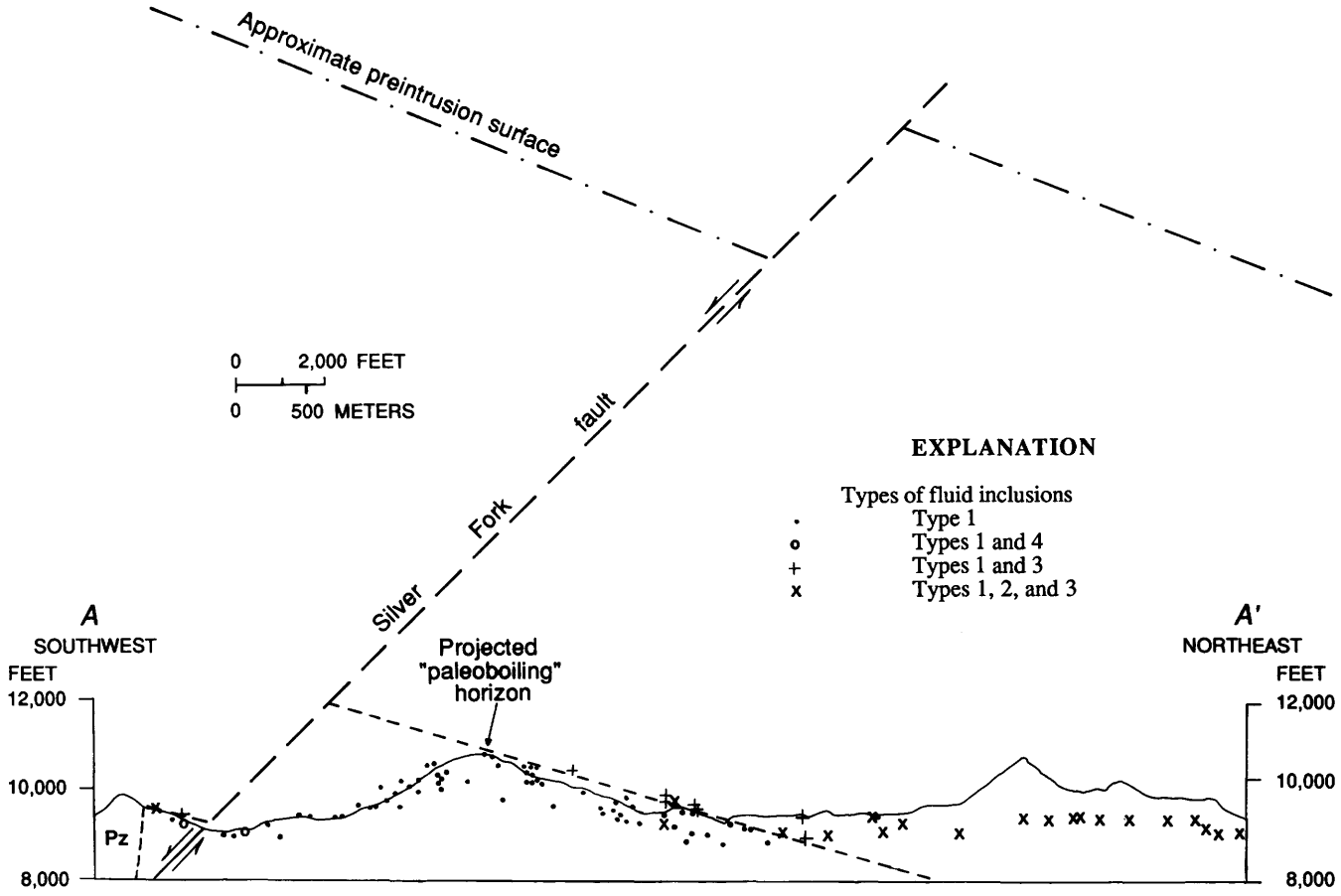

Figure 21. Cross section of Alta stock showing distribution of fluid-inclusion populations in igneous quartz. Samples shown are projected onto plane *A-A'* (fig. 20). Inferred high-temperature "paleoboiling" surface also is shown. Amount of offset of this surface by Silver Fork fault is similar to amount of stratigraphic offset estimated by Calkins and Butler (1943). Also shown is inferred preintrusion surface from John (1989). Pz, Paleozoic rocks. Arrows show direction of relative movement.

ences exist between homogenization temperatures and calculated salinities of fluid inclusions in igneous quartz and those in quartz veins (compare figs. 22, 23).

Igneous quartz in two of the western samples contains sparse fluid inclusions that homogenize at significantly higher temperatures than fluid inclusions in vein quartz (samples 83-PC-253 and 83-PC-279, fig. 22). These high measured homogenization temperatures and high apparent trapping temperatures after pressure corrections (table 6) suggest that some fluid inclusions may have been trapped prior to vein formation but at solidus or slightly subsolidus temperatures (≤720 °C).

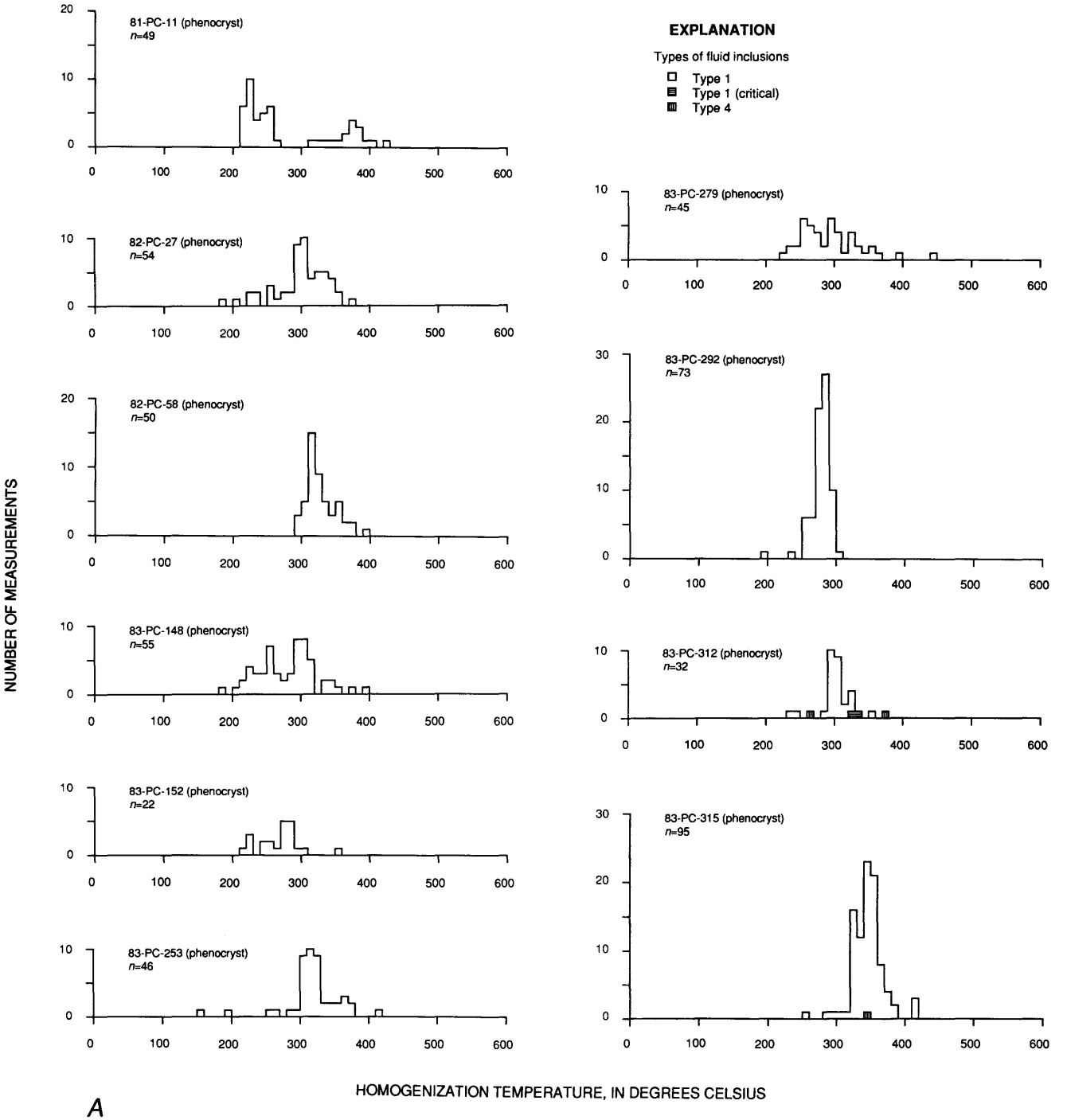

Figure 22. Measured homogenization temperatures of fluid inclusions in western part of Alta stock. *n*, total number of fluid inclusions measured in each sample. *A*, Igneous quartz samples. *B*, Vein quartz samples.

Pressure Corrections and Trapping Temperatures

Type 1 fluid inclusions were trapped at pressures greater than liquid-vapor equilibrium, and measured homogenization temperatures must be pressure corrected to estimate trapping temperatures. Pressure corrections for type 1 fluid inclusions were made using the data of Zhang and Frantz (1987) for the NaCl-H_2O system. Lithostatic pressure was assumed, and the effects of salts other than NaCl and the small amounts of dissolved CO_2 were ignored. Lithostatic pressures were estimated from figure 21 under the assumption that 1 kbar = 3.7 km.

Pressure-corrected homogenization temperatures of type 1 fluid inclusions in igneous quartz samples range from about 445 °C to 720 °C (table 6). These temperatures represent maximum possible trapping temperatures because of the assumptions of lithostatic pressure and negligible effects of CO_2 and salts other than NaCl. Pressures probably approached lithostatic during cooling of the Alta stock because of low fracture permeability, lack of major throughgoing fractures, and relatively great depths (3.7 to 6.3 km). Small amounts of dissolved CO_2 raise the vapor pressure of the fluid inclusion, which slightly decreases the pressure correction. The effects of salts other than NaCl are minor except at high Ca/Na, K/Na and Mg/Na ratios (Potter and Clynne, 1978; Zhang and Frantz, 1987).

Comparison of maximum pressure-corrected homogenization temperatures and salinities of fluid inclusions from various types of veins reveals few differences (table 6). Maximum trapping temperatures suggest formation of all of the veins studied between about 470 °C and 550 °C from moderately saline (≤10 weight percent NaCl equivalent) fluids. The notably high temperatures recorded in sample 83-PC-315 (654 °C) may be the result of measuring fluid inclusions trapped in a thin aplite dikelet that was later reopened and filled with quartz, biotite, epidote, magnetite, chalcopyrite, and molybdenite (appendix 1). Early hornblende veins yield the lowest maximum trapping temperatures (approximately 465–475 °C), yet they are consistently the oldest type of vein. The discrepancy between field relations and fluid-inclusion data could result from several processes, including (1) absence of primary fluid inclusions, (2) deposition of quartz after other minerals were deposited in the veins, (3) multiple periods of fluid flow and entrapment of fluid inclusions in the veins, (4) variations in the pressure regime, and (5) formation of all these veins from

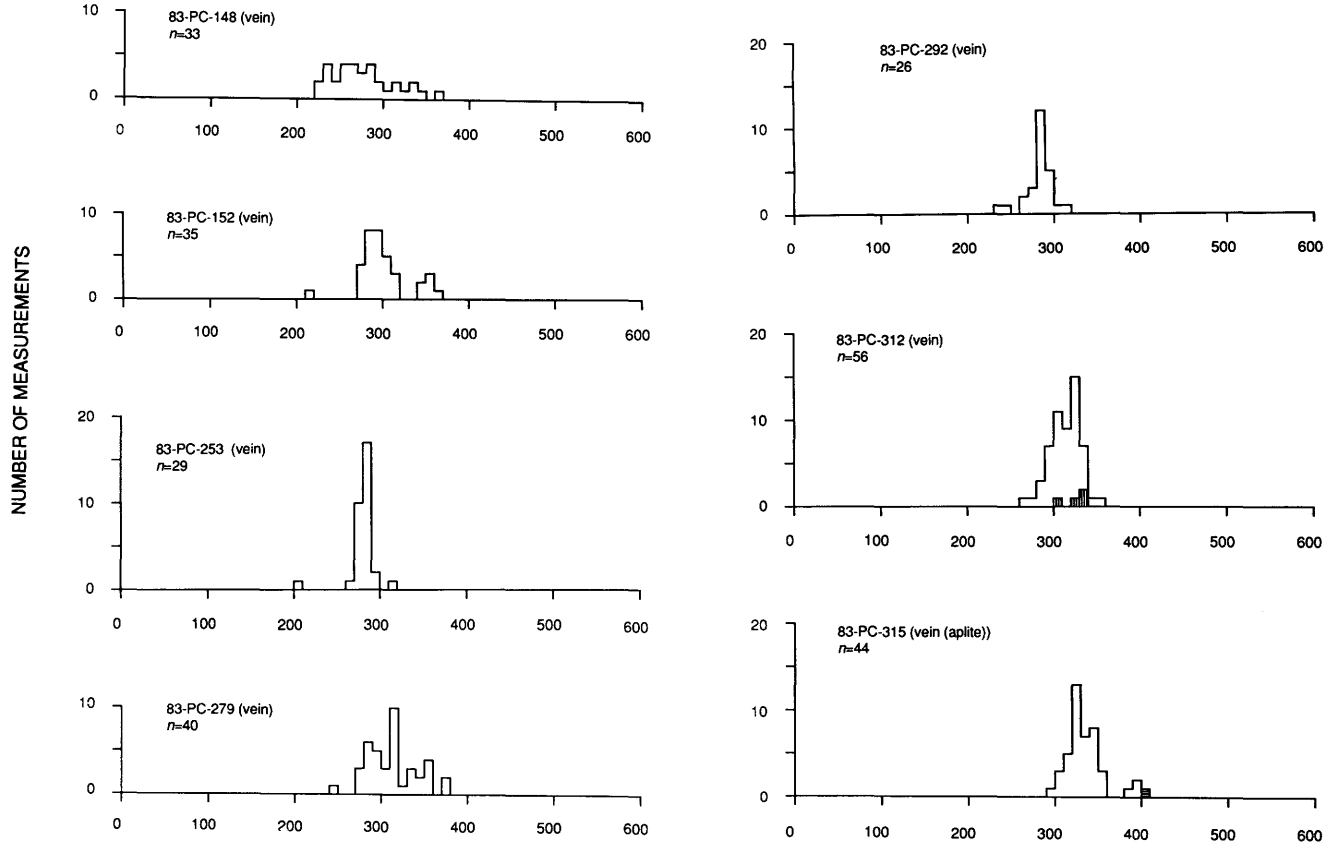

B

Figure 22. Continued.

fluids that had similar temperatures but slightly different compositions that are not reflected in the bulk estimates of salinity. Multiple periods of fluid circulation and entrapment of fluid inclusions are suggested by the wide range of homogenization temperatures (generally ≥200 °C) and partial alteration of early formed minerals, such as chloritization of biotite. The lack of contemporaneity of quartz and hornblende in type 1 veins is suggested by the lack of quartz in many type 1 veins and the textural relations between quartz and hornblende in the two type 1 veins studied (fig. 24). Variations in the pressure regime from early, near-lithostatic conditions to late, more nearly hydrostatic values also could lead to erroneously high pressure corrections for the late veins. The lack of evidence for boiling in late veins, however, suggests that large pressure decreases did not occur. The discrepancy between field relations and the fluid-inclusion data probably results from a combination of multiple generations of fluids, lack of contemporaneity of quartz and hornblende in type 1 veins, and slight variations in fluid chemistry.

Eastern Samples

Heating and freezing tests were made on fluid inclusions in 10 samples of igneous quartz from 9 outcrops

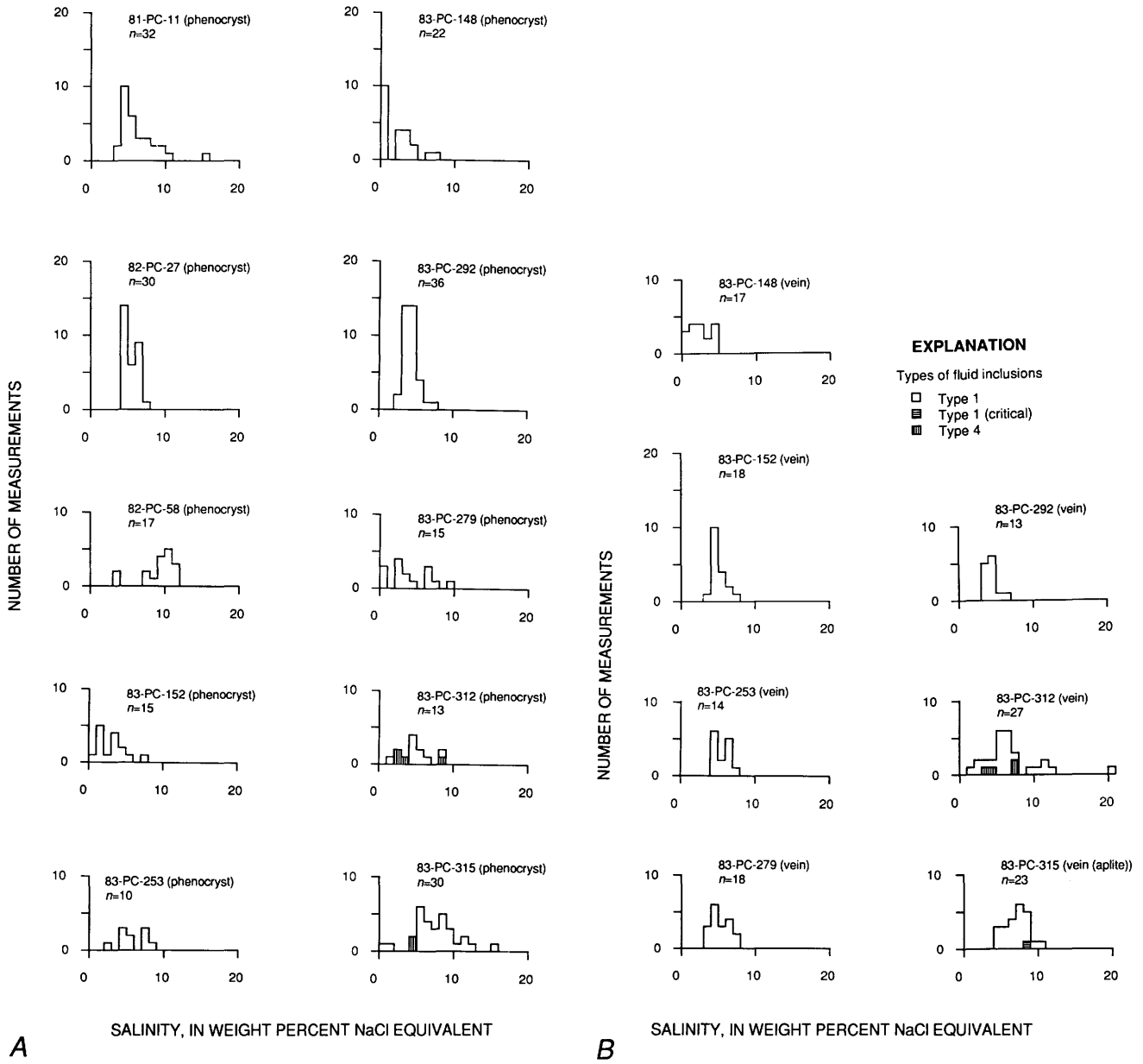

Figure 23. Calculated salinities of fluid inclusions in western part of Alta stock. *n*, total number of fluid inclusions measured in each sample. *A*, Igneous quartz samples. *B*, Vein quartz samples.

Table 6. Pressure corrections for type 1 fluid inclusions in the Alta stock

Sample		Pressure (bars)	Homogenization temperature (°C)	Salinity (wt % NaCl equiv.)	Pressure correction (°C)	Trapping temperature (°C)
Western Samples						
83-PC-148	Phenocryst	1,450	200–395	0–5	120–180	320–575
	Vein (type 3)	1,450	220–365	0–5	95–160	315–525
82-PC-27	Phenocryst	1,400	200–375	4–7	83–177	283–552
82-PC-58	Phenocryst	1,700	290–390	10	134–209	424–599
83-PC-312	Phenocryst	1,450	290–351	2–8	120–160	410–511
	Vein (type 5?)	1,450	290–353	2–12	120–160	410–513
83-PC-315	Phenocryst	1,700	255–414	0–15	121–195	376–609
	Vein (+aplite)	1,700	294–407	4–10	141–247	435–654
81-PC-11	Phenocryst	1,400	212–429	4–9	87–253	299–682
83-PC-253	Phenocryst	1,700	263–415	4–7	115–303	378–718
	Vein (type 1)	1,700	272–316	5–6	132–158	404–474
83-PC-292	Phenocryst	1,600	256–305	3–6	118–143	374–448
	Vein (type 1)	1,600	245–315	3–6	114–149	359–464
83-PC-152	Phenocryst	1,450	213–354	1–8	92–154	305–508
	Vein (type 6)	1,450	272–357	4–6	113–162	385–519
83-PC-279	Phenocryst	1,400	221–444	0–9	93–249	314–693
	Vein (type 6)	1,400	277–373	3–8	110–163	387–536
Eastern Samples						
83-PC-37A	Phenocryst	1,050	217–487	0–22	67–179	284–646
83-PC-276	Phenocryst	1,250	218–338	3–5	80–127	298–465
	Vein (type 4)	1,250	229–380	3–6	83–155	312–535
83-PC-275	Phenocryst	1,250	220–381	2–10	77–160	297–541
	Vein (type 5)	1,250	280–378	5–6	98–153	378–531
S-38	Phenocryst	1,000	160–540	variable		see text
84-PC-40	Vein (type 5)	1,000	265–399	5–10	64–124	329–523
83-PC-274	Vein (type 1)	1,100	257–349	0–8	83–123	340–472
83-PC-151	Phenocryst	1,400	194–420	5–20	79–130	273–550
S-30	Phenocryst	1,200	200–316	3–24	69–92	269–408
82-PC-51	Phenocryst	1,450	210–468 (409) [1]	5–20	90–156	300–≥565 [1]
84-PC-36	Phenocryst	1,150	210–384	7–23	67–104	277–488
	Vein (type 6)	1,150	230–391	3–16	75–108	305–499
83-PC-163	Phenocryst	1,250	200–353	4–7	75–134	275–487
	Vein (type 5)	1,250	218–376	3–7	80–151	298–527
83-PC-177	Phenocryst	1,300	187–348	3–8	75–142	262–490
	Vein (type 3)	1,300	200–336	2–4	79–134	279–470

[1]Salinity of fluid inclusions with highest homogenization temperatures unknown; calculations use fluid inclusion with lower homogenization temperature (in parentheses)

and in 7 quartz veins (fig. 11). Two of the samples were late igneous differentiates (pegmatite and aplite dikes). There were no obvious differences in fluid-inclusion populations between quartz in late igneous dikes and quartz phenocrysts in granitic wall rocks of the late dikes. Igneous quartz crystals contain three major types of fluid inclusions: liquid rich (type 1), high salinity (types 3a, 3b, and 3c), and, locally, vapor rich (type 2). Type 3a fluid inclusions are relatively sparse or are not present in several samples. Type 3c fluid inclusions are only found in one sample (83-PC-151). Type 4 fluid inclusions apparently are not present in the eastern part of the Alta stock.

Igneous Quartz—Homogenization Temperatures and Salinities

Type 1 fluid inclusions have a wide range in homogenization temperatures and estimated salinities. Homogenization temperatures range from <200 °C to 540 °C, although most type 1 fluid inclusions homogenize to the liquid phase between 250 °C and 370 °C (fig. 25). Calculated salinities span the continuum from 0 to 26 weight percent NaCl equivalent (fig. 26). Many halite-undersaturated fluid inclusions have first melting points at less than –30 °C (as low as –53 °C) and final melting points at less than –24 °C, indicating the presence of salts other than NaCl and KCl. These fluid inclusions probably contain appreciable amounts of $CaCl_2$ and (or) $FeCl_2$ as is suggested by their low melting temperatures (Crawford and others, 1979; Kwak and Tan, 1981) and by the presence of calcite and hematite daughter(?) crystals in some type 3 fluid inclusions in these samples (particularly in samples 83-PC-37A and S-38). No evidence for the presence of CO_2 was seen in fluid inclusions with low melting points, even when temperatures were lowered to less than –100 °C during many of the freezing runs.

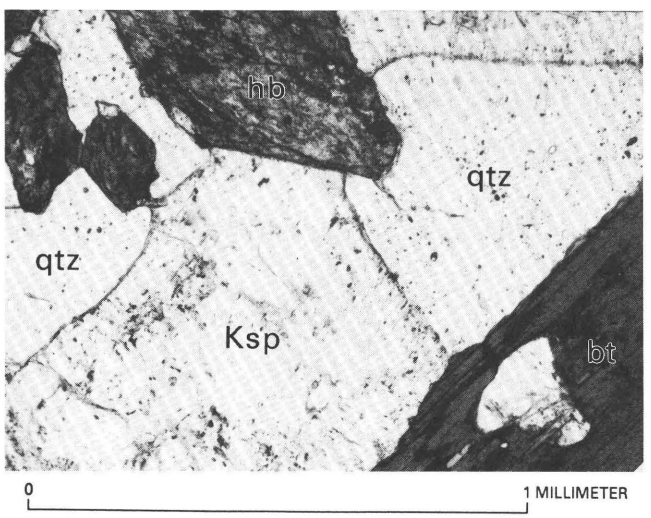

Figure 24. Photomicrograph of type 1 hornblende+K-feldspar vein in sample 83-PC-292, showing textures of hornblende, K-feldspar, and quartz. Euhedral hornblende (hb) is overgrown by subhedral, turbid perthitic K-feldspar (Ksp) and subhedral-to-anhedral quartz (qtz). Note abundant type 1 fluid inclusions in quartz. Biotite (bt) is in wall rock along edge of vein. Plane-polarized light.

Type 2 fluid inclusions vary considerably in abundance and are sparse or absent in several samples (fig. 20). Most type 2 fluid inclusions have vapor contents nearly filling the inclusion cavity (fig. 19*A*, *B*), and freezing-point depression and homogenization temperatures cannot be obtained for these fluid inclusions. However, homogenization temperatures were measured for 10 fluid inclusions, ranging from 300 °C to 542 °C. Bodnar and others (1985) have shown that apparent homogenization temperatures of vapor-rich fluid inclusions may be as much as 200 °C to 400 °C less than the actual homogenization temperatures. Thus, the measured homogenization temperatures should be regarded as minimum values. Freezing points were only measured for four type 2 fluid inclusions with calculated salinities ranging from 1.7 to 16 weight percent NaCl equivalent.

Most type 3a fluid inclusions have homogenization temperatures between 180 °C and 360 °C (fig. 25). Salinities calculated from halite dissolution temperatures range from about 26.5 to 39 percent NaCl equivalent (fig. 26). One type 3a fluid inclusion in sample 84-PC-36 has a much higher homogenization temperature (515 °C) and a higher estimated salinity (45 weight percent NaCl equivalent). Daughter minerals other than halite are uncommon in type 3a inclusions, except in sample 83-PC-37A, where calcite(?) and opaque daughter minerals are present locally.

Type 3b fluid inclusions have a much larger range in homogenization temperatures and calculated salinities than type 3a fluid inclusions (figs. 25, 26). Homogenization temperatures range from about 185 °C to 495 °C, corresponding to minimum salinities of 31 to 56 weight percent NaCl equivalent. Halite dissolution commonly occurs at temperatures 200 °C or more higher than liquid-vapor homogenization. Type 3b inclusions commonly contain several daughter minerals in addition to halite, including sylvite, hematite, calcite, anhydrite(?), and several other small birefringent and (or) opaque phases. The chemistry of the daughter minerals indicates that fluids in type 3b fluid inclusions are complex mixtures of Na, K, Ca, Fe, Cl, and so forth, and that the $NaCl\text{-}H_2O$ system may not adequately represent them (see Kwak and Tan, 1981).

NaCl-KCl compositions were estimated from the dissolution temperatures of halite and sylvite in four type 3c fluid inclusions from sample 83-PC-151 (which did not contain calcite) using $NaCl\text{-}KCl\text{-}H_2O$ relations from Sterner and others (1988). These fluid inclusions

have estimated total salinities of 41 to 47 weight percent NaCl+KCl equivalent and K/Na molar ratios of 0.22 to 0.27. First melting temperatures were not measured for these fluid inclusions; thus, the possible effects of Ca cannot be evaluated.

Vein Quartz—Homogenization Temperatures and Salinities

Heating and freezing measurements of fluid inclusions in seven quartz veins from six outcrops were made. In six of the seven veins, only type 1 liquid-rich fluid inclusions are present. In the other vein (sample 83-PC-274), vapor-rich (type 2) and high-salinity (types 3a and 3b) fluid inclusions are present in addition to liquid-rich fluid inclusions.

Type 1 fluid inclusions have measured homogenization temperatures ranging from 130 °C to 392 °C (fig. 25). With the exception of sample 83-PC-274, calculated salinities are relatively low, with most fluid inclusions having salinities of ≤7 weight percent NaCl equivalent (fig. 26). Eutectic temperatures significantly lower than –23 °C were not observed in these fluid inclusions.

Quartz crystals in a quartz+K-feldspar+amphibole vein (type 1) in sample 83-PC-274 contain types 1, 2, 3a, and 3b inclusions. Igneous quartz crystals in this sample also contain these types of fluid inclusions, but owing to optical problems with fluid-inclusion plates, heating and freezing measurements could not be made on fluid inclusions in igneous quartz. Homogenization temperatures of type 1 inclusions in vein quartz range from 257 °C to 349 °C, with most of the determinations in the range 320–350 °C (fig. 25). Calculated salinities range between 0 and 19 weight percent NaCl equivalent (fig. 26). Measured homogenization temperatures of type 3a fluid inclusions are between 269 °C and 313 °C and have salinities ranging from 29 to 34 weight percent NaCl equivalent. Type 3b inclusions have homogenization temperatures ranging from 260 °C to 560 °C, corresponding to estimated salinities of 35 to 70 weight percent NaCl equivalent. No homogenization or freezing data were obtained on the sparse type 2 fluid inclusions in the vein quartz.

Pressure Corrections and Trapping Temperatures

Vapor-rich (type 2) fluid inclusions are absent in several igneous quartz samples and in the quartz veins (except sample 83-PC-274). This suggests that most type 1 and possibly type 3a fluid inclusions were not trapped from boiling solutions and that homogenization temperatures for these inclusions must be pressure corrected to estimate trapping temperatures. Type 3b fluid inclusions homogenize by halite dissolution at temperatures greater than liquid-vapor homogenization and could not have been trapped from boiling solutions.

Maximum pressure-corrected homogenization temperatures for type 1 fluid inclusions in igneous quartz samples range from about 408 °C to 646 °C, whereas type 1 fluid inclusions in vein quartz range from about 470 °C to 535 °C (table 6). Salinities and pressure-corrected homogenization temperatures for type 1 fluid inclusions in paired samples of igneous and vein quartz are nearly identical, suggesting that most type 1 fluid inclusions in igneous quartz were trapped from fluids that formed the quartz veins. Fluid inclusions are very similar in all veins, except for sample 83-PC-274, with maximum salinities and trapping temperatures similar to those for corresponding types of veins in the western parts of the stock (table 6).

Several type 1 fluid inclusions in sample S-38 have measured homogenization temperatures higher than 500 °C. These fluid inclusions have estimated compositions and measured homogenization temperatures similar to those of other fluid inclusions in this sample that homogenize either to the vapor phase or homogenize by critical behavior. These high-temperature fluid inclusions may have been trapped near the critical point (540 °C, 750 bars, 16 weight percent NaCl; Sourirajan and Kennedy, 1962), and thus they do not require pressure correction.

Type 3a (high-salinity) fluid inclusions may have been trapped at pressures greater than vapor pressure. This is suggested by the lack of vapor-rich fluid inclusions in several samples containing type 3a fluid inclusions (fig. 20), by the unreasonably low pressures (<170 bars) implied by these fluid inclusions if they were trapped from boiling solutions (Sourirajan and Kennedy, 1962), and by the presence of type 1 fluid inclusions that have similar or higher homogenization temperatures and should have boiled if type 3a fluid inclusions were directly trapped from boiling solutions. Vapor pressures and densities of type 3a fluid inclusions at measured homogenization temperatures were estimated from the data of Urusova (1975) and Haas (1976). Approximate pressure corrections were then made assuming lithostatic pressure and using isochores interpolated from data in Urusova (1975). Estimated pressure corrections range from 75 °C to 150 °C and raise maximum trapping temperatures to 310 °C to 590 °C (table 7). These temperatures probably represent maximum temperatures possible at the time of trapping.

Type 3b fluid inclusions could not have been trapped under vapor-saturated conditions because halite dissolves after liquid-vapor homogenization, and homogenization temperatures must be pressure corrected. Densities of type 3b fluid inclusions calculated using the method of Roedder and Bodnar (1980, p. 285–286) assuming pure NaCl-H_2O solutions are quite high (1.08 to 1.41 g/cm^3). Most of the calculated densities are well outside the range of available *P-V-T-X* data and imply

high internal pressures that probably exceed estimated lithostatic pressures. The presence of other salts (KCl, $CaCl_2$, etc.) in the fluid-inclusion fluids, however, probably significantly lowers the pressures (Stewart and Potter, 1979; Roedder and Bodnar, 1980) and could lead to significant pressure corrections for these fluid inclusions. Unfortunately, the compositions of the solutions in these fluid inclusions are poorly known, and *P-V-T-X* data are not available for complex solutions at high pressures and temperatures. Thus, halite-dissolution temperatures must be regarded as minimum estimates of trapping temperatures of type 3b inclusions.

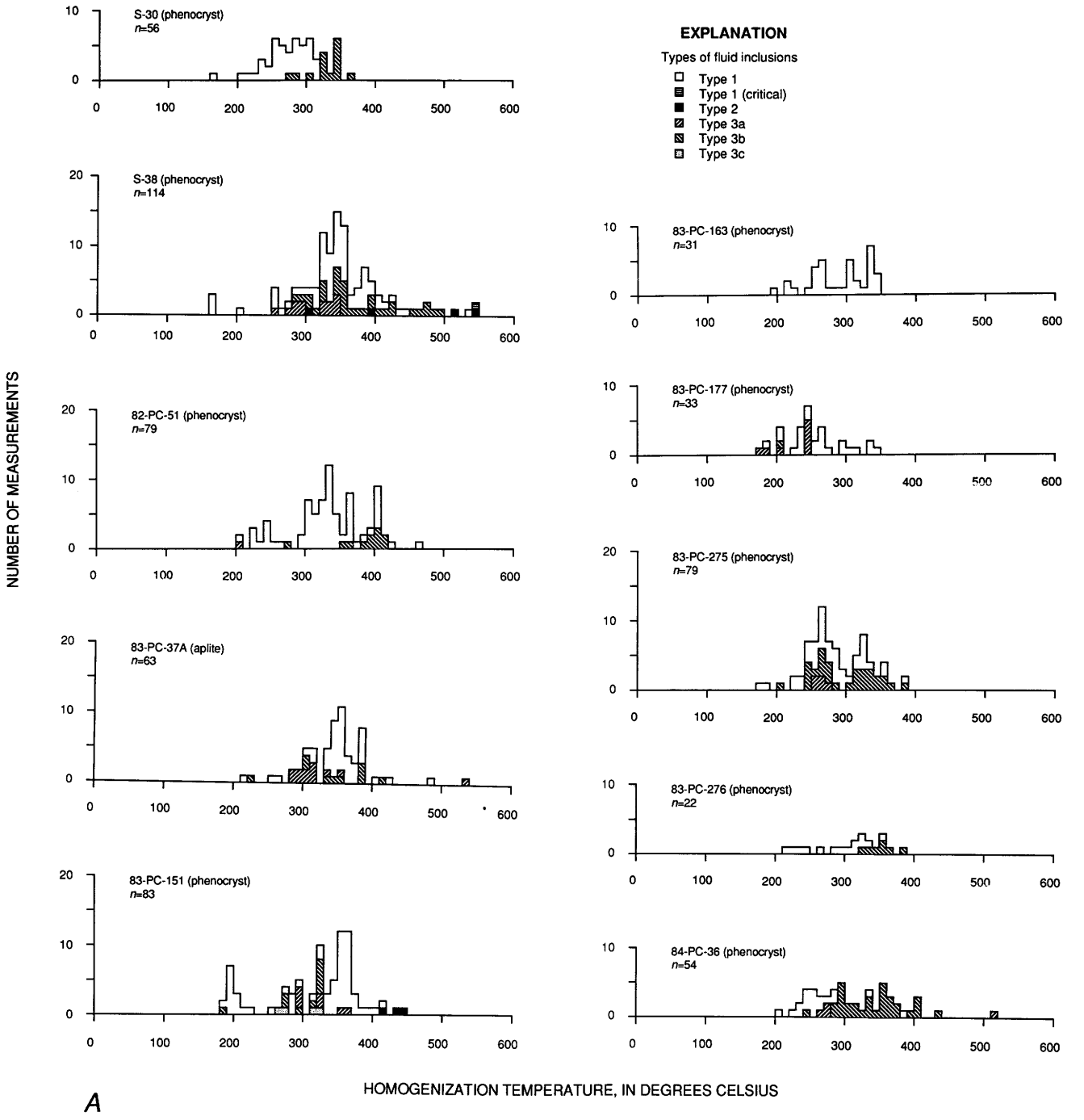

Figure 25. Measured homogenization temperatures of fluid inclusions in eastern part of Alta stock. *n*, total number of fluid inclusions measured in each sample. *A*, Igneous quartz samples. *B*, Vein quartz samples.

Origin of Fluid Inclusions in the Alta Stock

The origin of fluids and fluid inclusions in the Alta stock is constrained by several factors, as discussed above. First, stable-isotope data indicate that meteoric water has played an insignificant role in development of the hydrothermal system, and that fluids trapped in the stock were derived from magmatic fluids or fluids that equilibrated with the magma at high temperatures. Second, there is little evidence that CO_2 played a major role in the hydrothermal system. Third, high-salinity fluids appear to have formed early and, in most cases, predate low-salinity fluids that circulated through the fracture-controlled hydrothermal system. Fourth, there is a regular geometric distribution of high-salinity fluid inclusions (type 3) subparallel to the inferred preintrusion surface, with high-salinity fluid inclusions limited to depths of less than about 5 km. Finally, most, if not all, fluid inclusions were trapped at subsolidus temperatures, and most fluid inclusions were not trapped directly from boiling fluids. These observations suggest that high-salinity fluids formed at high temperatures from magmatic fluids, and that pressure probably exerted a major influence on the generation of high-salinity fluids.

The most likely explanation for the formation of high-salinity fluid inclusions in the Alta stock is that magmatic fluids, or fluids that isotopically equilibrated with a magma at high temperatures, either boiled in the upper parts of the Alta stock (paleodepths less than 4,600 to 5,200 m), forming high-salinity brines, or that high-salinity brines were directly exsolved from the crystallizing magma. The paleo-high-salinity horizon in the Alta stock, separating samples containing high-salinity fluid inclusions from samples lacking high-salinity fluid inclusions, may be thought of as a high-temperature "paleoboiling" horizon.

Direct exsolution of an immiscible high-salinity brine from crystallizing granitic magmas has been demonstrated in plutonic blocks from Ascensión Island (Roedder and Coombs, 1967; Harris, 1986) and has been suggested as the mechanism leading to formation of high-salinity brines lying on "halite trends" (Cloke and Kesler, 1979; Wilson and others, 1980). In the Alta stock, most high-temperature, high-salinity fluid inclusions homogenize by halite dissolution after liquid-vapor homogenization (type 3b), indicating that the fluids were not vapor saturated and thus were not boiling at the time of trapping. However, vapor-rich (type 2) fluid inclu-

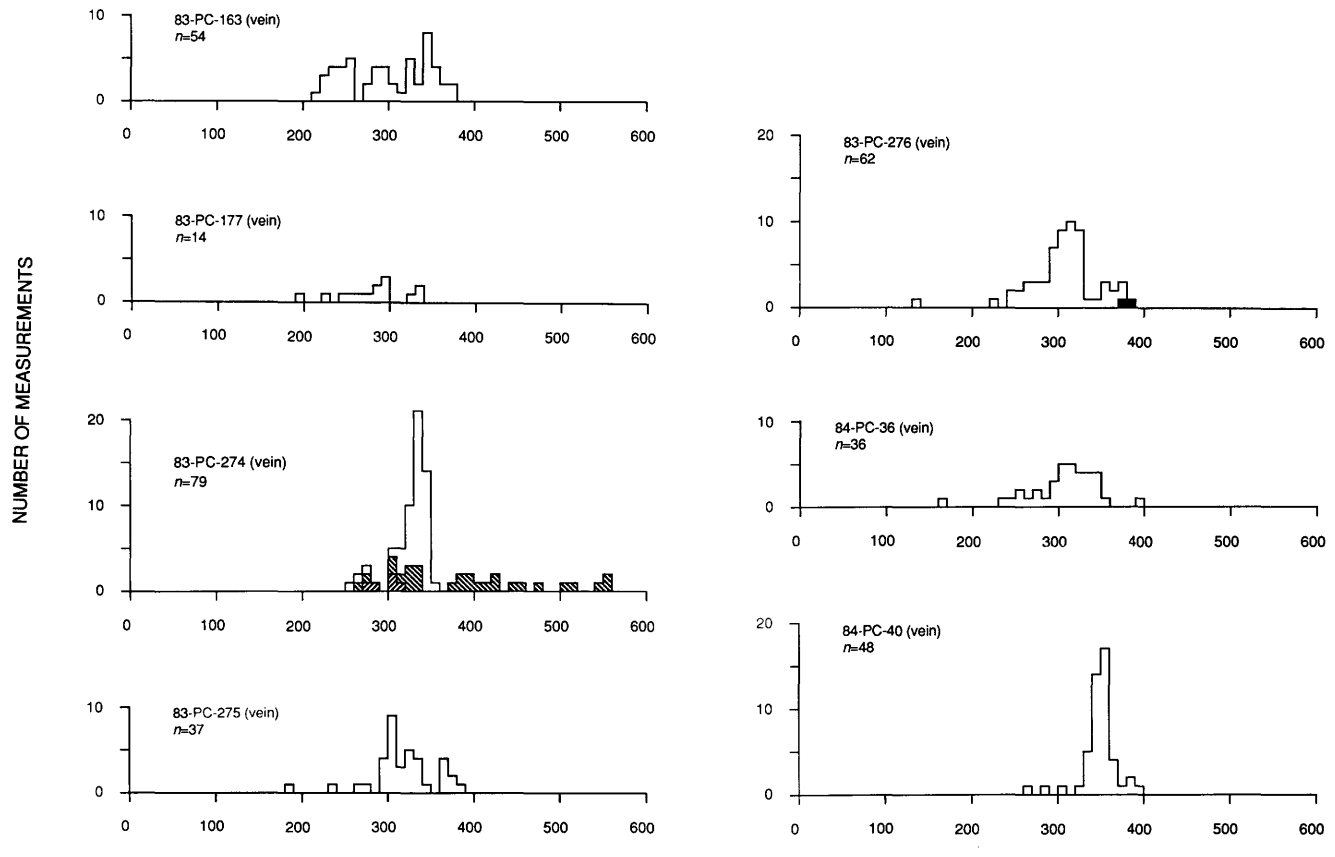

B

Figure 25. Continued.

sions are present in most samples that contain high-salinity fluid inclusions (fig. 21)—a fact that strongly suggests that boiling occurred at some point in time. The general lack of vapor-rich fluid inclusions in quartz veins in the Alta stock suggests that boiling occurred prior to formation of the veins and may have been contemporaneous with formation of high-salinity brines.

Sylvite daughter crystals are rare in high-salinity fluid inclusions in the Alta stock, and fluid inclusions defining a "halite trend" are not present. This fact suggests that high-salinity brines had low K/Na molar ratios (generally ≤0.2) that would not be in equilibrium with two feldspars (or granitic magmas) at magmatic or near-magmatic temperatures (Lagache and Weisbrod, 1977; Burnham, 1979a; Cloke and Kesler, 1979). However, the K/Na molar ratio of high-salinity fluid inclusions may not be an accurate indicator of the bulk composition of magmatic fluids, because if boiling has occurred near

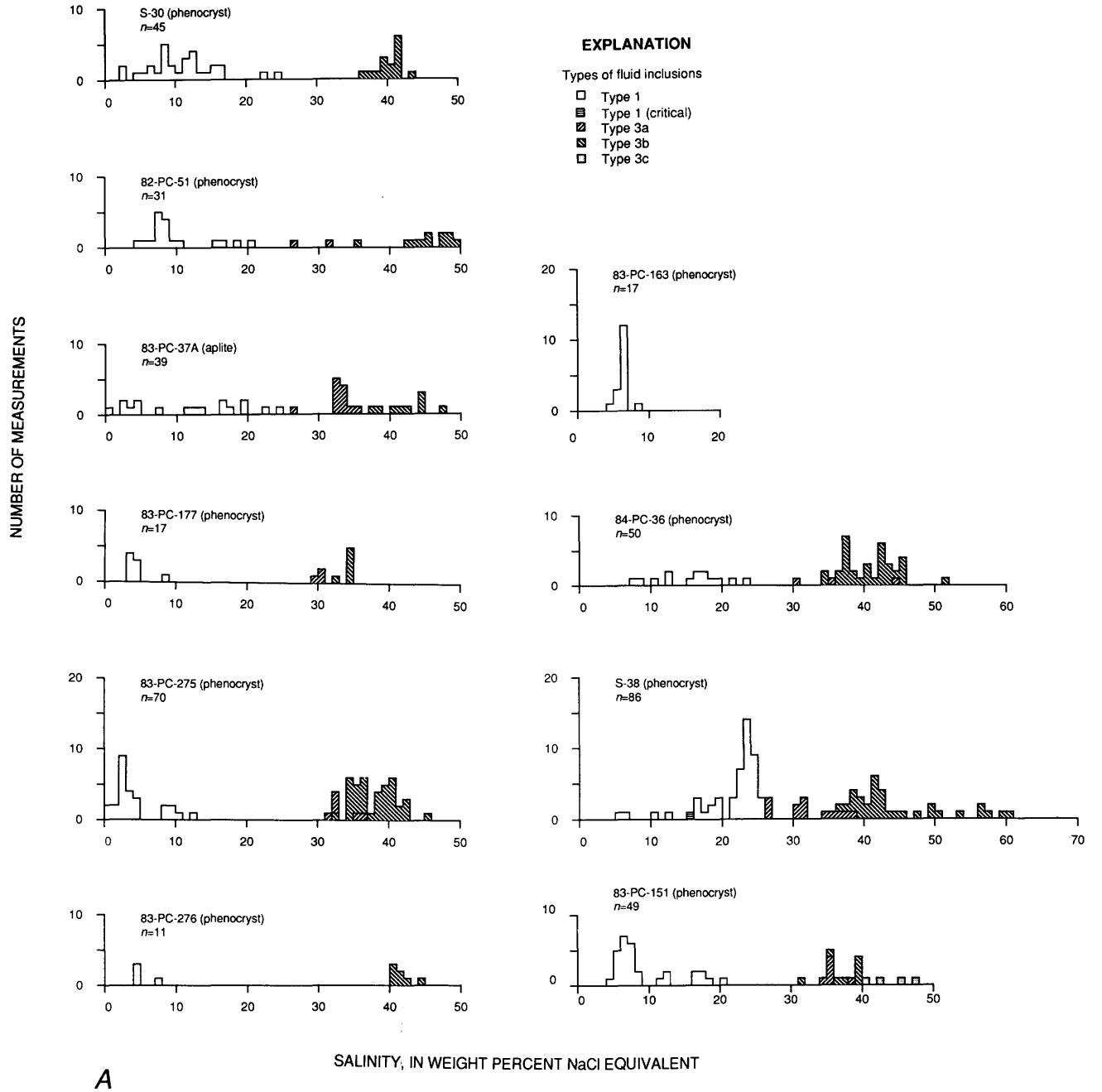

Figure 26. Calculated salinities of fluid inclusions in eastern part of Alta stock. *n*, total number of fluid inclusions measured in each sample. *A*, Igneous quartz samples. Values for type 3c fluid inclusions in sample 83-PC-151 are given in weight percent NaCl+KCl equivalent. *B*, Vein quartz samples.

700 °C, K is preferentially partitioned into the vapor phase, lowering the K/Na ratio of the brine phase (Sterner and Bodnar, 1986). Silicate-melt inclusions and mixed inclusions of high-salinity fluids and silicate melts similar to inclusions at Ascensión Island (Roedder and Coombs, 1967) also are absent in the Alta stock. These data suggest that at least minimal boiling occurred early in the hydrothermal history of the Alta stock. It is not possible, however, to determine if high-salinity brines formed by direct exsolution of an immiscible high-salinity brine from the crystallizing magmas with later boiling or by boiling of low- to moderate-salinity fluids released during crystallization of magmas.

The magma of the Alta stock probably contained about 3 to 4 weight percent H_2O, most of which was released as an aqueous vapor phase during crystallization and cooling of the stock, because less than 0.7 weight percent H_2O is contained in hydrous phases in the Alta stock (table 1). Burnham (1979a) suggested that the initial salinity of aqueous fluids separating from a granodioritic magma will be in the range of a few to 20 weight percent NaCl equivalent. Type 1 fluid inclusions in the western part of the stock with the highest estimated trapping temperatures suggest that such fluids may have had salinities of 5 to 12 weight percent NaCl equivalent.

The NaCl-H_2O system can be used as a simplified model for the fluids in the Alta stock. Chou (1987) has presented a temperature-composition diagram for this system showing two-phase liquid+vapor curves and the compositions of coexisting fluid phases at various pressures (fig. 27). At 1,300 bars pressure and temperatures higher than 750 °C, 10 weight percent NaCl solutions are unstable and will boil, separating into high-salinity liquid and lower salinity vapor phases. At 1,000 bars, 10 weight percent NaCl solutions will separate into two phases at temperatures greater than about 640 °C, whereas at 1,500 bars, 10 weight percent NaCl solutions will remain in the one-phase field at all temperatures lower than 850 °C.

Possible temperatures of boiling and probable temperatures of vapor saturation of the magma were estimated using NaCl-H_2O phase relations shown by Chou (1987), maximum salinities of type 3b inclusions estimated in each sample, and lithostatic pressures estimated from paleodepths in figure 21. The estimated temperatures range from about 725 °C to 860 °C, with most between 725 °C and 770 °C (table 7). Provided that the NaCl-H_2O system is applicable to the complex fluids of the Alta stock, the temperature estimates suggest that vapor saturation and boiling did not occur until relatively late during crystallization, possibly at only a few degrees above the solidus. These temperature estimates are probably maximum temperatures because lower salinities and (or) lower pressures both lead to

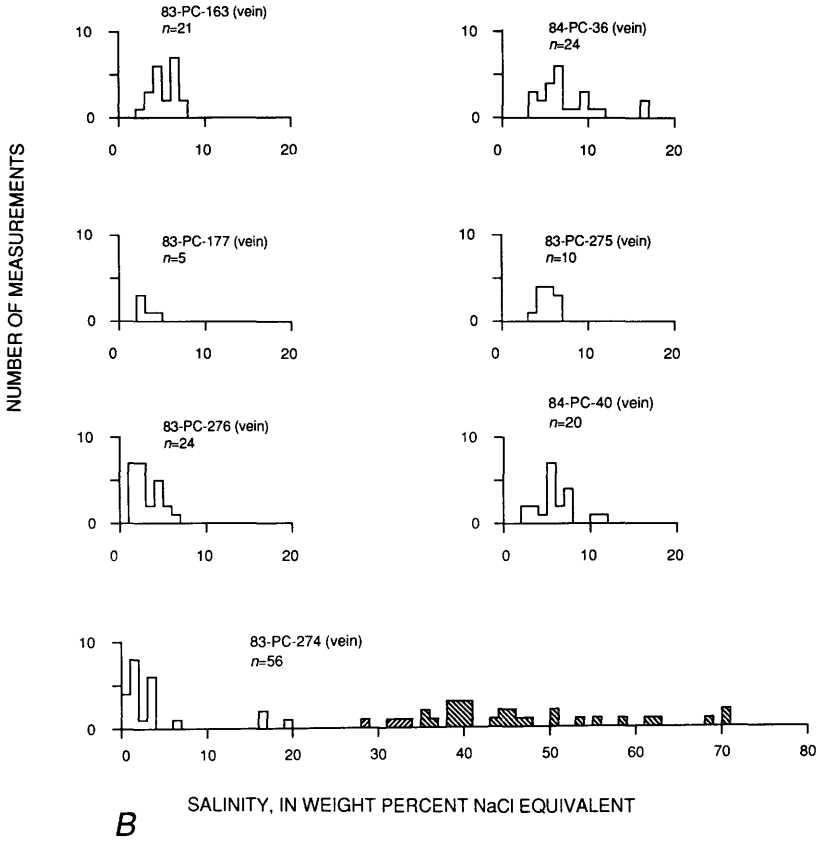

Figure 26. Continued.

Table 7. Summary of pressure corrections for type 3 fluid inclusions in the eastern part of the Alta stock

[T_H, homogenization temperature]

Sample	Pressure (bars)	Type 3a fluid inclusions				Type 3b fluid inclusions				
		T_H (°C)	Maximum salinity (wt % NaCl equiv.)	Pressure correction (°C)	Trapping temperature (°C)	T_H vapor (°C)	T_H halite (°C)	Maximum salinity (wt % NaCl equiv.)	Density (g/cm^3)	Maximum temperature of boiling (°C)
83-PC-151	1,400	360	38	150	510	311	322	39.5	1.08	770
S-30	1,200					196	370	43.4	1.21	730
82-PC-51	1,450	206	32	120	325	221	412	49.1	1.23	810
S-38	1,000	349	39	110	460	252	495	60.6	1.21	770
84-PC-36	1,150	515	45	75	590	238	431	51.3	1.23	735
83-PC-177	1,300	205	31	105	310	229	249	34.5	1.11	725
83-PC-37A	1,050	319	35	80	400	275	413	48.8	1.16	725
83-PC-276	1,250					160	381	44.3	1.26	735
83-PC-275	1,250	294	37	145	440	325	354	45.1	1.08	740
83-PC-274	1,100	312	34	120	430	213	550	70.1	1.41	860

lower temperature estimates for boiling (fig. 27). In general, the maximum salinity of type 3 fluid inclusions decreases with increasing pressure (table 7), which is consistent with vapor saturation and boiling at similar temperatures throughout the stock (fig. 27) and may explain the sharp, nearly planar break between rocks containing high-salinity fluid inclusions and those lacking high-salinity fluid inclusions that is interpreted as a high temperature paleoboiling horizon (fig. 21). The one sample that lies below this horizon and contains high-salinity fluid inclusions may have become vapor saturated at slightly higher temperatures or initially may have had a slightly more saline composition, allowing it to boil at lower temperatures and form high-salinity fluids (fig. 27).

High-salinity fluid inclusions were not trapped directly from these "boiling" fluids, and they may have been trapped at temperatures 100 °C to 300 °C lower than those at which the high-salinity fluids formed (table 7). An isoplethal pressure-temperature projection of the high-salinity portion of the NaCl-H_2O system (fig. 28) from Chou (1987), Bodnar and others (1985), and Gunter and others (1983) shows that a 10 weight percent NaCl solution exsolved at 725 °C and 1,000 bars (point A) will unmix into a small amount of brine with a composition of about 53 weight percent NaCl and a volumetrically dominant vapor phase with a salinity of about 3 weight percent NaCl (Sourirajan and Kennedy 1962; Chou, 1987). If the high-salinity brine is not trapped in fluid inclusions at the temperature of boiling (725 °C) but is allowed to cool along a nearly isobaric path similar to A–B without remixing with the low-salinity vapor, its density will increase as it moves through the field of liquid stability, and it will become vapor undersaturated. Trapping of this fluid somewhere along this path at temperatures above the liquidus (point C) will result in the formation of a fluid inclusion that homogenizes by halite dissolution and has a bulk composition of 53 weight percent NaCl. If the brine is allowed to cool to still lower temperatures without dilution, it will cross the liquidus surface at point C (about 450 °C) and begin precipitating halite. Further cooling will result in fluids that have salinities less than 53 weight percent NaCl equivalent, and because of the fixation of NaCl into precipitating halite, any fluid inclusions trapped from the residual solutions will also homogenize by halite dissolution (type 3b fluid inclusions).

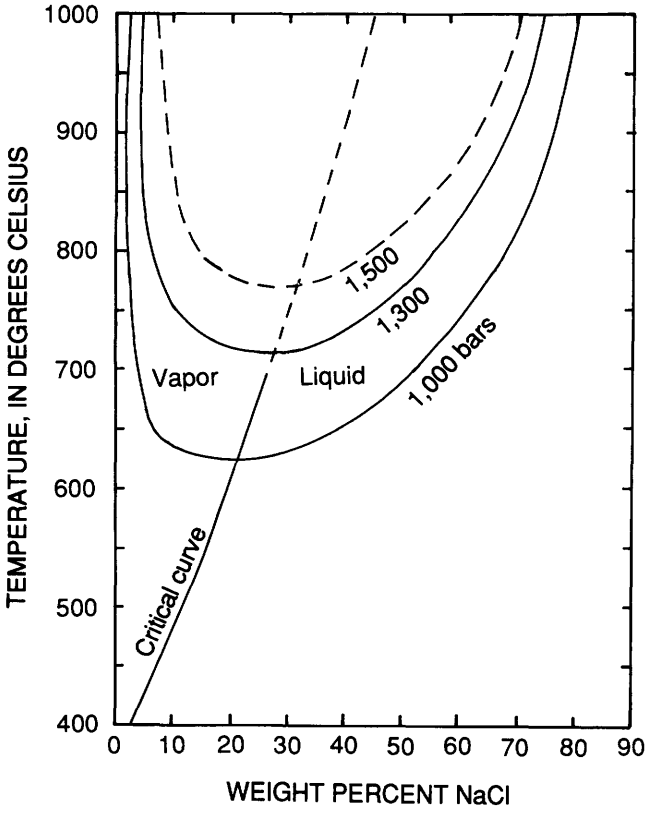

Figure 27. Temperature-composition diagram for high-temperature part of NaCl-H_2O system (from Chou, 1987), showing isobars for the two-phase liquid+vapor field and compositions of coexisting liquid and vapor phases. Dashed curves are extrapolated. Critical curve is loci of critical points.

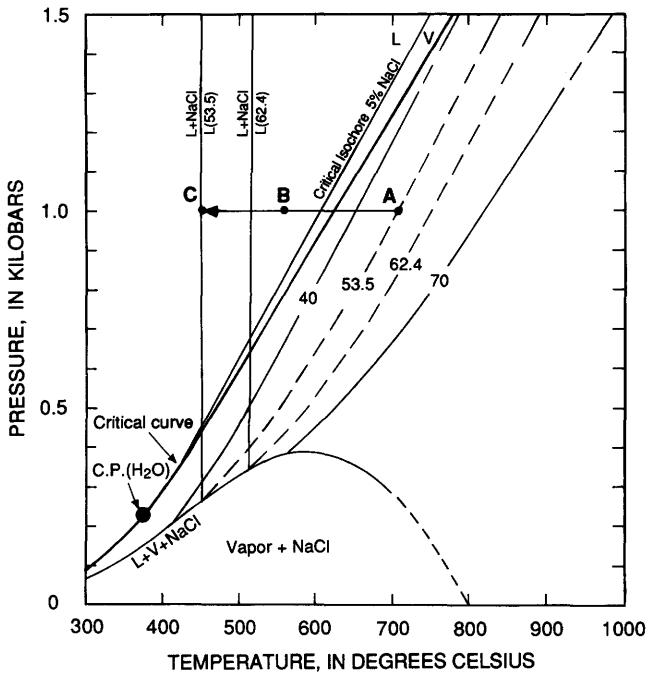

Figure 28. Isoplethal pressure-temperature diagram for part of NaCl-H_2O system (modified from Chou, 1987). Liquidus surfaces from Gunter and others (1983). Critical isochore for 5 weight percent NaCl estimated from Roedder (1984, fig. 17-17). Path A–B–C is described in text. Lines labeled 40, 53.5, 62.4, and 70 are isopleths of liquid composition in weight percent NaCl. Dashed curves are interpolated. Abbreviations: L, liquid; V, vapor; C.P. (H_2O), critical point of H_2O.

Type 3a fluid inclusions may have formed by partial mixing of the high-salinity brines with lower salinity, less dense fluids. Type 3a fluid inclusions generally have lower salinities, lower densities, and lower homogenization temperatures than type 3b fluid inclusions (figs. 25, 26; table 7). With the exception of one fluid inclusion in sample 84-PC-36, maximum pressure-corrected homogenization temperatures of type 1 fluid inclusions are equal to or greater than pressure-corrected homogenization temperatures for type 3a fluid inclusions. These data suggest that type 3a fluid inclusions may have formed by partial mixing of the high-salinity brines with the lower salinity fluids that were trapped as type 1 fluid inclusions. Fluid inclusions trapping mixtures of these fluids will have intermediate salinities and densities and could homogenize either by halite dissolution (type 3b) or by vapor disappearance (type 3a), depending on the bulk density of the fluid inclusion.

Type 1 fluid inclusions in the eastern samples could have formed in several ways. They may represent low-salinity fluids that flowed into this part of the stock either from the wall rocks (meteoric or metamorphic waters) or from deeper parts of the stock, or they could represent small portions of the low-salinity vapor phase that formed during high-temperature boiling. Stable-isotope relations suggest that large volumes of meteoric or metamorphic water did not circulate through the stock. The sharp interface between rocks containing high-salinity fluid inclusions and those that lack high-salinity fluid inclusions suggests that there probably was not widespread circulation of fluids upward in the stock. Gravitational sinking of the high-density brines would be expected if lower density fluids were flowing upward, as discussed by Henley and McNabb (1978) and Fournier (1983). Apparent trapping temperatures of types 1, 3a, and 3b fluid inclusions suggest that they were all trapped at similar temperatures. These data further suggest that type 1 fluid inclusions represent either small portions of the vapor phase formed by boiling at high temperatures and not trapped until temperatures ≤620 °C or low-salinity fluids released during crystallization of the deeper parts of the stock.

The composition of the vapor phase formed during boiling of a 10 weight percent NaCl solution at 725–770 °C and 1,000–1,400 bars will vary between about 3 and 8 weight percent NaCl (Sourirajan and Kennedy, 1962; Bodnar and others, 1985; Chou, 1987). Most type 2 vapor-rich fluid inclusions may represent a small fraction of this fluid, although salinity and homogenization data are too limited, and actual homogenization temperatures too uncertain, to test this hypothesis. If the vapor cools isobarically and does not mix with the high-salinity brine, its density will increase, and eventually it will cross its critical isochore between 600 °C and 700 °C (fig. 28). Fluid inclusions trapped at temperatures lower than the critical isochore will homogenize to the liquid phase. Partial mixing of the high-salinity brines with the low-salinity fluids may have led to the higher salinities locally found in type 1 fluid inclusions. This suggestion is supported by the strong correlation between type 3 fluid inclusions that probably have high Ca contents, as exemplified by the presence of calcite daughter crystals, and the presence of relatively high salinity type 1 fluid inclusions.

Type 1 fluid inclusions in the western part of the Alta stock probably represent residual intergranular fluids exsolved during the late stages of igneous crystallization. These fluids locally circulated through small fractures forming the relatively sparse veins. High-salinity fluids apparently were not formed at depths corresponding to lithostatic pressures greater than about 1,400 bars (approximately 5.2 km). For fluids containing about 10 weight percent NaCl equivalent, this suggests that vapor saturation of the magma did not occur until temperatures fell below about 800 °C (Chou, 1987), which is consistent with the temperatures estimated above for vapor saturation in the eastern parts of the stock.

Most overall fluid-inclusion populations in igneous quartz in the western samples are similar regardless of their proximity to megascopic veins (table 6). Measurements of fluid-inclusion properties in three or more igneous quartz crystals in most samples indicate that there are large differences in the salinities and homogenization temperatures of fluid inclusions contained in different crystals within single samples. These data suggest that most fluid inclusions formed during repeated microfracturing and healing of quartz crystals, and that an intergranular pore fluid was present throughout subsolidus cooling of the stock. A pore fluid also is suggested by the pervasive weak deuteric alteration of the stock.

COMPARISON OF THE EVOLUTION OF HYDROTHERMAL FLUIDS IN THE ALTA STOCK TO PORPHYRY COPPER SYSTEMS

Porphyry copper systems associated with calc-alkaline magmatism are characterized by a number of features that may vary in detail but are distinct enough to have been described as "variations on a common theme" (Gustafson and Hunt, 1975). These features include (1) close association with stocklike, epizonal or subvolcanic granitic bodies that commonly are porphyritic; (2) extensive development of steeply dipping fractures centered on the apical portions of intrusions; and (3) strong hydrothermal alteration centered on the fractured part of the intrusion, including early potassic alteration (biotite and potassium feldspar stable) containing sulfide minerals with high Cu:Fe ratios (chalcopyrite ±

bornite) and later biotite and potassium feldspar-destructive alteration (generally sericitic) containing sulfide minerals with low Cu:Fe ratios (pyrite ± chalcopyrite). Pressure also may vary from early, near-lithostatic values to late, near-hydrostatic values corresponding to a change from dominantly magmatic to dominantly meteoric processes. The hydrothermal system of the Alta stock appears to have evolved in several ways distinct from hydrothermal systems in typical porphyry copper intrusions. These differences include apparent timing of vapor saturation of the crystallizing magma; types and extents of hydrothermal alteration; salinities of vein-forming fluids; interaction of meteoric fluids with the stock; fracturing and fracture permeability of the intrusions; and, most importantly, lack of significant copper mineralization within the stock.

Vapor saturation and fluid exsolution from the crystallizing magma occurred relatively late in the Alta stock, probably at near-solidus temperatures. Late vapor saturation is suggested by the mineral crystallization sequence, the fracture pattern, and the compositions and densities of early fluid inclusions. In most porphyry copper stocks, timing of vapor saturation is poorly known, although generally it is thought to be relatively early (for example, see Burnham, 1979a; Dilles, 1984, 1987). Relatively late vapor exsolution in the Alta stock compared with porphyry copper systems also is consistent with both H_2O solubility in silicate melts, which increases with increasing pressure (Burnham, 1979a, 1985), and the somewhat greater depths of crystallization of the Alta stock (approximately 3.7 to 6.3 km) compared with most porphyry copper systems [for example, Bingham, 1–3 km (Einaudi, 1982); Yerington, 1–2.5 km (Dilles, 1987); Ann Mason (Yerington district), 3–4.5 km (Dilles, 1987); Ely, 2–3 km (James, 1976); El Salvador, 2 km (Gustafson and Hunt, 1975)]. Late vapor saturation and (or) lower initial H_2O contents of the magma of the Alta stock may have led to the low fracture permeability, which resulted in weak fracture-related alteration, inhibited incursion of large volumes of meteoric water into the stock, and allowed pressure to remain near lithostatic values throughout cooling of the stock. Late vapor saturation also may have prevented removal of copper from the melt and formation of copper-rich hydrothermal fluids, as shown by the somewhat high copper contents of biotite, hornblende, and magnetite phenocrysts in the Alta stock compared with copper contents of these minerals in porphyry copper intrusions (Hendry and others, 1985).

Five features of hydrothermal alteration in the Alta stock are notably different from hydrothermal alteration in most intrusion-hosted porphyry copper systems (for example, see Lowell and Guilbert, 1970; Gustafson, 1978). First, hornblende is stable in early alteration assemblages, and large areas of pervasive biotitization are not present. Second, alteration zones, which typically form in porphyry copper systems in areas where one type of fracture-controlled alteration becomes dominant and commonly are more or less concentrically distributed around one or more intrusive phases, are absent in the Alta stock. Most hydrothermal alteration is weak, pervasive deuteric alteration. Fracture-controlled alteration is relatively sparse and nowhere strongly developed, and the same vein assemblages are present throughout the Alta stock (fig. 7). Third, the youngest and most common vein assemblage in the Alta stock is pyrite+chlorite, in contrast to the quartz+sericite+pyrite vein assemblage that occurs in nearly all continental porphyry copper systems. Quartz+sericite+pyrite alteration locally is present in the Alta stock, but it is cut by pyrite+chlorite veins that are much more abundant. Fourth, no argillic or advanced argillic alteration is present in the Alta stock. Finally, the results of reconnaissance stable-isotope studies indicate that meteoric water did not play a significant role in the late stages of the hydrothermal system of the Alta stock. These features suggest that fluid abundance, composition, and circulation patterns in the Alta stock were markedly different from those in "typical" porphyry copper systems.

Early hydrothermal fluids circulating through megascopic fractures in the Alta stock were in equilibrium with an essentially magmatic assemblage (hornblende, potassium feldspar, biotite, magnetite, sphene, and, locally, oligoclase), and over time fluids evolved from compositions that were in equilibrium with biotite and magnetite, similar to early veins in porphyry copper systems, to compositions in equilibrium with combinations of sericite, chlorite, and pyrite. The distribution of vein types (fig. 7) suggests that fluids with similar compositions were present throughout most of the Alta stock at some point during its cooling. It is not possible, however, to determine if different parts of the stock saw identical types of fluids at similar stages of cooling. Also, as a result of the relatively low abundance of fractures, the volume of rock that interacted with these fluids at any location probably was small.

Activity diagrams for the systems CaO-MgO-K_2O-Al_2O_3-SiO_2-H_2O-HCl and MgO-K_2O-Al_2O_3-SiO_2-H_2O-HCl at 1,000 bars and 500 °C and 300 °C, calculated from hydrolysis reactions in Bowers and others (1984), are displayed in figure 29. Early vein assemblages in the Alta stock contain calcic amphibole (hornblende) and (or) epidote, suggesting that they have higher $a_{Ca}{}^{2+}/a^2{}_{H}{}^{+}$ ratios than do typical early vein assemblages in porphyry copper systems, where biotite replaces calcic amphibole (fig. 29*A*). Potassium feldspar+amphibole (actinolitic hornblende) is only stable over a narrow range of $a_{Mg}{}^{2+}/a^2{}_{H}{}^{+}$ and $a_{Ca}{}^{2+}/a^2{}_{H}{}^{+}$, and increasing $a_{Mg}{}^{2+}/a^2{}_{H}{}^{+}$ ratios will result in biotite saturation, whereas increasing $a_{Ca}{}^{2+}/a^2{}_{H}{}^{+}$ ratios will result in formation of clinopyroxene (diop-

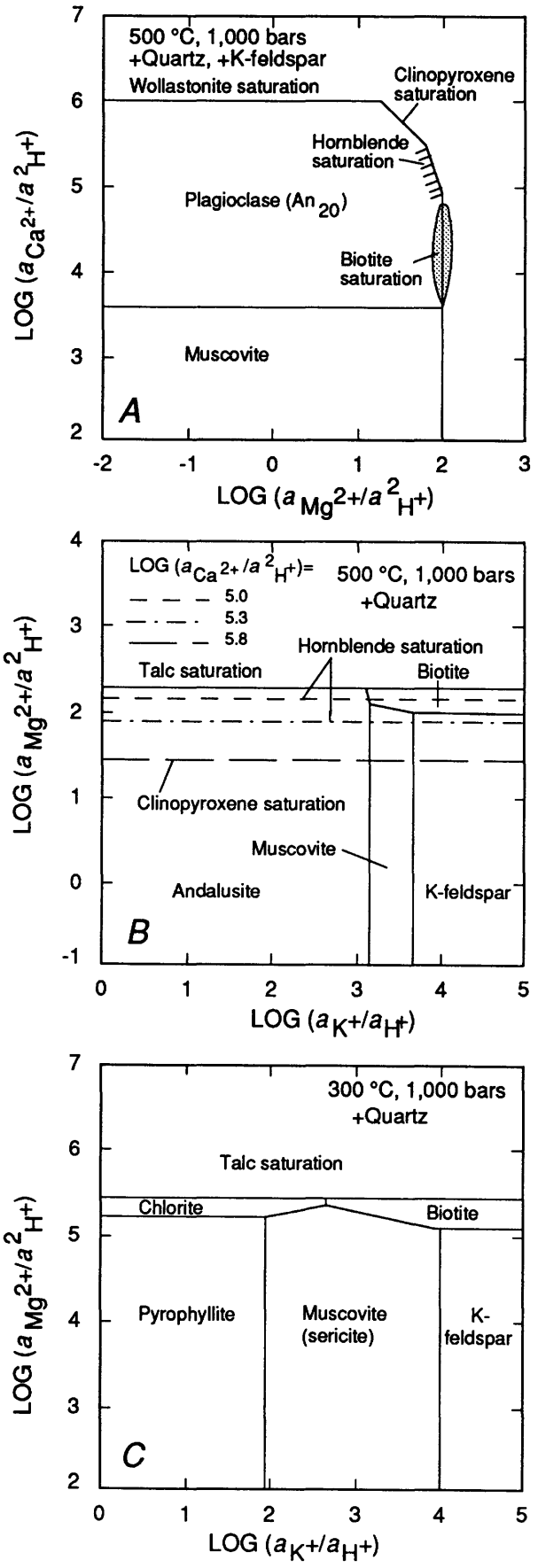

side), which has not been found in the Alta stock (fig. 29*B*). Stoichiometric clinozoisite is unstable at 500 °C, and the presence of epidote in early veins implies significant Fe^{+3} substitution (Bird and Helgeson, 1981). The lack of anhydrite is apparently due to relatively low activity of SO_2 in the fluids.

In the upper part of the Alta stock, either early fluids boiled at hypersolidus temperatures, forming high-salinity brines, or else high-salinity brines were directly exsolved from the crystallizing magma. These brines, however, mostly remained as interstitial pore fluids and did not circulate through fractures. High-salinity fluids also did not lead to the formation of disseminated copper mineralization within the stock, although most silver-lead-zinc fissure and replacement ores in the Cottonwood mining district and the small iron-copper skarns, such as the Big Cottonwood mine, are spatially associated with parts of the stock where high-salinity fluids were present. The behavior of the high-salinity fluids in the Alta stock is quite different from that of most porphyry copper systems, where early fluid inclusions in quartz veins forming potassic alteration generally are of high salinity (for example, see Nash, 1976; Chivas and Wilkins, 1977; Eastoe, 1978; Roedder, 1984), and commonly there is a strong correlation between copper grade and the abundance of high-salinity fluid inclusions (for example, see Moore and Nash, 1974). The lack of high-

◀ **Figure 29.** Activity diagrams for fluids in equilibrium with various vein assemblages in Alta stock. Diagrams are calculated using hydrolysis reactions in Bowers and others (1984), ideal ionic solid-solution models for biotite and amphibole (Bohlen and others, 1980), activity relations from Orville (1972) for plagioclase and Waldbaum and Thompson (1969) for potassium feldspar, and mineral compositions determined by microprobe analyses. All diagrams are for 1,000 bars water pressure. *A*, Log $(a_{Ca}^{2+}/a^2_{H^+})$-log $(a_{Mg}^{2+}/a^2_{H^+})$ diagram for system CaO-MgO-K_2O-Al_2O_3-SiO_2-H_2O-HCl at 500 °C with excess quartz and potassium feldspar and unit activity of water. Hachured field shows possible range of compositions of early fluids forming hornblende-stable veins in Alta stock; stippled field shows possible range of fluid compositions in early alteration in typical porphyry copper systems (biotite replaces hornblende). *B*, Log$(a_{Mg}^{2+}/a^2_{H^+})$-log(a_K^+/a_{H^+}) diagram for system CaO-MgO-K_2O-Al_2O_3-SiO_2-H_2O-HCl at 500 °C with excess quartz and unit activity of water. Biotite+K-feldspar assemblages in porphyry copper systems requires lower $(a_{Ca}^{2+}/a^2_{H^+})$ ratios than in Alta stock, where hornblende+K-feldspar is stable in early veins. *C*, Log $(a_{Mg}^{2+}/a^2_{H^+})$-log(a_K^+/a_{H^+}) diagram for system MgO-K_2O-Al_2O_3-SiO_2-H_2O-HCl at 300 °C with excess quartz and unit activity of water. Chlorite (+pyrite) assemblages in late veins in Alta stock suggest higher $(a_{Mg}^{2+}/a^2_{H^+})$ ratios and (or) lower (a_K^+/a_{H^+}) ratios than in typical porphyry copper systems, where sericite (+pyrite) is stable late assemblage.

salinity fluid inclusions in quartz veins may result from the low fracture permeability and the near-lithostatic pressures, which did not allow hydrothermal fluids to boil. Unlike most porphyry copper systems, late hydrothermal fluids that formed quartz veins in the Alta stock did not have markedly different salinities from early, vein-forming hydrothermal fluids. Late veins in the Alta stock also deposited large amounts of chlorite instead of sericite, which is present in nearly all continental porphyry copper systems. This suggests that late fluids in the Alta stock may have had higher $a_{Mg}{}^{2+}/a^2{}_{H}{}^{+}$ ratios than in typical porphyry copper systems (fig. 23*C*). Late fluids in the Alta stock may have remained undiluted by Mg-poor meteoric water, leading to higher $a_{Mg}{}^{2+}/a^2{}_{H}{}^{+}$ values than for late fluids in typical porphyry copper systems.

SUMMARY AND CONCLUSIONS

The evolution of the hydrothermal system associated with the Alta stock was a complex process that has been partially deciphered through field, petrographic, stable-isotope, fluid-inclusion, and electron-microprobe studies. The Alta stock is a small, composite granodioritic body that was emplaced in two main pulses closely spaced in time. Present exposures represent paleodepths ranging from about 3.7 km on the east to 6.3 km on the west. Compositions of the two intrusions are similar, and the main difference between the two phases is a variable, but generally small, amount of aplitic groundmass that probably resulted from pressure quenching of residual magma of the younger (porphyritic) phase. The magma of both bodies was moderately H_2O rich (probably 3 to 4 weight percent H_2O), as shown by the presence of phenocrystic hornblende and biotite and the lack of pyroxene, but H_2O contents may have been somewhat less than in typical porphyry copper intrusions because biotite crystallized earlier than hornblende. Relatively deep emplacement, strong zones of regional weaknesses, and relatively late vapor saturation of the magma led to low fracture abundance and low fracture permeability and probably prevented the formation of fracture patterns typical of porphyry copper systems (Haynes and Titley, 1980; Burnham, 1985; Titley and others, 1986).

Biotite and amphibole show a wide range of compositions and compositional zoning. Both minerals generally are characterized by decreasing Fe/(Fe+Mg), Ti, and Al during progressive crystallization from early inclusions in plagioclase to phenocrysts to hydrothermal crystals. Compositions and zoning patterns of both minerals are similar to those of minerals reported in porphyry copper deposits and other shallow intrusions (for example, see Jacobs and Parry, 1979; Chivas, 1981; Dilles, 1984, 1987). Biotite compositions and temperatures estimated from its Fe-Ti contents suggest that crystallization occurred under moderately oxidizing conditions, probably slightly above the Ni-NiO oxygen buffer, and that the oxidation state may have slightly increased (less than one log unit) during crystallization. Biotite in the western, deeper part of the stock generally has a higher Fe/(Fe+Mg) ratio than does the eastern, shallower parts of the stock, but calculations suggest that this biotite may have crystallized at a slightly higher oxidation state than the more Mg-rich biotite in the eastern parts of the stock. Generally increasing Mg, Si, and Ca contents in amphibole with crystallization also suggest an increase in the oxidation state during crystallization. Overall amphibole compositional trends are nearly identical to those of the Inamumu zoned pluton, which Chivas (1981) suggested may have crystallized under vapor-saturated conditions.

The compositions and densities of early fluids varied markedly within the Alta stock and were strongly dependent on pressure. At depths less than about 5.2 km, low- to moderate-salinity fluids (probably released during crystallization of magma) boiled, forming low-density vapor and high-density, high-salinity (35 to 70 weight percent NaCl equivalent) brine phases; alternatively, a high-salinity brine was directly exsolved from the crystallizing magma. Maximum salinities of fluid inclusions in this part of the stock suggest that vapor saturation of the crystallizing magma may have occurred at temperatures between about 725 °C and 770 °C. At depths greater than about 5.2 km, early fluids were supercritical and of low to moderate salinity (<12 weight percent NaCl equivalent), and there is no fluid-inclusion evidence for the presence of fluids at temperatures greater than approximately 720 °C.

Hydrothermal alteration is characterized by pervasive, generally weak deuteric alteration and only weak fracture-controlled alteration. Deuteric alteration generally consists of partial to complete chloritization of biotite, partial sericitization of plagioclase, and formation of turbid perthite crystals. Oxygen-isotope fractionation between quartz and potassium feldspar, δD values for biotite and chlorite, fluid-inclusion data, and two-feldspar thermometry suggest that deuteric alteration occurred at temperatures around 500 °C probably from magmatically derived fluids. In particular, deuterium enrichment of chlorite by about 10 to 30 permil relative to fresh biotite suggests that little meteoric water circulated through the Alta stock during deuteric alteration. The lack of meteoric water probably is due to the relatively low fracture permeability of the Alta stock. Fracture abundance is about an order of magnitude lower than in the nearby Mayflower stock (Villas and Norton, 1977) and considerably lower than measured in the proximity of porphyry copper deposits (Haynes and Titley, 1980; Titley and others, 1986).

A wide variety of veins formed during cooling of the Alta stock. Early veins were calcic-amphibole (hornblende)+K-feldspar+sphene±quartz±magnetite± epidote. These were followed by epidote ± magnetite ± pyrite, biotite+magnetite±K-feldspar ± quartz ± sulfide minerals, quartz±K-feldspar, quartz+pyrite±sericite, quartz+pyrite+chlorite, and pyrite+chlorite veins. Little wall-rock alteration is associated with the veins. Pyrite+chlorite veins are the most abundant type. All veins predominantly have northeast orientations that parallel regional structures. Fluid inclusions in these veins suggest that all veins except pyrite+chlorite may have formed initially at similar temperatures between about 465 °C and 535 °C from low- to moderate-salinity (≤10 weight percent NaCl equivalent) nonboiling fluids. Early high-salinity fluids in the upper part of the stock apparently did not widely circulate through fractures and remained as intergranular fluids. The $\delta^{18}O$ values of quartz from quartz+pyrite+sericite and quartz+pyrite+chlorite veins and the δD value of chlorite in a quartz+pyrite+chlorite vein also suggest that fluids forming these veins were derived from magmatic sources.

There are several major differences in the evolution of the hydrothermal system of the Alta stock compared with that of typical porphyry copper intrusions. These include (1) relatively low fracture abundance and low fracture permeability, resulting in relatively weak fracture-controlled alteration in the Alta stock; (2) early amphibole-stable veins and relatively little biotite replacement of hornblende, suggesting that early fluids in the Alta stock had relatively high $a_{Ca}{}^{2+}/a^2{}_{H}{}^{+}$ ratios compared with early fluids in porphyry copper systems; (3) widespread late pyrite+chlorite veins in the Alta stock instead of quartz+pyrite±sericite veins, suggesting that late fluids had higher $a_{Mg}{}^{2+}/a^2{}_{H}{}^{+}$ ratios than in most porphyry copper systems; (4) a general lack of high-salinity fluid inclusions in quartz veins in the Alta stock despite abundant high-salinity fluid inclusions in igneous quartz in the upper parts of the stock; (5) similar salinities and pressure-corrected homogenization temperatures of fluid inclusions in all types of quartz veins, regardless of age, in the Alta stock; (6) the lack of isotopic evidence for the interaction of meteoric water during the late stages of alteration (quartz+pyrite±sericite and pyrite+chlorite veins) in the Alta stock, again probably resulting from the low fracture permeability; and (7) no evidence for a change in the pressure regime from early lithostatic pressures to late hydrostatic pressures. These differences mostly result from the slightly greater depths of emplacement and possibly the lower initial water contents of the Alta stock, which resulted in relatively late vapor saturation of the magma and did not allow development of an extensive fracture system typical of porphyry copper systems. Late vapor saturation of the magma may have prevented removal of copper from the melt and concentration of it in hydrothermal fluids

REFERENCES CITED

Ague, J. J., and Brimhall, G. H., 1988, Regional variations in bulk chemistry, mineralogy, and the compositions of mafic and accessory minerals in the batholiths of California: Geological Society of America, v. 100, p. 891–911.

Aiken, S.A., 1982, Magmatic history, alteration, and mineralization of the Clayton Peak stock, Utah: Baltimore, Md., Johns Hopkins University, Ph.D. thesis, 255 p.

Barriere, M., and Cotten, J., 1979, Biotites and associated minerals as markers of magmatic fractionation and deuteric equilibration in granites: Contributions to Mineralogy and Petrology, v. 70, p. 183–192.

Baker, A.A., Calkins, F.C., Crittenden, M.D., and Bromfield, C.S., 1966, Geologic map of the Brighton quadrangle, Utah: U.S. Geological Survey Geologic Quadrangle Map GQ-534, scale 1:24,000.

Belt, C.B., Jr., 1969, Preliminary geochemical study of the Alta and Clayton Peak intrusives: Utah Geological and Mineralogical Survey Bulletin, v. 82, p. 111–124.

Bigeleisen, J., Perlman, M.L., and Prosser, H.C., 1952, Conversion of hydrogenic materials to hydrogen for isotopic analysis: Analytical Chemistry, v. 24, p. 1356–1362.

Bird, D.K., and Helgeson, H.C., 1981, Chemical interaction of aqueous solutions with epidote-feldspar mineral assemblages in geologic systems. II. Equilibrium constraints in metamorphic/geothermal processes: American Journal of Science, v. 281, p. 576–614.

Bodnar, R.J., Burnham, C.W., and Sterner, S.M., 1985, Synthetic fluid inclusions in natural quartz: III. Determination of phase equilibrium properties in the system H_2O-NaCl to 1000°C and 1500 bars: Geochimica et Cosmochimica Acta, v. 49, p. 1861–1873.

Bohlen, S.R., Peacor, D.R., and Essene, E.J., 1980, Crystal chemistry of a metamorphic biotite and its significance in water barometry: American Mineralogist, v. 65, p. 55–62.

Borthwick, J., and Harmon, R.S., 1982, A note regarding ClF_3 as an alternative to oxygen isotope analysis: Geochimica et Cosmochimica Acta, v. 46, p. 1665–1668.

Bottinga, Y., and Javoy, M., 1973, Comments on oxygen isotope geothermometry: Earth and Planetary Science Letters, v. 20, p. 250–265.

——— 1975, Oxygen isotope partitioning among the minerals in igneous and metamorphic rocks: Reviews in Geophysics and Space Physics, v. 13, p. 401–408.

Bowers, T.S., Jackson, K.J., and Helgeson, H.C., 1984, Equilibrium Activity Diagrams: New York, Springer-Verlag, 397 p.

Bowman, J.R., and Cook, S.J., 1981, Physical-chemical conditions of contact skarn formation at Alta, Utah [abs.]: Geological Society of America Abstracts with Programs, v. 13, p. 414.

Bowman, J.R., Parry, W.T., Kropp, W.P., and Kruer, S.A., 1987, Chemical and isotopic evolution of hydrothermal solutions at Bingham, Utah: Economic Geology, v. 82, p. 395–428.

Bozzo, A.T., Chen, J.R., Kass, J.R., and Barduhn, A.J., 1975, The properties of hydrates of chlorine and carbon dioxide: Desalination, v.16, p. 303–320.

Brigham, R.H., 1984, K-feldspar genesis and stable isotope relations of the Papoose Flat pluton, Inyo Mountains, California: Stanford, Calif., Stanford University, Ph.D. thesis, 172 p.

Bromley, K.S., Bowman, J.R., and Parry, W.T., 1985, A stable isotope study of the Wasatch fault zone at Corner Creek, Utah [abs.]: Eos (American Geophysical Union, Transactions), v. 66, p. 1066.

Brown, W. L., and Parsons, I., 1981, Towards a more practical two-feldspar geothermometer: Contributions to Mineralogy and Petrology, v. 76, p. 321–335.

Burnham, C.W., 1979a, Magmas and hydrothermal fluids, *in* Barnes, H.L., ed., Geochemistry of hydrothermal ore deposits (2nd ed.): New York, Wiley-Interscience, p. 71-136.

——— 1979b, The importance of volatile constituents, *in* Yoder, H.S., Jr., ed., The evolution of the igneous rocks fiftieth anniversary perspectives: Princeton, N.J., Princeton University Press, p. 439–482.

——— 1981, Physicochemical constraints on porphyry mineralization, *in* Dickinson, W.R. and Payne, W.D., eds., Relations of tectonics to ore deposits in the southern Cordillera: Arizona Geological Society Digest, v. 14, p. 71–77.

——— 1985, Energy release in subvolcanic environments: Implications for breccia formation: Economic Geology, v. 80, p. 1515–1522.

Burnham, C.W., Holloway, J.R., and Davis, N.F., 1969, Thermodynamic properties of water to 1,000°C and 10,000 bars: Geological Society of America Special Paper 132, 96 p.

Burnham, C.W. and Ohmoto, H., 1980, Late-stage processes of felsic magmatism: Mining Geology, Special Issue 8, p. 1–11.

Burruss, R.C., 1981, Analysis of phase equilibria in C-O-H-S fluid inclusions, *in* Hollister, L.S., and Crawford, M.L., eds., Short course in fluid inclusions: Applications to petrology: Calgary, Mineralogical Association of Canada, p. 39–74.

Calkins, F.C., and Butler, B.S., 1943, Geology and ore deposits of the Cottonwood–American Fork area: U.S. Geological Survey Professional Paper 201, 152 p.

Candela, P.A., 1986, The evolution of aqueous vapor from silicate melts: Effect on oxygen fugacity: Geochimica et Cosmochimica Acta, v. 50, p. 1205–1211.

Chivas, A.R., 1981, Geochemical evidence for magmatic fluids in porphyry copper mineralization. Part I. Mafic silicates from the Koloula Igneous Complex: Contributions to Mineralogy and Petrology, v. 78, p. 389–403.

Chivas, A.R., and Wilkins, R.W.T., 1977, Fluid inclusion studies in relation to hydrothermal alteration and mineralization at the Koloula porphyry copper prospect, Guadalcanal: Economic Geology, v. 72, p. 153–169.

Chou, I-Ming, 1978, Calibration of oxygen buffers at elevated *P* and *T* using the hydrogen fugacity sensor: American Mineralogist, v. 63, p. 690–703.

——— 1987, Phase relations in the system NaCl-KCl-H_2O. III: Solubilities of halite in vapor-saturated liquids above 445°C and redetermination of phase equilibrium properties in the system NaCl-H_2O to 1000°C and 1500 bars: Geochimica et Cosmochimica Acta, v. 51, p. 1965-1975.

Clayton, R.N., and Mayeda, T.K., 1963, The use of bromine pentafluoride in the extraction of oxygen from oxides and silicates for isotopic analysis: Geochimica et Cosmochimica Acta, v. 27, p. 43–52.

Cloke, P.L., and Kesler, S.E., 1979, The halite trend in hydrothermal solutions: Economic Geology, v. 74, p. 1823–1831.

Craig, H, 1961, Isotopic variations in meteoric waters: Science, v. 133, p. 1702–1703.

Cranor, J.I., 1974, Petrology and geochemistry of the calc-silicate zone adjacent to the Alta and Clayton Peak stocks near Brighton, Utah: Brigham Young University Geological Studies, v. 21, p. 151–176.

Crawford, M.L., Krauss, D.W., and Hollister, L.W., 1979, Petrologic and fluid inclusion study of calc-silicate rocks, Prince Rupert, British Columbia: American Journal of Science, v. 279, p. 1135-1159.

Criss, R.E., and Taylor, H.P., 1983, An $^{18}O/^{16}O$ and D/H study of Tertiary hydrothermal systems in the southern half of the Idaho batholith: Geological Society of America Bulletin, v. 94, p. 640–663.

Crittenden, M.D., Jr., 1965, Geologic map of the Dromedary Peak quadrangle, Utah: U.S. Geological Survey Geologic Quadrangle Map GQ-378, scale 1:24,000.

Czamanske, G.K., Ishihara, S., and Aiken, S.A., 1981, Chemistry of rock-forming minerals of the Cretaceous-Paleocene batholith in southwestern Japan and implications for magma genesis: Journal of Geophysical Research, v. 86, p. 10431–10469.

Czamanske, G.K., and Moore, W.J., 1973, Compositions of biotites from unaltered and altered monzonitic rocks in the Bingham mining district: Economic Geology, v. 68, p. 269–274.

Czamanske, G.K., and Wones, D.R., 1973, Oxidation during magmatic differentiation, Finnmarka Complex, Oslo area, Norway: Part 2, the mafic silicates: Journal of Petrology, v. 14, p. 349–380.

Dilles, J.H., 1984, The petrology and geochemistry of the Yerington batholith and the Ann-Mason porphyry copper deposit, western Nevada: Stanford, Calif., Stanford University, Ph.D. thesis, 389 p.

——— 1987, Petrology of the Yerington batholith, Nevada: Evidence for evolution of porphyry copper ore fluids: Economic Geology, v. 82, p. 1750–1789.

Dodge, F.C.W., Papike, J.J., and Mays, R.E., 1968, Hornblendes from granitic rocks of the central Sierra Nevada batholith, California: Journal of Petrology, v. 9, p. 378–410.

Dodge, F.C.W., and Ross, D.C., 1971, Coexisting hornblendes and biotites from granitic rocks near the San Andreas fault, California: Journal of Geology, v. 79, p. 158–172.

Dodge, F.C.W., Smith, V.C., and Mays, R.E., 1969, Biotites from granitic rocks of the central Sierra Nevada batholith, California: Journal of Petrology, v. 10, p. 250–271.

Eastoe, C.J., 1978, A fluid inclusion study of the Panguna porphyry copper deposit, Bougainville, Papua New Guinea: Economic Geology. v. 73, p. 721–748.

Einaudi, M.T., 1982, General features and origin of skarns as-

sociated with porphyry copper plutons, southwestern North America, *in* Titley, S. R., ed. Advances in geology of the porphyry copper deposits, southwestern North America: Tucson, Ariz., University of Arizona Press, p. 185–209.

Fournier, R.O., 1983, Active hydrothermal systems as analogues of fossil systems: Geothermal Resources Council, Special Report 13, p. 263–284.

Graham, C.M., Viglino, J.A., and Harmon, R.S., 1987, Experimental study of hydrogen-isotope exchange between aluminous chlorite and water and of hydrogen diffusion in chlorite: American Mineralogist, v. 72, p. 566-579.

Gunter, W.D., Chou, I., and Girsperger, S., 1983, Phase relations in the system NaCl-KCl-H_2O II: Differential thermal analysis of the halite liquidus in the NaCl-H_2O binary above 450°C: Geochimica et Cosmochimica Acta, v. 47, p. 863–873.

Gustafson, L.B., 1978, Some major factors of porphyry copper genesis: Economic Geology, v. 73, p. 600–607.

Gustafson, L.B., and Hunt, J.P, 1975, The porphyry copper deposit at El Salvador, Chile: Economic Geology, v. 70, p. 856–912.

Haas, J.W., 1976, Physical properties of the coexisting phases and thermochemical properties of the H_2O component in boiling NaCl solutions: U.S. Geological Survey Bulletin 1421-A, 73 p.

Hammarstrom, J.M., and Zen, E-an, 1986, Aluminum in hornblende: An empirical igneous geothermometer: American Mineralogist, v. 71, p. 1297–1313.

Harris, C., 1986, A quantitative study of magmatic inclusions in the plutonic ejecta of Ascensión Island: Journal of Petrology, v. 27, p. 251–276.

Haynes, F.M., and Titley, S.R., 1980, The evolution of fracture-related permeability within the Ruby Star Granodiorite, Sierrita porphyry copper deposit, Pima County, Arizona: Economic Geology, v. 75, p. 673-683.

Helz, R.T., 1982, Phase relations and compositions of amphiboles produced in studies of the melting behavior of rocks, *in* Veblen, D.R., and Ribbe, P.H., eds., Amphiboles: Petrology and experimental phase relations, v. 9B *of* Reviews in Mineralogy: Washington, D.C., Mineralogical Society of America, p. 279–353.

Hendry, D.A.F., Chivas, A.R., Long, J.V.P., and Reed, S.J.B., 1985, Chemical differences between minerals from mineralizing and barren intrusions from some North American porphyry copper deposits: Contributions to Mineralogy and Petrology, v. 89, p. 317–329.

Henley, R.W., and McNabb, A., 1978, Magmatic vapor plumes and ground-water interaction in porphyry copper emplacement: Economic Geology, v. 73, p. 1–20.

Hildreth, W., 1979, The Bishop Tuff: Evidence for the origin of compositional zonation in silicic magma chambers: Geological Society of America Special Paper 180, p. 43–75.

Hintze, L.F., compiler, 1980, Geologic map of Utah: Salt Lake City, Utah Geological and Mineralogical Survey, scale 1:500,000.

Hollister, L.S., Griscom, G.C., Peters, E.K., Stowell, H.H., and Sisson, V.B., 1987, Confirmation of the empirical correlation of Al in hornblende with pressure of solidification of calc-alkaline plutons: American Mineralogist, v. 72, p. 231–239.

Huebner, J.S., and Sato, M., 1970, The oxygen fugacity–temperature relationships of manganese oxide and nickel oxide buffers: American Mineralogist, v. 55, p. 934–952.

Jacobs, D.C., and Parry, W.T., 1979, Geochemistry of biotite in the Santa Rita porphyry copper deposit, New Mexico: Economic Geology, v. 74, p. 860–887.

Jahns, R.H., and Tuttle, O.F., 1964, Layered pegmatite-aplite intrusives: Mineralogical Society of America Special Paper No. 1, p. 78–92.

James, L.P., 1976, Zonal alteration in limestone at porphyry copper deposits, Ely, Nevada: Economic Geology, v. 71, p. 488–512.

——— 1978, Geology, ore deposits, and history of the Big Cottonwood mining district, Salt Lake County, Utah: Utah Geological and Mineral Survey Bulletin 114, 98 p.

John, D.A., 1987, Evolution of hydrothermal fluids in intrusions of the central Wasatch Mountains, Utah: Stanford, Calif., Stanford University, Ph.D. thesis, 236 p.

——— 1989, Geologic setting, depths of emplacement, and regional distribution of fluid inclusions in intrusions of the central Wasatch Mountains, Utah: Economic Geology, v. 84, p. 386–409.

Johnson, M.C., and Rutherford, M.J., 1989a, Experimentally determined conditions in the Fish Canyon Tuff, Colorado, magma chamber: Journal of Petrology, v. 30, p. 711–737.

——— 1989b, Experimental calibration of the aluminum-in-hornblende geobarometer with application to Long Valley caldera (California) volcanic rocks: Geology, v. 17, p. 837–841.

Kemp, W.W., III, and Bowman, J.R., 1984, A stable isotope and fluid inclusion study of contact Al(Fe)-Ca-Mg-Si skarns in the Alta stock aureole, Alta, Utah [abs.]: Geological Society of America Abstracts with Programs, v. 16, p. 558.

Kwak, T.A.P., and Tan, T.H., 1981, The importance of $CaCl_2$ in fluid composition trends—evidence from the King Island (Dolphin) skarn deposit: Economic Geology, v. 76, p. 955–960.

Lagache, M., and Weisbrod, A., 1977, The system: two alkali feldspars-KCl-NaCl-H_2O at moderate to high temperatures and low pressures: Contributions to Mineralogy and Petrology, v. 62, p. 77–101.

Lanier, G., Raab, W.J., Folsom, R.B., and Cone, S., 1978, Alteration of equigranular monzonite, Bingham mining district, Utah: Economic Geology, v. 73, p. 1270–1286.

Leake, B.E., 1968, A catalog of analyzed califerous and subcaliferous amphiboles together with their nomenclature and associated minerals: Geological Society of America Special Paper 98, 210 p.

——— 1978, Nomenclature of amphiboles: American Mineralogist, v. 63, p. 1023-1052.

Lipman, P.W., 1971, Iron-titanium oxide phenocrysts in compositionally zoned ash-flow sheets from southern Nevada: Journal of Geology, v. 79, p. 438–456.

Lowell, J.D., and Guilbert, J.M., 1970, Lateral and vertical alteration-mineralization zoning in porphyry ore deposits: Economic Geology, v. 65, p. 378–408.

Luhr, J. F., Carmichael, I. S. E., and Varekamp, J. C., 1984,

The 1982 eruptions of El Chichon volcano, Chiapas, Mexico: Mineralogy and petrology of the anhydrite-bearing pumices: Journal of Volcanology and Geothermal Research, v. 23, p. 69–108.

Mason, D.R., 1978, Compositional variations in ferromagnesium minerals from porphyry copper-generating and barren intrusions of the Western Highlands, Papua, New Guiena: Economic Geology, v. 73, p. 878–890.

Moore, J.N., and Kerrick, D.M., 1976, Equilibria in siliceous dolomites of the Alta aureole, Utah: American Journal of Science, v. 276, p. 502–524.

Moore, W.J., and Nash, J.T., 1974, Alteration and fluid inclusion studies of the porphyry copper ore body at Bingham, Utah: Economic Geology, v. 69, p. 631–645.

Murakami, N., 1969, Two contrastive trends of evolution of biotite in granitic rocks: Journal of the Japanese Association of Mineralogists, Petrologists, and Economic Geologists, v. 62, p. 223–247.

Nabelek, P.I., O'Neil, J.R., and Papike, J.J., 1983, Vapor phase exsolution as a controlling factor in hydrogen isotope variation in granitic rocks: The Notch Peak granitic stock, Utah: Earth and Planetary Science Letters, v. 66, p. 137–150.

Naney, M.T., 1983, Phase equilibria of rock-forming ferromagnesium silicates in granitic systems: American Journal of Science, v. 283, p. 993–1033.

Nash, J.T., 1976, Fluid-inclusion petrology—data from porphyry copper deposits and applications to exploration: U.S. Geological Survey Professional Paper 907D, 16 p.

——— 1982, Petrology of igneous rocks and wall rock alteration, Mayflower mine, Wasatch County, Utah. Part 1: Primary rock and mineral compositions: U.S. Geological Survey Open-File Report 82-1056, 54 p.

Norton, D., and Knapp, R., 1977, Transport phenomena in hydrothermal systems: The nature of porosity: American Journal of Science, v. 277, p. 913–936.

Orville, P.M., 1972, Plagioclase cation exchange equilibria with aqueous chloride solution: American Journal of Science, v. 272, p. 259–272.

Piwinskii, A.J., 1968, Experimental studies of igneous rock series, central Sierra Nevada batholith, California: Journal of Geology, v. 76, p. 548–570.

Potter, R.W., II, and Brown, D.L., 1977, The volumetric properties of aqueous sodium chloride solutions from 0° to 500°C at pressures up to 2000 bars based on a regression of available data in the literature: U.S. Geological Survey Bulletin 1421-C, 36 p.

Potter, R.W., and Clynne, M.A., 1978, Solubility of highly soluble salts in aqueous media—part 1, NaCl, KCl, $CaCl_2$, Na_2SO_4, and K_2SO_4 solubilities to 100°C: U.S. Geological Survey Journal of Research, v. 5, p. 389–395.

Potter, R.W., II, Clynne, M.A., and Brown, D.L., 1978, Freezing point depressions of aqueous sodium chloride solutions: Economic Geology, v. 73, p. 284–285.

Roedder, E., 1971, Fluid inclusion studies on the porphyry-type ore deposits at Bingham, Utah, Butte, Montana, and Climax, Colorado: Economic Geology, v. 66, p. 98-120.

——— 1984, Fluid inclusions, v. 12 *of* Reviews in Mineralogy: Washington, D.C., Mineralogical Society of America, 644 p.

Roedder, E., and Bodnar, R.J., 1980, Geologic pressure determinations from fluid inclusion studies: Annual Review of Earth and Planetary Sciences, v. 8, p. 263–301.

Roedder, Edwin, and Coombs, D.S., 1967, Immiscibility in granitic melts indicated by fluid inclusions in ejected granite blocks from Ascensión Island: Journal of Petrology, v. 8, p. 417–451.

Smith, R.K., 1972, The mineralogy and petrology of the contact metamorphic aureole around the Alta stock, Utah: Iowa City, University of Iowa, Ph.D. thesis, 215 p.

Snow, D.T., 1970, The frequency and apertures of fractures in rocks: International Journal of Rock Mechanical Mining Science, v. 7, p. 23–40.

Sourirajan, S., and Kennedy, G.C., 1962, The system H_2O-NaCl at elevated temperatures and pressures: American Journal of Science, v. 260, p. 115–141.

Sterner, S.M., and Bodnar, R.J., 1986, Experimental determination of phase relations in the system NaCl-KCl-H_2O at 1 kbar and 700° and 800°C using synthetic fluid inclusions [abs.]: Geological Society of America Abstracts with Programs, v. 18, p. 763.

Sterner, S.M., Hall, D.L., and Bodnar, R.J., 1988, Synthetic fluid inclusions. V. Solubility relations in the system NaCl-KCl-H_2O under vapor-saturated conditions: Geochimica et Cosmochimica Acta, v. 52, p. 989–1006.

Stewart, D.B. and Potter, R.W., II, 1979, Application of physical chemistry of fluids in rock salt at elevated temperature and pressure to repositories for radioactive waste, *in* McCarthy, G.J., ed., Scientific basis for nuclear waste management: New York, Plenum Press, v. 1, p. 297–311.

Streckeisen, A.L., 1976, To each plutonic rock its proper name: Earth Science Reviews, v. 12, p. 1–33.

Suzuoki, T., and Epstein, S., 1976, Hydrogen isotope fractionation between OH-bearing minerals and water: Geochimica et Cosmochimica Acta, v. 40, p. 1229-1240.

Taylor, B.E., 1988, Degassing of rhyolitic magmas: Hydrogen isotope evidence and implications for magmatic-hydrothermal ore deposits, *in* Taylor, R.P., and Strong, D.F., eds., Recent advances in geology of granite-related mineral deposits: Montreal, The Canadian Institute of Mining and Metallurgy, Special Volume 39, p. 33–49.

Taylor, H.P., Jr., 1968, The oxygen isotope geochemistry of igneous rocks: Contributions to Mineralogy and Petrology, v. 19, p. 1–71.

——— 1974, The application of oxygen and hydrogen isotope studies to problems of hydrothermal alteration and ore deposition: Economic Geology, v. 69, p. 843–883.

Titley, S.R., 1982, The style and progress of mineralization and alteration in porphyry copper systems: American Southwest, *in* Titley, S.R., ed., Advances in geology of the porphyry copper deposits, southwestern North America: Tucson, Ariz., University of Arizona Press, p. 93–116.

Titley, S.R., Thompson, R.C., Haynes, F.M., Manske, S.L., Robison, L.C., and White, J.L., 1986, Evolution of fractures and alteration in the Sierrita-Esperanza hydrothermal system, Pima County, Arizona: Economic Geology, v. 81, p. 243–270.

Urusova, M.A., 1975, Volume properties of aqueous solutions

of sodium chloride at elevated temperatures and pressures: Russian Journal of Inorganic Chemistry, v. 20, p. 1717-1721.

Villas, R.N., and Norton, D., 1977, Irreversible mass transfer between circulating hydrothermal fluids and the Mayflower stock: Economic Geology, v. 72, p. 1471–1504.

Waldbaum, D.R., and Thompson, J.B., Jr., 1969, Mixing properties of sanidine crystalline solutions: IV. Phase diagrams from equations of state: American Mineralogist, v. 54, p. 1274–1298.

Whitney, J.A., and Stormer, J.C., Jr., 1977, The distribution of $NaAlSi_3O_8$ between coexisting microcline and plagioclase and its effect on thermometric calculation: American Mineralogist, v. 62, p. 687-691.

——— 1985, Mineralogy, petrology, and magmatic conditions from the Fish Canyon Tuff, Central San Juan volcanic field, Colorado: Journal of Petrology, v. 26, p. 726–762.

Wilson, J.C., 1961, Geology of the Alta stock, Utah: Pasadena, Calif., California Institute of Technology, Ph.D. thesis, 236 p.

Wilson, J.W.J., Kesler, S.E., Cloke, P.C., and Kelly, W.C., 1980, Fluid inclusion geochemistry of the Granisle and Bell porphyry copper deposits: Economic Geology, v. 75, p. 45–61.

Wones, D.R., 1972, Stability of biotite: A reply: American Mineralogist, v. 57, p. 316–317.

——— 1981, Mafic silicates as indicators of intensive variables in granitic magmas: Mining Geology, v. 31, p. 191–212.

——— 1989, Significance of the assemblage titanite + magnetite + quartz in granitic rocks: American Mineralogist, v. 74, p. 744–749.

Wones, D.R., and Eugster, H.P., 1965, Stability of biotite: Experiment, theory and application: American Mineralogist, v. 50, p. 1228–1272.

Zhang, Yi-Gang, and Frantz, J.D., 1987, Determination of the homogenization temperatures and densities of supercritical fluids in the system NaCl-KCl-$CaCl_2$-H_2O using synthetic fluid inclusions: Chemical Geology, v. 64, p. 335–350.

APPENDIX 1. DESCRIPTIONS OF SAMPLES USED IN FLUID-INCLUSION STUDIES

83-PC-37A: 1-cm aplite dikelet cutting equigranular phase of Alta stock, with weak deuteric alteration in stock; aplite has 4–5 mm aplitic quartz+K-feldspar center line with 3-mm graphic intergrowths of quartz and K-feldspar on either side; fluid inclusions—moderately abundant types 1, 2, and 3 [type 3 have several birefringent daughter minerals including calcite(?)] in both aplite and host rock

83-PC-148: Equigranular phase with generally weak deuteric alteration; cut by 1-mm-wide quartz+biotite+magnetite+chalcopyrite vein; biotite largely chloritized; fluid inclusions—both igneous and vein quartz have moderately abundant type 1

83-PC-151: Pod of quartz+K-feldspar pegmatite in equigranular phase; fluid inclusions—abundant type 1 and sparse type 3, with some type 3 having sylvite daughters in addition to halite

83-PC-152: Equigranular phase, weak deuteric alteration; cut by 2 mm quartz+pyrite+chlorite vein (trace epidote and chalcopyrite) with stronger sericite and chlorite alteration along vein edge; fluid inclusions—igneous quartz has sparse type 1, and vein quartz moderately abundant type 1

83-PC-163: Porphyritic phase, moderate deuteric alteration; cut by 7-mm vuggy quartz+K-feldspar vein with vug-filling pyrite; fluid inclusions—both igneous and vein quartz have moderately abundant type 1

83-PC-177: Equigranular phase, weak to moderate deuteric alteration; cut by 1-mm quartz+biotite+magnetite vein, with biotite largely chloritized; fluid inclusions—igneous quartz has sparse types 1, 2, and 3, and vein quartz sparse type 1

83-PC-253: Equigranular phase, moderate deuteric alteration; cut by 1-cm quartz+hornblende+K-feldspar+sphene vein, with quartz interstitial to euhedral hornblende, K-feldspar strongly perthitic; plagioclase phenocrysts along vein margin overgrown with K-feldspar; fluid inclusions—both igneous and vein quartz have abundant type 1

83-PC-274: Porphyritic phase, generally weak deuteric alteration; cut by 2–3 mm quartz+(actinolite) vein with thin K-feldspar center line; weak sericitic alteration along vein margin; fluid inclusions—both igneous and vein quartz have abundant types 1 and 3 and sparse type 2

83-PC-275: Equigranular phase, moderate deuteric alteration, biotite partially replaces hornblende; cut by 5–7 mm vuggy quartz+pyrite vein with 1-cm sericitic selvage; fluid inclusions—igneous quartz has sparse types 1 and 3, and vein quartz sparse type 1

83-PC-276: Subporphyritic (same outcrop as 83-PC-275), weak deuteric alteration; cut by 3-mm vuggy quartz vein with thin K-feldspar center line; biotite weakly chloritized along vein edge; fluid inclusions—igneous quartz has moderately abundant types 1 and 3, and vein quartz sparse type 1

83-PC-279: Equigranular phase, weak deuteric alteration; cut by 5 mm, vuggy quartz+pyrite+chlorite vein (pyrite+chlorite may be late vug filling), trace calcite in vugs, moderate to strong sericitic alteration along vein

edge; fluid inclusions—both igneous and vein quartz have sparse type 1

83-PC-292: Equigranular phase, weak to strong deuteric alteration; cut by 2-mm quartz+hornblende+K-feldspar+sphene vein, with quartz interstitial to euhedral hornblende and sphene; fluid inclusions—igneous quartz has sparse type 1, and vein quartz moderately abundant type 1

83-PC-312: Equigranular phase, weak to moderate deuteric alteration; cut by 1-cm granular quartz vein with weak sericitic envelope; fluid inclusions—igneous quartz has moderately abundant type 1 and sparse type 4, and vein quartz abundant type 1 and sparse type 4

83-PC-315: Equigranular phase, weak to strong deuteric alteration; cut by two veins: (1) 5-mm quartz+K-feldspar aplite that was opened and filled by (2) 5-mm quartz+biotite+epidote+magnetite+chalcopyrite+molybdenite vein; fluid inclusions—both igneous and vein quartz have moderately abundant type 1 and sparse type 4

81-PC-11: Porphyritic phase, moderate deuteric alteration; fluid inclusions—sparse type 1

82-PC-27: Porphyritic phase, moderate deuteric alteration; fluid inclusions—sparse type 1

82-PC-51: Fine-grained, equigranular phase, weak to moderate deuteric alteration; fluid inclusions—moderately abundant types 1, 2, and 3

82-PC-58: Equigranular phase, weak to moderate deuteric alteration; fluid inclusions—moderately abundant type 1

84-PC-36: Equigranular phase, generally moderate deuteric alteration; cut by 3-mm quartz+pyrite+chlorite+(epidote) vein with weak sericitic envelope; fluid inclusions—igneous quartz has abundant types 1, 2, and 3, and vein quartz abundant type 1

S-30: Equigranular phase, moderate deuteric alteration; fluid inclusions—abundant types 1 and 3, sparse type 2

S-38: Equigranular phase, generally weak deuteric alteration; fluid inclusions—abundant types 1, 2, and 3

84-PC-40: 4–5 cm vuggy granular quartz+(pyrite) vein with broad sericitic envelope cutting sample S-38; fluid inclusions—sparse to abundant type 1

SELECTED SERIES OF U.S. GEOLOGICAL SURVEY PUBLICATIONS

Periodicals

Earthquakes & Volcanoes (issued bimonthly).
Preliminary Determination of Epicenters (issued monthly).

Technical Books and Reports

Professional Papers are mainly comprehensive scientific reports of wide and lasting interest and importance to professional scientists and engineers. Included are reports on the results of resource studies and of topographic, hydrologic, and geologic investigations. They also include collections of related papers addressing different aspects of a single scientific topic.

Bulletins contain significant data and interpretations that are of lasting scientific interest but are generally more limited in scope or geographic coverage than Professional Papers. They include the results of resource studies and of geologic and topographic investigations; as well as collections of short papers related to a specific topic.

Water-Supply Papers are comprehensive reports that present significant interpretive results of hydrologic investigations of wide interest to professional geologists, hydrologists, and engineers. The series covers investigations in all phases of hydrology, including hydrogeology, availability of water, quality of water, and use of water.

Circulars present administrative information or important scientific information of wide popular interest in a format designed for distribution at no cost to the public. Information is usually of short-term interest.

Water-Resources Investigations Reports are papers of an interpretive nature made available to the public outside the formal USGS publications series. Copies are reproduced on request unlike formal USGS publications, and they are also available for public inspection at depositories indicated in USGS catalogs.

Open-File Reports include unpublished manuscript reports, maps, and other material that are made available for public consultation at depositories. They are a nonpermanent form of publication that may be cited in other publications as sources of information.

Maps

Geologic Quadrangle Maps are multicolor geologic maps on topographic bases in 7 1/2- or 15-minute quadrangle formats (scales mainly 1:24,000 or 1:62,500) showing bedrock, surficial, or engineering geology. Maps generally include brief texts; some maps include structure and columnar sections only.

Geophysical Investigations Maps are on topographic or planimetric bases at various scales; they show results of surveys using geophysical techniques, such as gravity, magnetic, seismic, or radioactivity, which reflect subsurface structures that are of economic or geologic significance. Many maps include correlations with the geology.

Miscellaneous Investigations Series Maps are on planimetric or topographic bases of regular and irregular areas at various scales; they present a wide variety of format and subject matter. The series also includes 7 1/2-minute quadrangle photogeologic maps on planimetric bases which show geology as interpreted from aerial photographs. Series also includes maps of Mars and the Moon.

Coal Investigations Maps are geologic maps on topographic or planimetric bases at various scales showing bedrock or surficial geology, stratigraphy, and structural relations in certain coal-resource areas.

Oil and Gas Investigations Charts show stratigraphic information for certain oil and gas fields and other areas having petroleum potential.

Miscellaneous Field Studies Maps are multicolor or black-and-white maps on topographic or planimetric bases on quadrangle or irregular areas at various scales. Pre-1971 maps show bedrock geology in relation to specific mining or mineral-deposit problems; post-1971 maps are primarily black-and-white maps on various subjects such as environmental studies or wilderness mineral investigations.

Hydrologic Investigations Atlases are multicolored or black-and-white maps on topographic or planimetric bases presenting a wide range of geohydrologic data of both regular and irregular areas; principal scale is 1:24,000 and regional studies are at 1:250,000 scale or smaller.

Catalogs

Permanent catalogs, as well as some others, giving comprehensive listings of U.S. Geological Survey publications are available under the conditions indicated below from the U.S. Geological Survey, Books and Open-File Reports Section, Federal Center, Box 25425, Denver, CO 80225. (See latest Price and Availability List.)

"Publications of the Geological Survey, 1879-1961" may be purchased by mail and over the counter in paperback book form and as a set of microfiche.

"Publications of the Geological Survey, 1962-1970" may be purchased by mail and over the counter in paperback book form and as a set of microfiche.

"Publications of the U.S. Geological Survey, 1971-1981" may be purchased by mail and over the counter in paperback book form (two volumes, publications listing and index) and as a set of microfiche.

Supplements for 1982, 1983, 1984, 1985, 1986, and for subsequent years since the last permanent catalog may be purchased by mail and over the counter in paperback book form.

State catalogs, "List of U.S. Geological Survey Geologic and Water-Supply Reports and Maps For (State)," may be purchased by mail and over the counter in paperback booklet form only.

"Price and Availability List of U.S. Geological Survey Publications," issued annually, is available free of charge in paperback booklet form only.

Selected copies of a monthly catalog "New Publications of the U.S. Geological Survey" available free of charge by mail or may be obtained over the counter in paperback booklet form only. Those wishing a free subscription to the monthly catalog "New Publications of the U.S. Geological Survey" should write to the U.S. Geological Survey, 582 National Center, Reston, VA 22092.

Note.--Prices of Government publications listed in older catalogs, announcements, and publications may be incorrect. Therefore, the prices charged may differ from the prices in catalogs, announcements, and publications.